Experimental Study of a Solar Air Heater With New Arrangement of Transverse Longitudinal Baffles and Wire Mesh Layers

Afaq Jasim Mahmood

Submitted to the
Institute of Graduate Studies and Research
in partial fulfillment of the requirements for the degree of

Doctor of Philosophy
in
Mechanical Engineering

Eastern Mediterranean University
August 2015
Gazimağusa, North Cyprus

Approval of the Institute of Graduate Studies and Research

Prof. Dr. Serhan Çiftçioğlu
Acting Director

I certify that this thesis satisfies the requirements as a thesis for the degree of Doctor of Philosophy in Mechanical Engineering.

Prof. Dr. Uğur Atikol
Chair, Department of Mechanical Engineering

We certify that we have read this thesis and that in our opinion it is fully adequate in scope and quality as a thesis for the degree of Doctor of Philosophy in Mechanical Engineering.

Prof. Dr. Fuat Egelioğlu
Co-Supervisor

Prof. Dr. Loay Aldabbagh
Supervisor

Examining Committee

1- Prof. Dr. Uğur Atikol

2- Prof. Dr. Fuat Egelioğlu

3- Prof. Dr. Hüsamettin Bulut

4-Prof.Dr. Can Ertekin

5- Prof. Dr. Ibrahim Sezai

ABSTRACT

In this study, experiments were conducted on single- and double-pass solar air heaters (SAHs) with baffles and sixteen wire mesh layers inserted between the baffles. The baffles and mesh layers were inserted in the collector and tested to observe their effects on the thermal performance of the SAHs.

Three cases of single- and double-pass SAHs were considered with bed heights of 3, 5, and 7.5 cm. The different bed heights were considered to improve the thermal efficiency and outlet temperature. For all cases, the airflow rate was varied between 0.011 and 0.032 kg/s, and the height of the upper channel for the double-pass SAH was fixed at 2.5 cm. The effects of the airflow rate and number of baffles in each case on the thermal efficiency and outlet temperature of the SAHs were experimentally investigated.

The results showed that the efficiency could be improved by increasing the airflow rate, increasing the number of baffles, and decreasing the bed height. However, the temperature difference (ΔT) increased when the airflow rate was decreased, number of baffles was increased, and bed height was decreased. In all cases, the double-pass SAHs showed a greater thermal efficiency and outlet temperature than the single-pass SAHs.

A maximum efficiency of 68.1% was obtained using a double-pass SAH with seven baffles, an airflow of 0.032 kg/s, and a bed height of 3 cm. The maximum average temperature difference between the ambient and outlet air temperatures of 54 °C

was achieved using a double-pass SAH with seven baffles, airflow of 0.011 kg/s, and bed height of 3 cm.

The pressure drop increased with the number of baffles and airflow rate. When the airflow was kept the same, the pressure drop decreased as the bed height was increased. A comparison of the pressure drops for the single- and double-pass SAHs showed that the latter had a higher pressure drop than the former, as expected.

Keywords: Solar air heater, single- and double-pass, mesh layers, thermal efficiency, airflow.

ÖZ

Bu çalışmada tek ve çift geçişli bölmeli ve bölmeler arasına yerleştirilen on altı tel örgü katmanlı güneş hava ısıtıcıları (GHI) üzerine deneyler yapıldı. Akış bölme komponentleri ve tel katmanlar kollektör içerisine yerleştirilerek GHI'ların termal performansı üzerindeki etkilerini gözlemlemek için test edilmiştir.

Tek ve çift geçişli GHI'lar için yatak yüksekliği 3, 5, ve 7.5 cm olmak üzere üç durum göz önünde bulunduruldu. Farklı yatak yükseklikleri termal verimliliği ve çıkış sıcaklığı artırmak için düşünüldü. Tüm durumlarda, hava akış hızı 0.011 ve 0.032 kg/s arasında değiştirildi, ve çift geçişli ısıtıcı için her durumda üst kanalın derinliği 2.5 cm olarak sabit kalmıştır.Farklı hava akış hızları ve farklı akış bölme komponentleri sayılarının her durumda, çıkış sıcaklığı ve GHI'ların ısıl verimliliği üzerindeki etkileri deneysel olarak incelenmiştir.

Sonuçlar hava akış hızınınve akış bölme komponentleri sayısının artırıldığı, ve yatak yüksekliğinin azaldığı durumlarda verimliliğin iyileştiği gösterdi. Ancak,azalan hava akışhızı, artan akış bölme komponent sayısı ve azalan yatak yüksekliği sıcaklık farkını (ΔT) artırmıştır. Tüm durumlarda, çift geçişli GHI'nın ısıl verimliliği ve çıkış sıcaklıkları tek geçişli GHI'dan daha yüksek bulunmuştur.

Çift geçişli GHI için elde edilen % 68.1maksimum verimlilik, 7 akış bölme komponenti, 0.032 kg/s hava akış hızı ve 3 cm yatak yüksekliği kullanılarakelde edilmiştir.Çevre giriş ve çıkış havası arasında elde edilen maksimum ortalama sıcaklık farkı çift geçişli, 7 akış bölme komponentli, 0.011 kg/s hava akış hızı ve 3 cm yatak yüksekliğindeki durumda 54^{o}C olduğu belirlenmiştir.

Basınç düşüşü akış bölme komponenti sayısı ve hava akış hızının arttırılması ile artmıştır.Yatak yüksekliği arttıkça aynı hava akışı için, basınç düşüşünün azaldığı görülmüştür. maktadır. Ayrıca beklendiği gibi çift geçişli GHI'daki basınç düşüşünün tek geçişli GHI'dan daha yüksek olduğu tespit edilmiştir.

Anahtar Kelimeler: Güneş hava ısıtıcısı, tek ve çift geçişli, örgü katmanları, ısıl verim, hava akış hızı

To My Life

My Mother,

My Husband Othman,

My sons, Ahmed, Yahya and Ibraheem,

My Daughter, Maryam

ACKNOWLEDGMENT

I would like to express my sincere gratitude to my supervisor Assoc. Prof. Dr. Loay Aldabbagh and my co-supervisor Prof. Dr. Fuat Egelioglu for the continuous support of my PhD study and research.

Besides my supervisors, I would like to thank the rest of my thesis committee members, Prof. Dr. Can Ertekin, Prof. Dr. Hüsamettin Bulut and Prof. Dr. Ibrahim Sezai.

My sincere thanks also go to the department chair Prof. Dr. Ugur Atikol for his support, and help.

TABLE OF CONTENTS

ABSTRACT iii

ÖZ v

DEDICATION vii

ACKNOWLEDGMENT viii

LIST OF TABLES xi

LIST OF FIGURES xii

LIST OF SYMBOLS xviii

1 INTRODUCTION 1

1.1 Background and Problem Description..... 1

1.2 Thesis Objectives..... 3

1.3 Thesis Motivations and Organisation..... 4

2 SOLAR AIR HEATER..... 7

2.1 Types of Solar Air Collectors..... 7

2.1.1 Bare-plate Solar Collector..... 9

2.1.2 Cover-Plate Solar Collector..... 9

2.2 Literature Review..... 11

2.2.1 Single-pass Solar Collectors..... 13

2.2.2 Double-pass Solar Collectors..... 22

3 THERMAL ANALYSIS..... 29

3.1 Conservation of Energy Equation..... 29

3.1.1 An Energy Balance on the absorber plate of the Flat-Plate SAH..... 30

3.1.2 An Energy Balance on the Air Stream…..... 31

3.1.3 An Energy Balance on the Back Plate..... 31

3.2 Solar Air Heater Energy Losses..... 34

4 DESCRIPTION OF EXPERIMENTAL SETUP..... 35

4.1 Solar Air Heater with Various Arrangements..... 35

4.2. Experimental Setup..... 41

4.3. Experimental Proceedings..... 43

4.4 Measurements and Calibration of the Instruments..... 44

4.4.1 Airflow..... 44

4.4.2 Blower..... 46

4.4.3 Solar Radiation..... 46

4.4.4 Wire Mesh Layers..... 46

4.5 Uncertainty Analysis.....47

5 RESULTS AND DISCUSSION.....50

5.1 Heat Flux and Inlet Temperature.....50

5.2 Temperature Differences between the Outlet and Inlet Temperatures (**ΔT**)... 53

5.3 Temperature Differences of Bed ΔT_{bed} and Glass ΔT_g..... 68

5.4 Thermal Efficiency (η)..... 77

5.5 Pressure Drop..... 98

5.6 Performance Implications of the New Porous Media and Baffles Arrangement... ……..…….104

6 CONCLUSION and future work..... 105

6.1 Conclusions of Present Work..... 105

6.2 Future Work..... 109

REFERENCES.....110

LIST OF TABLES

Table 4.1: Different set-ups of the SAH..... 36

Table 4.2. The basic design and operating parameters used for the experimental study..... 41

Table 4.3: The mean average value for single and double- pass SAH..... 49

Table 5.1: Maximum temperature differences of the solar air heater with different height of collectors and number of baffles at minimum airflow rate 0.011 kg/s..... 66

Table 5.2: Maximum bed temperatures differences and glass temperatures differences of the SAH with different height of collectors and number of baffles at airflow rate 0.011 kg/s…….……...……. 75

Table 5.3: The thermal efficiencies for single- and double-pass SAHs with different height of bed and number of baffles at airflow rate 0.032 kg/s.....93

Table 5.4: The average thermal efficiencies from single- and double-pass SAHs with different height of bed and number of baffles at airflow rate 0.032 kg/s..... 94

Table 5.5: shows the maximum pressure drop from with different height of bed and number of baffles at airflow rate 0.032 kg/s..... 100

LIST OF FIGURES

Figure 2.1: Classification of solar air heaters.....8

Figure 2.2: Transpired collectors (Naveed et al., 2006).....10

Figure 2.3: Section of a bare-plate collector (Chongjie et al., 2006).....10

Figure 2.4: Conventional solar air heater.....12

Figure 2.5: Conventional single-pass solar collector with single glass cover (Ekenchukwu and Norton, 1999).....12

Figure 2.6: single- pass with double cover solar collector (Ekenchukwu and Norton, 1999)..... 13

Figure 2.7: Flat plate solar air heater (Gupta and Kaushi, 2008)..... 15

Figure 2.8: Schematic solar air heater (Hegazy, 1996)..... 15

Figure 2.9: Photograph of experimental set-up for testing of solar air heaters(Gill et al., 2012)..... 17

Figure 2.10: Sub regions for single channel solar collector (Al-Kamil et al., 1996).....18

Figure 2.11: Schematic view of the solar air collector with offset strip fin attached (Ming et al., 2014)..... 20

Figure 2.12: Schematic assembly of the double pass solar air heater, Aldabbagh et al. (2010)..... 21

Figure 2.13: Schematic of packed bed solar air heater, Mittal and Varshney (2006)……..…. 23

Figure 2.14: Parallel pass solar air heater (Ekenchukwu and Norton, 1999)....23

Figure 2.15: Double pass solar air heater..... 24

Figure 3.1: A schematic digram of the single pass SAH.....30

Figure 3.1: A schematic diagram of the single- pass SAH and thermal network.....31

Figure 4.1: Pictorial view of the experimental set up of SAH..... 37

Figure 4.2: Assembly scheme of the single-pass SAH system 3 baffles and wire mesh layers, section A-A, side view of single-pass SAH..... 38

Figure 4.3: Schematic assembly of the double-pass SAH, 5 baffles and wire mesh layers, section A-A, side view of double-pass SAH..... 39

Figure 4.4: Schematic assembly of the double-pass SAH, 7 baffles and wire mesh layers, section A-A, side view of double-pass SAH..... 40

Figure 4.5: Digital thermometer (OMEGASAYS)..... 44

Figure 4.6: Cross sectional view of the designed orifice meter.....45

Figure 4.7: An Eppley pyranometer.....46

Figure 5.1: Solar intensity versus time of the day for double- pass SAH, during testing of the SAHs having (a) 3 baffles (b) 5 baffles and (c) 7 baffles, with7.5 cm bed height……..……..…..……...51

Figure 5.2: Inlet temperature versus time of the day for: (a) 3 baffles (b) 5 baffles and (c) 7 baffles, for double- pass SAH, with 7.5 cm bed height.....52

Figure 5.3: Temperature difference versus time of the day at different mass flow rates: (a) Single- pass SAH, (b) Double- pass SAH, 3 baffles, 3cm bed height.....55

Figure 5.4: Temperature difference versus standard local time of the day at different mass flow rates: (a) Single- pass SAH, (b) Double- pass SAH, 5 baffles, 3cm bed height.....56

Figure 5.5: Temperature difference versus standard local time of the day at different mass flow rates: (a) Single- pass SAH, (b) Double- pass SAH, 7 baffles, 3cm bed height…….…...…….….... 57

Figure 5.6: Temperature difference versus standard local time of the day at different mass flow rates : (a) 3 baffles (b) 5 baffles and (c) 7 baffles, for single- pass SAH, 5cm bed height……..... 58

Figure 5.7: Temperature difference versus standard local time of the day at different mass flow rates: (a) 3 baffles (b) 5 baffles and (c) 7 baffles, for double- pass SAH, 5cm bed height..... 59

Figure 5.8: Temperature difference versus standard local time of the day at different mass flow rates: (a) Single- pass SAH, (b) Double- pass SAH, 3 baffles, 7.5cm bed height…….60

Figure 5.9: Temperature difference versus standard local time of the day at different mass flow rates: (a) Single- pass SAH, (b) Double- pass SAH, 5 baffles, 7.5cm bed height..... 61

Figure 5.10: Temperature difference versus standard local time of the day at different mass flow rates: (a) Single- pass SAH, (b) Double- pass SAH, 7 baffles, 7.5cm bed height..... 62

Figure 5.11: Effect of number of baffles (3, 5 and 7) on the temperature difference at different mass flow rates: a) Single- pass SAH, b) Double- pass SAH, 5cm height of bed..... 63

Figure 5.12: Temperature difference versus solar intensity at 0.011kg/s airflow rate for single- pass SAH with 5 cm bed height..... 64

Figure 5.13: Outlet temperature versus Inlet temperature for: a) Single- pass SAH, b) Double- pass SAH with 5cm bed height..... 65

Figure 5.14: Maximum temperature differences of the solar air heater with different height of collectors and number of baffles, as 3D columns.....67

Figure 5.15: Bed temperature difference versus standard local time of the day at

different mass flow rates for: (a) single- pass SAH, (b) double- pass SAH, 3 baffles and 3cm bed height.....70
Figure 5.16: Glass temperature difference versus standard local time of the day at different mass flow rates for: (a) single- pass SAH, (b) double- pass SAH, 3 baffles and 3cm bed height……..... 71
Figure 5.17: Bed temperature difference versus standard local time of the day at airflow rates 0.011 kg/s for double- pass SAH, 3 baffles……..... 72
Figure 5.18: Glass temperature difference versus standard local time of the day at airflow rates 0.011 kg/s for double- pass SAH, 3 baffles..... 72
Figure 5.19: Bed temperature difference and Glass temperature difference versus standard local time of the day, at airflow rates 0.011 kg/s, for a) Single- pass SAH, b) Double- pass SAH, 7 baffles with 5 cm bed height..... 73
Figure 5.20: Glass temperature difference versus standard local time of the day, for double- pass SAH: 3,5,7 baffles, 5 cm height of bed..... 74
Figure 5.21: Bed temperature difference versus standard local time of the day, for double- pass SAH: 3,5,7 baffles, 5 cm height of bed..... 74
Figure 5.22: Variation of collector efficiency at different mass flow rates for (a) Single- pass SAH, (b) Double- pass SAH, for 3 baffles, 3cm bed height..... 80
Figure 5.23: Variation of collector efficiency at different mass flow rates for (a) Single- pass SAH, (b) Double- pass SAH, for 5 baffles, for 3cm bed height..... 81
Figure 5.24: Variation of collector efficiency at different mass flow rates for (a) Single-pass SAH, (b) Double-pass SAH, for 7 baffles, 3cm bed height..... 82
Figure 5.25: Average efficiency across the single- and double-pass SAHs versus mass flow rate, for 3cm bed height..... 83
Figure 5.26: Efficiency comparison between single- pass and double- pass SAHs, for 5cm bed height..... 84

Figure 5.27: Average efficiency across the single- and double- pass SAHs versus mass flow rate, for 5cm bed height..... 85

Figure 5.28: Average efficiency across the single- and double- pass SAHs versus mass flow rate, for 5cm bed height as 3D columns..... 86

Figure 5.29: Variation of collector efficiency at different mass flow rates for: (a) Single- pass SAH, (b) Double- pass SAH, for 3 baffles, for 7.5cm bed height.....87

Figure 5.30: The maximum thermal efficiencies for single- and double- pass SAHs with different height of bed and number of baffles at mass flow rate 0.032 kg/s.....88

Figure 5.31: The maximum average thermal efficiencies from single- and double-pass SAHs with different height of bed and number of baffles at airflow rate 0.032 kg/s..…….…….....….....88

Figure 5.32: Average efficiency versus air flow rate for 7.5 cm with 3,5 and 7 baffles, for 7.5cm bed height..... 89

Figure 5.33: Efficiency comparison between single- pass and double- pass SAHs for 3baffles..... 89

Figure 5.34: Thermal efficiency versus solar intensity for 5 cm with 3,5 and 7 baffles, for single- pass SAH..... 90

Figure 5.35: Thermal efficiency versus inlet temperature for 5 cm with 3,5 and 7 baffles, for single- pass and double- pass SAHs.....91

Figure 5.36: Efficiency comparison between the double- pass SAH (7 baffles- 3cm) with same double- pass SAHs in literature.....92

Figure 5.37: The thermal efficiency of the collectors versus $(T_o - T_i)/I$, for 3cm bed height, 3baffles.....96

Figure 5.38: The thermal efficiency of the collectors versus $(T_o - T_i)/I$, for 5cm bed height, 3baffles.....96

Figure 5.39: The thermal efficiency of the collectors versus (T_o - T_i)/I, for 7.5cm bed height, 3baffles.....97

Figure 5.40: Pressure drop across the bed versus mass flow rates for: (a) 3 baffles (b) 5 baffles and (c) 7 baffles, for double pass SAH, 5cm bed height.....101

Figure 5.41: Pressure drop across the bed of 3 baffles versus mass flow rates for single and double pass. For 3cm bed height.....101

Figure 5.42: Pressure drop across the bed versus mass flow rates for single- pass and double- pass SAHs, for 3 baffles, for 7.5cm bed height.....102

LIST OF SYMBOLS

A_c	Collector area, (m^2).
C_p	Specific heat of air, (kJ/kg.K).
D	Outer diameter of orifice pipe outer diameter, (m).
d	Inner diameter of orifice pipe outer diameter, (m).
h	Fluid deflection inside the incline manometer, (m).
I	Solar radiation, (W/m^2).
m	Mass flow rate of air, (kg/s).
Q	Volumetric flow rate, (m^3/s).
T_{air}	Film air temperature between the outlet and inlet, (°C).
T_{in}	Inlet air temperature, (°C).
T_{out}	Outlet air temperature, (°C).
T_{bed}	Temperature of bed, (°C), $T_{bed} = (T_{bed1} + T_{bed2} + T_{bed3})/3$.
T_g	Temperature of glass, (°C), $T_g = (T_{g1} + T_{g2} + T_{g3})/3$.

Greek symbols

η	Thermal efficiency of collector.
ρ	Density of air, (kg/m^3).
ΔP	Pressure difference, $\Delta P = \rho.g.h \sin 15^o$, ($N/m^2$).
ΔT	Temperature difference ($T_{out} - T_{in}$), (°C).
ΔT_{bed}	Temperature difference of bed ($T_{bed} - T_{in}$), (°C).
ΔT_g	Temperature difference of glass ($T_g - T_{in}$), (°C).
ω	Uncertainty.
Φ	Porosity.

Subscripts

bed	Bed.
f	Fluid.
g	Glass.
in	Inlet.
out	Outlet.

Chapter 1

INTRODUCTION

1.1 Background and Problem Description

Energy is vital to human life. The rapid increases in the global population and economic development and growth have increased the demand for energy. At present, most energy is being produced from non-renewable sources, such as fossil fuels, because of the large supply and low cost of production (Kalogirou, 2004). Fossil fuels are being consumed at such a rate that they will be completely exhausted within a century or so. The combustion of fossil fuels to generate heat and power causes various hazards to human health and ecosystems (Jesko, 2008). Emissions from the combustion process have been linked to phenomena such as global warming, acid rain, and photochemical smog. Several international treaties have been made to protect the environment and control emissions: the 1979 Convention on Long-Range Transboundary Air Pollution and its protocols, the 1985 Vienna Convention for the Protection of Ozone Layer, the 1987 Montreal Protocol on Substances that Deplete the Ozone Layer as amended in London in 1990, the 1992 United Nations Framework Convention on Climate Change (UNFCCC), the United Nations Conference on Environment and Development in Rio de Janeiro in 1992, and the Kyoto Protocol in 1997 that extended the UNFCCC with the aim of reducing global warming and manmade CO_2 emissions. The energy consumption of residential and other buildings forms a large part of the global and regional energy demand. In the residential sector, almost half of the energy

consumption is for space heating. Globally, biomass is the dominant fuel used for heating buildings (Ürge-Vorsatz*et al*., 2015). Electrical energy and natural gas are extensively used in developed regions. The use of electricity for space heating is showing substantial growth, and it is one of the most resource-intensive forms of consumption in cold climates (Heiskanen*et al.*, 2011). Hannema*et al*. (2013) indicated that, in developed countries, residential energy consumption is mostly due to space heating and is a large component of the energy demand. Ahren and Norton (2015) indicated that 27% of the total energy consumption by the European Union (EU) in 2010 was by the residential sector. Fan *et al*. (2015) indicated that the residential sector is one of the greatest contributors of CO_2 emissions in China. They found that the largest portion of carbon emissions is from space heating and cooling. The countries that signed the Kyoto Protocol set targets to decrease the emission of greenhouse gases. Heiskanen*et al*. (2011) indicated that there are many cost-effective ways to decrease the resource use and CO_2 emissions of space heating, such as the use of heat pumps. For the EU, their target is to reduce greenhouse gas emissions by 20% by 2020. The countries that signed the Kyoto Protocol are trying to meet the 2020 targets; one of the most important aspects in the near future is energy utilisation in a built environment. Policymakers and researchers are searching for cost-effective technologies to reduce energy consumption and CO_2 emissions. Using alternative and energy-efficient technologies with better building construction will help decrease the heat demand for space heating and thus reduce resource consumption and emissions. As the global population continues to grow and the limited supply of fossil fuels begins to diminish, it may not be possible to meet the global energy demand by only using fossil fuels.

The rise in fuel costs, exhaustion of fossil fuels, and their adverse effects due to combustion have renewed interest in alternative energy sources such as renewable. Utilising solar energy to heat air, such as through the use of solar air heaters (SAHs), is an effective way to decrease resource consumption and CO_2 emissions.

1.2 Thesis Objectives

A literature review showed that there is a shortage of experimental work involving the use of baffles with porous media as an absorber plate in single- and double-pass SAHs. To the best of our knowledge, there has been no experimental work on SAHs that use porous media with a 3 cm channel depth to create a large turbulent flow, which increases the heat transfer rate from the porous media to the airflow. In this work, single- and double-pass counter-flow SAHs were introduced with aluminium baffles and porous media (steel mesh layers) in a new arrangement. The proposed design has baffles and porous media as an absorber plate to increase the heat-transfer area, increase the length of the airflow path inside the ducts, and improve the airflow distribution inside the collector. To increase the length of the airflow path inside the bed, the transverse baffles were arranged and fixed inside the duct to produce a path shaped like a figure-eight. A double-pass SAH was constructed to reduce the heat loss from the cover and preheat the inlet air. The effect of increasing the number of baffles on the SAH performance was investigated. Increasing the number of baffles increases the length of the airflow path from the inlet to the outlet of the collector, so the airflow gains more heat from the wire mesh layers.

In cover-plate SAHs, the cover decreases convective heat losses from the absorber plate and reduces long-wave radiative heat losses. The present study was focused on improving the SAH performance; to achieve this goal, the cover and absorber plate of conventional solar collectors were modified. In order to increase the heat transfer

area between the air and absorber, wire mesh layers were used instead of an absorber plate. Using wire mesh instead of sheet metal as the absorber reduces the construction cost of the collector because the former is cheaper than the latter. The main objectives of this study can be summarised as follows:

1. To construct and test single- and double-pass (counter-flow collector) SAHs.
2. To replace the absorber plate with steel wire mesh layers (porous media) to reduce the construction cost and increase the heat transfer area.
3. To change the collector's bed height and examine the effect of the bed height on the thermal performance of the solar collector.
4. To examine the effect of the bed height on the thermal performance of the solar collector.
5. To perform experiments under the same weather conditions of Famagusta, North Cyprus in order to compare the collected data and recommend the optimum arrangement for achieving the highest level of performance.

1.3 Thesis Motivations and Organisation

Conventional SAHs mainly consist of panels, an insulated hot air duct, and air blowers in active systems. The panel consists of an absorber plate and transparent covers to allow solar radiation to penetrate into the collector. Such heaters have low thermal efficiency because of the low coefficient of the convective heat transfer between the absorber plate and air. Also, a higher temperature of the absorber plate which results in higher heat losses to the surroundings. This study is aimed to design and construct cheap and efficient SAHs packed with wire mesh layers. Similar studies carried by Nowzari*et al.*, (2015) and El- Khawajah*et al.*, (2011) at the EMU. El- Khawajah*et al.*, (2011) used transverse steel fins and the air moved in a snake path within the collector. The collector was packed with 12 layers of wire

meshes. The channel depth was fixed to 7 cm and the effect of the channel depth on the efficiency was not investigated. Nowzari*et al.*, (2015) investigated single and double- pass SAHs packed with wire mesh layers. The design philosophy was different; the second cover was partially perforated Plexiglas and no fins or baffles are employed. The bed height was varied between 3 and 8 cm. The effect of bed heights on the efficiency and exit air temperature with different mass flow rates were investigated. As mentioned above in Nowzari*et al.*, (2015) baffles or fins were not employed to increase the air path length and El- Khawajah*et al.*, (2011) had not investigated the effect of bed height. In this study the effect of the bed height and the air path length on the efficiency and exit air temperatures were investigated. The main contribution of science in this study was examined using porous materials like steel wire mesh layers (alternative of absorber plate) and transverse aluminium baffles (increase the air path to gain more heat) in the duct of the SAH to enhance the thermal performance. The use of a double-pass counter-flow collector minimises heat loss to the surroundings and maximises heat transfer to the airstream in the upper channel. The comparison of the average efficiencies in the present work with the reported data for double-pass SAHs shows that there is an improvement in the proposed SAH.

The thesis is organised as follows. Chapter 1 introduces the reasons for utilising SAH and the main objectives of this work. Chapter 2 presents SAH along with a literature review discussing research works which are related to the thesis topic. Chapter 3 explains the theoretical model of the proposed SAH in detail. Chapter 4 describes the experimental set up of the solar air collector and the equipment used to collect data. Chapter 5 presents the experimental results obtained from SAHs with different configurations. The collected data on various days of the tests are

illustrated with figures and discussed in detail. Chapter 6 presents the general conclusions and recommendations along with future works.

Chapter 2

SOLAR AIR HEATER

A SAH converts solar energy into useful thermal energy. In general, a SAH works as a heat exchanger that transfers heat to the working fluid *i.e.* air. The thermal performance of a SAH is influenced by different factors, such as the solar radiation, collector type, absorption area, orientation, inlet temperature, and air volume flow rate. SAHs are generally used to produce energy at low to moderate temperatures. These types of heating systems are cheap and easy to maintain, but suffer from the disadvantage of low thermal efficiency (Singh and Dhiman, 2014). SAHs have several advantages compared to other solar energy applications:

- Minimal maintenance is required.
- There are no freezing or corrosion problems compared with liquid-type collectors.
- If a perforated plate system is used, the fresh air improves the indoor air quality.

2.1 Types of Solar Air Collectors

The first SAH was designed and built by the American E. Morse in 1881 (Kumar and Singh, 2014). The International Energy Agency (IEA) classifies solar air heating systems into six different types:

1. Collector/room/collector,
2. Collector-heated air circulated through the cavity of the building envelope,
3. Closed loop collector/storage and radiant discharge to building spaces,
4. Open single-loop collector to building spaces,

5. Collector-heated air transferred to water via an air/water heat exchanger, and
6. Solar heating of ventilated air.

SAHs can be classified on the basis of the mode, as shown in Figure 2.1.

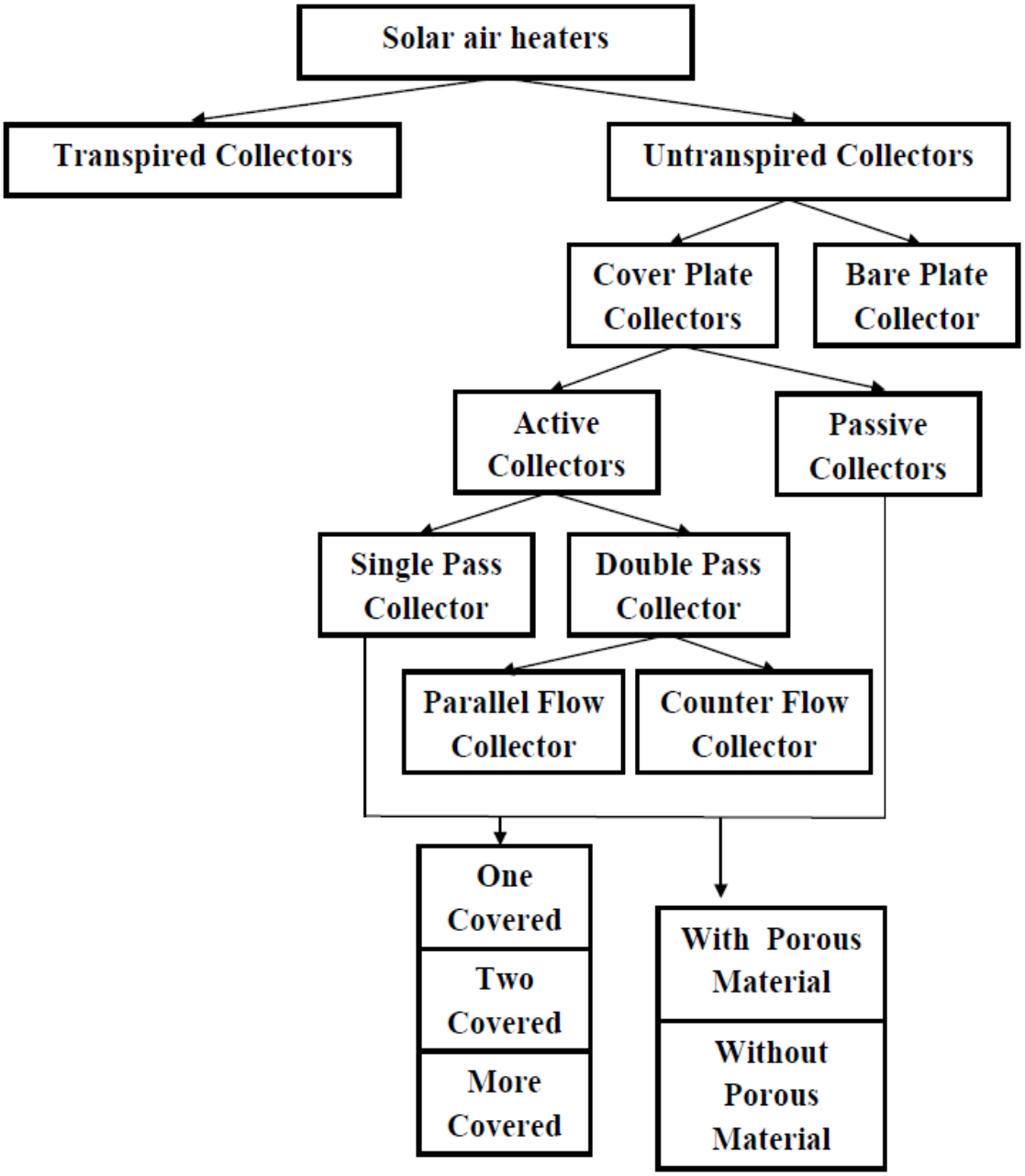

Figure 2.1: Classification of SAHs.

1. Transpired collectors

Transpired or perforated collectors (Figure 2.2) are relatively new solar collector technologies that were developed in the late 1980s for ventilation air heating. The absorber plate of the transpired collector is perforated so that ambient air is continuously withdrawn through the perforations (Naveed*et al.*, 2006).

2. Untranspired collectors

Untranspired collectors are more widely used compared to transpired collectors. The absorber heats the air as it passes above or below the absorber plate.

There are many types of untranspired collectors, and it is not an easy task to classify all. However, they can be classified into two main groups (Ekechukwu and Norton, 1999).

2.1.1 Bare-plate Solar Collector

This type of SAH is widely used in many applications, especially for agricultural drying operations. As shown in Figure 2.3, the air flows in a single pass between the absorber plate and insulated back bed. Researchers have studied the thermal performance of this type of solar collector and found that it has high thermal losses through the exposed surface. Thus, this type of SAH has the disadvantage of low thermal efficiency at moderate temperatures. In contrast, bare-plate SAHs are less expensive than cover-plate solar collectors (Chongjie*et al*., 2006).

2.1.2 Cover-Plate Solar Collector

The cover plate is an important component that affects the thermal efficiency of the SAH. One or more transparent covers parallel to the absorber plate can be used to minimise the heat losses from the SAH in order to increase the outlet air temperature and improve the efficiency. A double-glazed cover is used with either a

single or double airflow pass to increase the coefficient of the heat transfer between the working fluid and absorbing plate (Kalogirou, 1997).

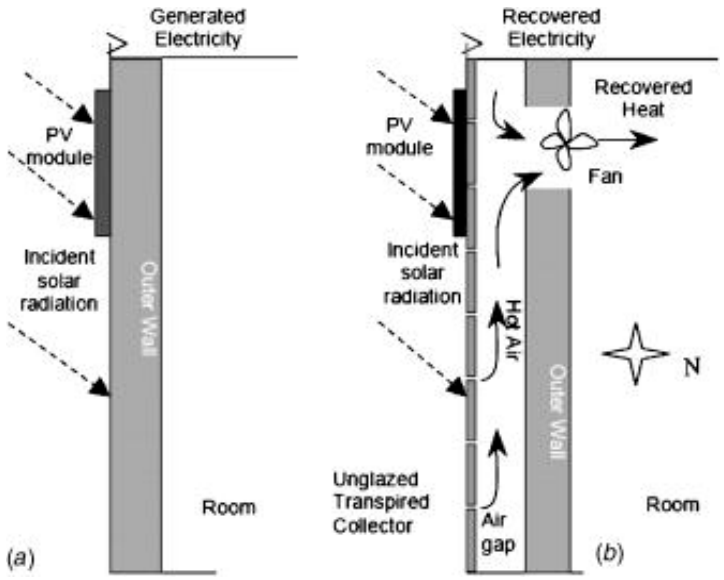

Figure 2.2: Transpired collectors (Naveed *et al.*, 2006).

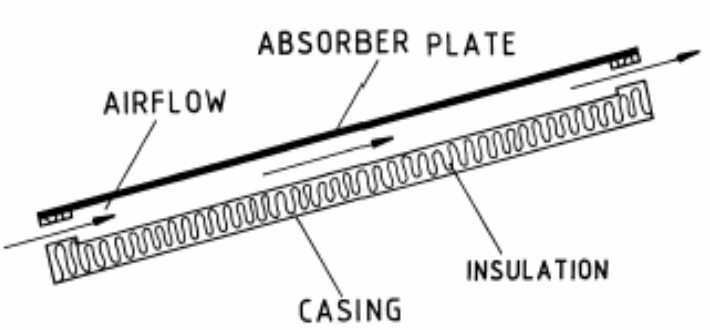

Figure 2.3: Section of a bare-plate collector (Chongjie et al., 2006).

A SAH consists of a rectangular shape collector made from metal or wood that is connected with an air blower in active systems and an absorber plate that absorbs the solar radiation and transfers it to the working fluid. The glazed SAH uses glass or a transparent material to trap the solar energy inside the collector and decrease the heat losses to the surroundings. All sides of the solar bed must be thermally

well-insulated to minimise the convection and radiation heat losses to the environment (Omojaro and Aldabbagh, 2010).

Struckmann (2008) indicated that a typical flat-plate air heater heats the air at temperatures of less than 80 °C. There are many designs of flat-plate solar collectors. The most common types are given below:

1. Active or passive solar collector: The active method employs fans to enhance the heat transfer by increasing the airflow rate. In the passive method, the thermal energy flows by natural convection.
2. Collector absorbing plates: Flat, corrugated, or grooved plates, fins, etc. The plate may be integrated with the obstacles.
3. Number of covers: Collectors that are designed to reduce heat losses can be classified by the number of covers that they can hold: one, two, or more covers. Increasing the number of covers reduces the heat losses from the cover, but less solar radiation is transmitted to the absorber plate.
4. Glazing materials: Glass is widely used for glazing the solar collectors because it can transmit as much as 90% of the incoming shortwave solar irradiation while transmitting virtually none of the long wave radiation emitted outward by the absorber plate.

2.2 Literature Review

Much technological and financial effort has gone into solar research on improving the thermal efficiency of SAHs because of its use of a renewable energy resource, lack of implementation, and environmental friendliness. Solar energy can be used to heat air and water, dry agricultural products, and light our homes. As mentioned earlier conventional SAHs mainly consist of a panel made of wood or other

materials, an absorber plate placed inside the duct, a thin glazing or transparent plastic at the top as a cover, and air blowers (Figure 2.4). The hot air duct is thermally insulated on all the sides except for the covered top. Multiple factors affect the SAH.

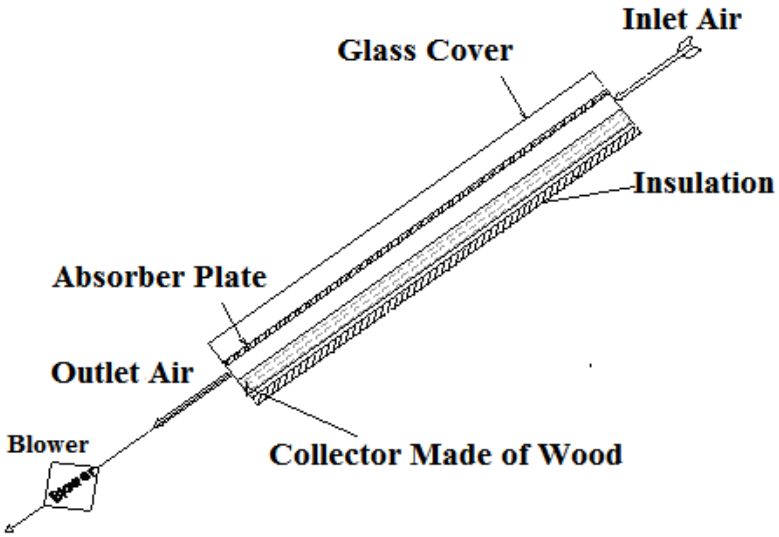

Figure 2.4: Conventional solar air heater.

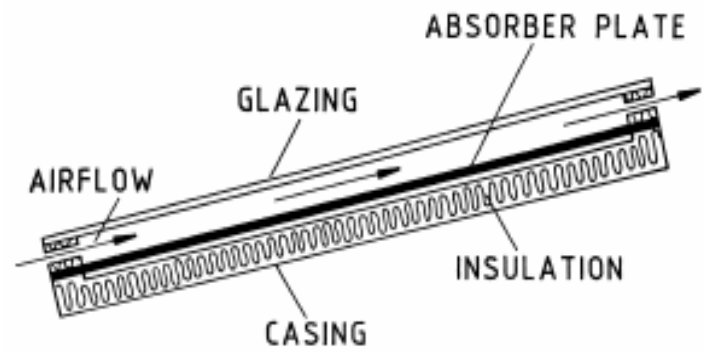

Figure 2.5: Conventional single-pass solar collector with single glass cover (Ekenchukwu and Norton, 1999).

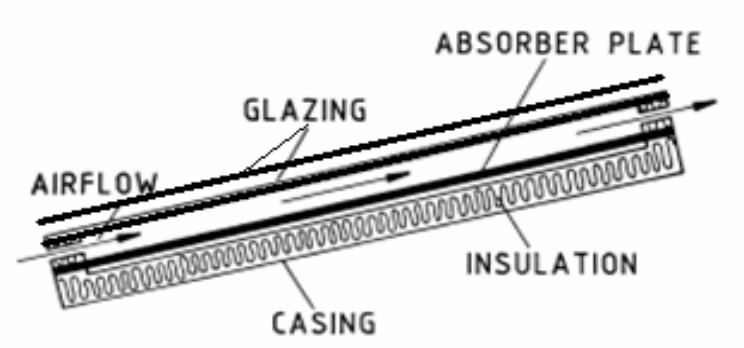

Figure 2.6: single- pass with double cover solar collector (Ekenchukwu and Norton, 1999).

efficiency are meteorological parameters (*e.g.* ambient temperature, wind speed, humidity, and solar intensity), design parameters (*e.g.* collector materials, size, and type), flow parameters (*e.g.* flow pattern, airflow rate, mode of flow, collector cover, absorber shape), and the material (*e.g.* black-coloured wood, aluminium, thin steel plate). The most important parameters are the absorber plate, collector cover, airflow pattern inside the duct, and height of the collector (Aboul-Enein*et al.*, 2000; Gupta and Kaushi, 2008).

2.2.1 Single-pass Solar Collectors

The conventional single-pass solar collector is classified as a front-pass cover-plate SAH, where air passes through the bed between the cover plate and absorber plate, or back-pass cover-plate SAH, where air flows between the backside of the absorber plate and end of the bed (Figure 2.5). Single-pass SAHs are classified in two types depending on the cover bed: single-cover (Figure 2.5) and double-cover (Figure 2.6). The absorber plate and cover type are the most important parameters which affect the thermal performance and outlet air temperature.

Increasing the absorber area increases the heat gain to the airflow. Different configurations can be applied to increase the absorber plate area and heat transfer

coefficient of the airflow. Fins and baffles or a wire mesh layer can be used to increase the surface area of the absorber plate while also increasing the turbulence inside the flow channel. Double-glass covers are used to improve the thermal performance of a SAH because they minimise the thermal energy lost from the cover to the environment (Aboul-Enein*et al.*, 2000).

Cleaning the glass cover of the solar collector increases the thermal efficiency, as demonstrated by Denga*et al.* (2015); the thermal efficiency of a very dusty surface can be 10.7%–21.0% less than that of a clean glass.

Gupta and Kaushi (2008) theoretically studied air passing between the absorber plate and bottom bed in a single pass with a single glass cover as shown in Figure 2.7. They predicted the most important parameters of any design of the solar collector to be the channel height (H) (*i.e.* space between the bottom plate and absorber), aspect ratio (AR; length-to-width ratio of the absorber plate), and mass flow rate per unit area (G). They noted that increasing the collector AR or G increases the air velocity inside the channel because of the reduced cross-sectional area of the channel. This results in a greater heat gain to the passing air, but also increases the pressure drop and power consumption of the fan.

Hegazy (1996) optimised the flow channel height for a conventional flat-plate SAH and derived an expression to estimate the channel depth-to-length ratio. This expression is of great importance for designers of this type of SAH. A parametric study was also carried out to investigate the effect of the channel depth on the useful heat gain by the collector over a wide range of D/L (depth of flow channel/length of absorber plate) ratios and pumping power requirements (Figure 2.8).

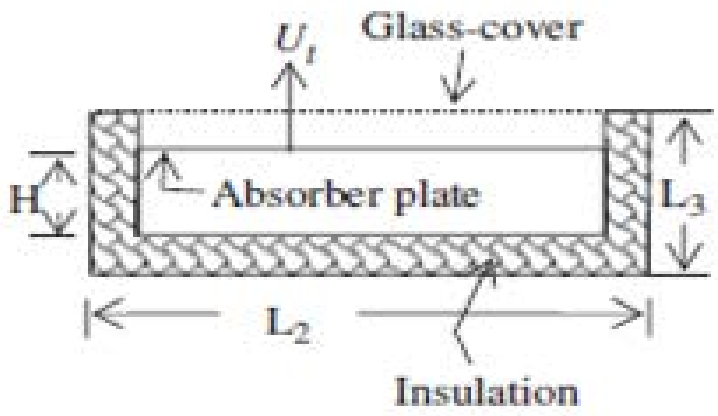

Figure 2.7: Flat plate solar air heater (Gupta and Kaushi, 2008).

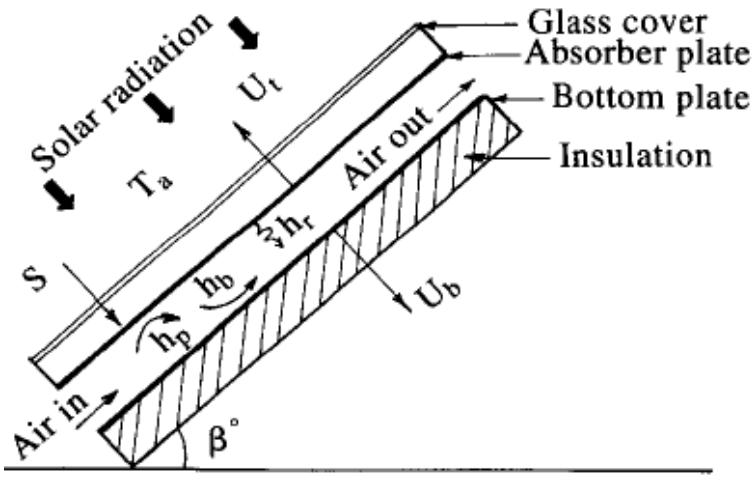

Figure 2.8: Schematic of solar air heater (Hegazy, 1996).

Gill *et al.* (2012) described three types of single-pass SAH models. Two had the same bed area with an obstacle sheet as the absorber plate, where the first bed had one glass cover and the second bed had two glass covers. The third collector had a packed bed and a smaller area than the others as shown in Figure 2.9. They found that the heater with the packed bed absorbed heat more effectively than the other two beds with obstacles and produced a higher outlet air temperature. The maximum rise in air temperature was found to be 35 °C for the packed bed at

airflow rate of 0.013 kg s^{-1} m^2, while the rise in air temperature was 12 °C for the single cover and 18 °C for the double glass cover at an airflow rate of 0.025 kg s^{-1} m^2. The SAHs efficiencies were 71.68% for the packed bed, 45.05% for the double cover, and 30.29% for the single cover at an airflow rate of 0.025 kg s^{-1} m^2.

Al-Kamil and Al-Ghareeb A.A (1996) experimentally and theoretically studied the performance of a flat plate SAH. They investigated the effect of blackening the collector rear plate and the thermal radiation inside the heaters. The constructed SAH had dimensions of 1690 mm × 1030 mm × 60 mm and was made of 1.1-mm-thick galvanised steel (Figure 2.10). The absorber was a dull, matte, and blackened plate. A single glass cover with a thickness of 4 mm was used as glazing. The temperature distribution inside the SAH was evaluated numerically. Blackening the rear plate was concluded to enhance the heat transfer up to 10%. The sectioning method was found to be suitable for solving SAH problems and can be used for future studies.

Baffles and obstacles have been used in many applications to increase the turbulence of the airflow through a duct. The artificial obstacle surface provided by the absorber plates has been found to have a positive effect on the heat transfer. The obstacle geometry creates turbulent flow because of the reattachment between the two repeated ribs and airflow separation, this can increase the coefficient of the heat transfer between the airflow and absorber plate in a SAH (Saxena*et al.*, 2015). Creating a turbulent flow inside the collector is an effective way of improving the performance of a SAH. Turbulence is observed in the forms of ribs, obstacles, delta winglets, baffles, fins, vortex generator, and rings. The heat transfer coefficient and thermal efficiency increase with the airflow rate through the ducts (Yongsirie*et al.*,

2014; Alam*et al.*, 2014). Ribs, baffles, fins, and different combinations of these have been found to augment heat transfer and improve the thermo-hydraulic performance.

However, turbulence in the fluid flow increases the pressure drop, which is undesirable in heat exchanger applications. Therefore, because of the contrasting effects of turbulators, careful considerations should be taken in the modelling and designing of such structures (Aghaie*et al.*, 2015).

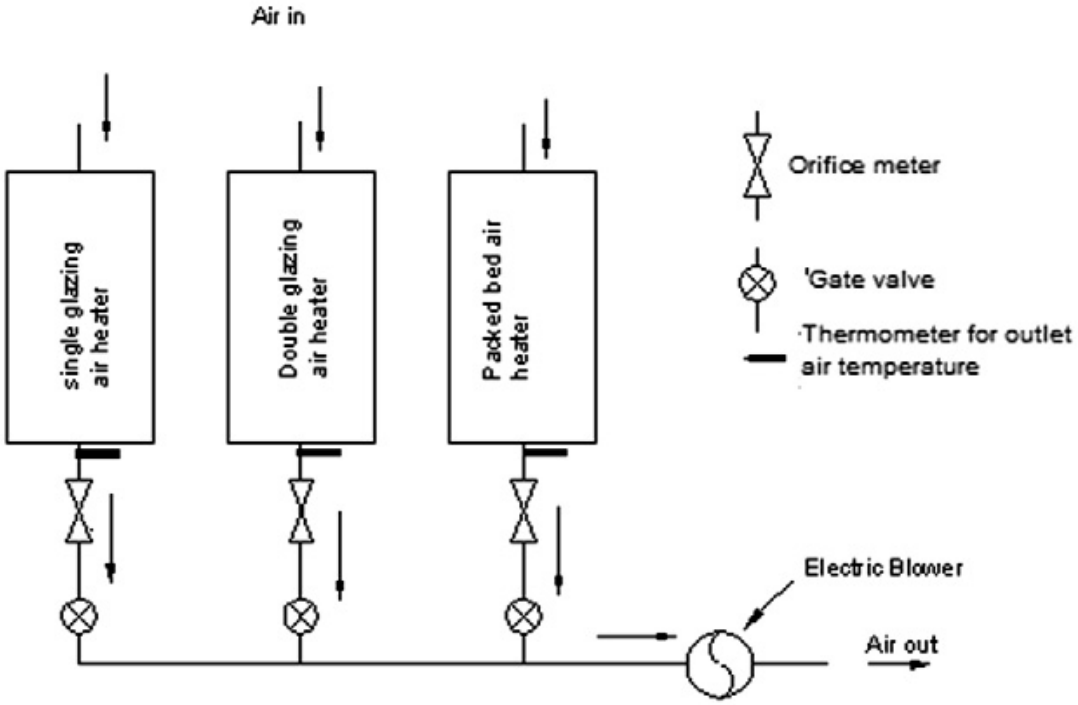

Figure 2.9: Experimental set-up for testing of solar air heaters (Gill *et al.*, 2012).

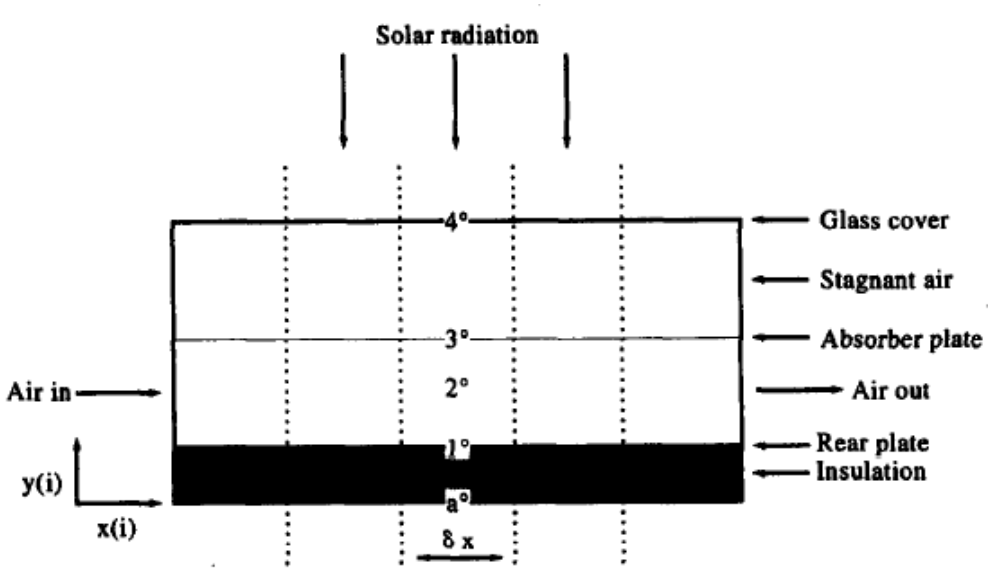

Figure 2.10: Subregions for single channel solar collector (Al-Kamil et *al*., 1996).

Similarly, Bahrehmand and Ameri (2015) and Mohammadi and Sabzpooshani (2013, 2014) presented single-pass SAHs that utilised baffles and fins over the absorber plate. They illustrated that increasing the baffle width and space between baffles in the turbulent flow regime are not economically feasible owing to the extreme increase in the pressure drop and required pump work.

Ben Salma (2007) suggested treating the problem of dead zones in the bed (*i.e.* places where air gets stuck and does not move) by using longitudinal fins between the main transverse fins. These longitudinal fins extend the airflow and do not contact the absorber. He found that the efficiency increased to a maximum of 81.5% at an airflow rate of 0.017 kg s^{-1} m^{-2}.

Adnane*et al.* (2012) experimentally compared the thermal performances of three single-pass SAHs: (a) with a new form of obstacles in the airflow duct, (b) with rectangular obstacles, and (c) without obstacles. They then compared the best system with (d) a double-pass solar bed having the same type of obstacles in order

to determine the best-performing model. The single-pass SAH having trapezoidal obstacles achieved efficiencies of 66.8% and 77% for airflow rates of 0.028 and 0.045 kg/s, respectively. With the double-pass SAH and at the same flow rates, the efficiencies were 67.5% and 78.3%, respectively.

Ming *et al.* (2014) optimised a new SAH with rectangular offset strip fins to strengthen the convective heat transfer in the airflow pass (Figure 2.11). The thermal efficiency increased from 64.1% to 72.3% as the airflow rate was changed from 0.034 kg/s to 0.063 kg/s.

Suleyman(2006)fixed fins on both the upper and lower faces of the absorber to maximise the heat absorbed from the sun to the absorber plate with fins. These fins were inclined at 75° to the air direction; therefore, this fin shape caused a turbulent airflow inside the duct. In addition, vortices developed around the absorber plate edges, which increased the absorber heat and heat transfer coefficient and decreased the thermal heat loss. This improved the thermal efficiency. The maximum thermal efficiency was 80% at 13:00 PM; the thermal efficiency results depend on the solar radiation and size of the solar air collectors.

Pakdaman*et al.* (2011) evaluated the performance of a natural convection SAH with a rectangular finned absorber plate. Their aim was to develop an empirical model which can predict various significant parameters for natural convection SAHs. The collector dimensions were 2000 mm × 1000 mm × 150 mm. A galvanised-iron plate, which was painted black, was used with a thickness of 1 mm. Forty-six rectangular fins were attached to the absorber plate 20 mm apart from each other. The attached fins had dimensions of 2000 mm × 10 mm with a thickness of 1 mm.

A single glass cover with a thickness of 4 mm was used as glazing. They concluded that a longitudinal rectangular fin arrangement enhances the heat transfer of SAHs. Some researchers have used porous packed materials to increase the turbulence of air inside the collector and thus increase the coefficient of the convective heat transfer between the absorber packed bed and airflow.

Aldabbagh*et al.*(2010) investigated single- and double-pass (counter-flow) SAHs with porous media (porosity 0.85). They used wire mesh layers as an absorber plate between the back bed and glass cover (Figure 2.12). The purpose of their study was to experimentally expand the similar work conducted theoretically by Mohamad (1997). They achieved a maximum efficiency of 45.93% at a mass flow rate of 0.038 kg/s.

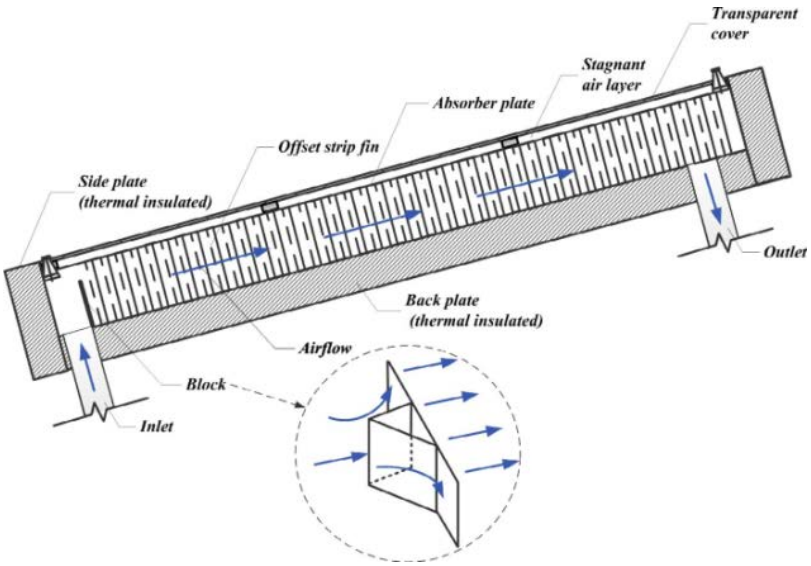

Figure 2.11: Schematic view of the solar air collector with offset strip fin attached (Ming *et al.*, 2014)

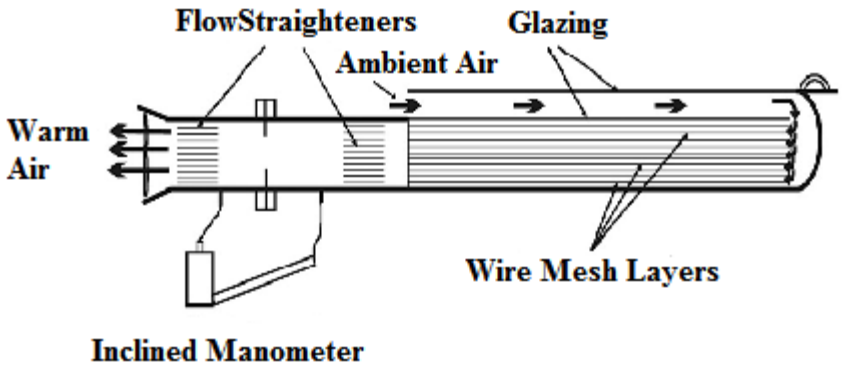

Figure 2.12: Schematic assembly of the double pass solar air heater, Aldabbagh*et al.*(2010)

Omojaro and Aldabbagh (2010) investigated the performance of single- and double-pass solar collectors with fins and wire mesh layers. They used wire mesh layers to create a turbulent flow inside the duct and improve the heat transfer coefficient. Their results showed that increasing the airflow rate inside the duct increases the thermal efficiency and decreases the outlet temperature.

Bhargava *et al.* (1990) modified a conventional SAH by using two metal plates as an absorber plate and single glazing. The air flowed through the lower channel (*i.e.* between the second metal plate and back bed), while the air stagnated between the metal plate and glazing to decrease heat loss. The upper channel had a higher thermal efficiency than the lower channel. They showed that keeping the upper channel completely open decreased the thermal efficiency of the lower channel by 5% because of the natural flow in the upper channel.

Alta *et al.*(2010) compared three types of single-pass collectors: a double glass cover without fins, single cover with fins, and double glass cover with fins. Two covers were used to minimise the heat losses from the cover to the surrounding. Using fins not only increased the absorbed heat gain but also allowed the absorbed

heat to be transferred to the airflow inside the bed. The maximum temperature difference was 11 °C at an airflow rate of 0.034 kg s^{-1} m^2 for the double glass finned collector.

Bahrehmand and Ameri (2015) presented a theoretical analysis for single-pass SAHs with two glass covers for various cases: i) an absorber plate (tin metal sheet) suspended in the middle of the air channel, ii) longitudinal fins with rectangular or triangular shapes, and iii) depth or length variations of the channel. Their results showed that a collector with two glass covers provided a better heat transfer to the airflow than a single-glass collector.

Mittal and Varshney (2006) considered the use of porous media in a packed bed with blackened wire screen matrices having different geometric parameters (*i.e.* wire diameter and pitch) with two glasses (Figure 2.13). They determined the thermo-hydraulic performance of the air heater in terms of the effective efficiency based on subtracting the primary energy required to generate the power for pumping air through the packed bed from the actual thermal energy gain.

2.2.2 Double-pass Solar Collectors

In a double-pass solar collector, the absorber plate is between the cover plate and insulation layer. Air flows on both sides of the absorber plate. There are two main types of double-pass solar collectors: the parallel-pass cover-plate solar collector (Figure 2.14) and double-pass counter-flow solar collector (Figure 2.15).

The thermal performance of a SAH can be improved by enhancing the rate of heat transfer. The thermal efficiency of a double-pass SAH is higher than that of a

single-pass SAH owing to the concept of doubling the heat transfer area without increasing the system cost (Chamolia*et al*., 2012).

Minimising the heat loss from the cover definitely enhances the thermal performance of a SAH. This is why double glazing or a counter-flow (*i.e.* double pass) is used. In a double-pass SAH,

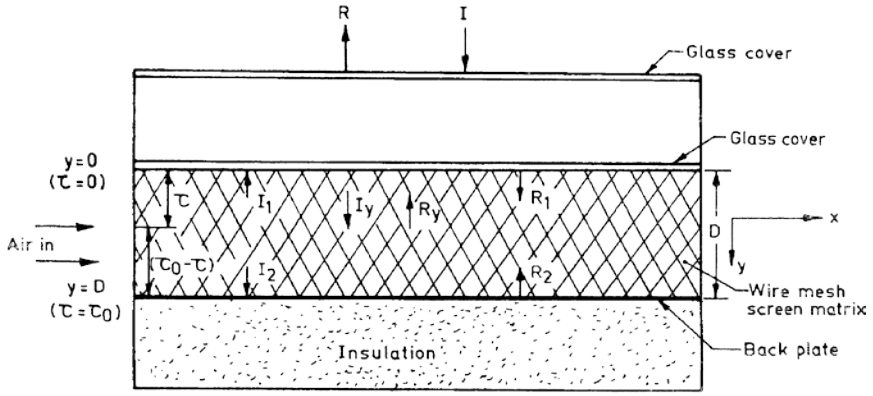

Figure 2.13: Schematic of packed bed solar air heater, Mittal and Varshney (2006).

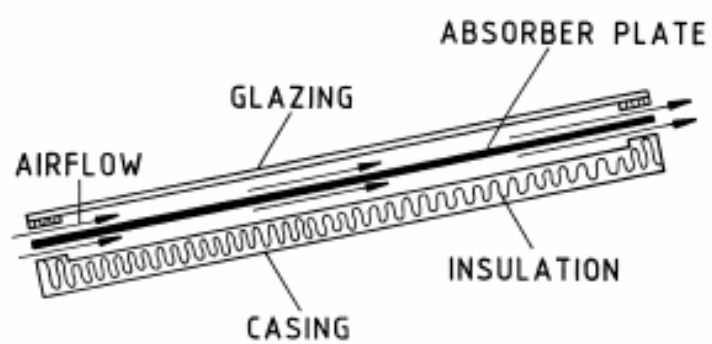

Figure 2.14: Parallel pass solar air heater (Ekenchukwu and Norton, 1999).

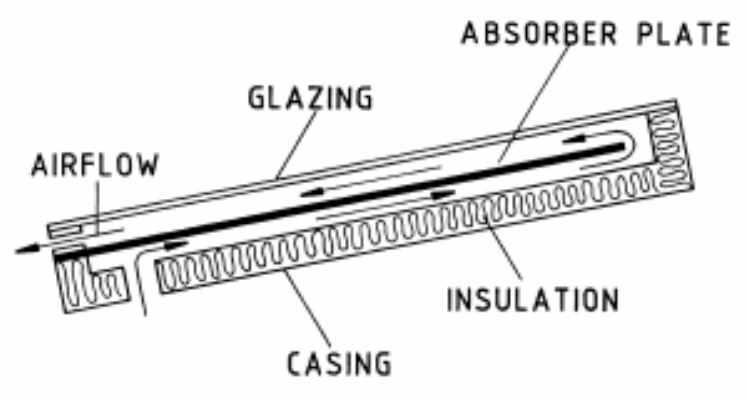

Figure 2.15: Double pass solar air heater (Ekenchukwu and Norton, 1999).

air passes through the upper channel (between the first and second glass covers) and then changes direction to pass between the second glass and bottom bed. Several research groups have suggested inserting the absorber plate mid-channel to divide the channel into two equal parts (Ramadan *et al.* 2007; El-Sebaii*et al.* 2007; Fudholi*et al.* 2013; Ramani*et al.* 2010; Yeh and Ho 2009; Youcef and Desmons 2006; Fudholi*et al.* 2011; Sopian *et al.* 2009). In this case, the air passes above and under the absorber plate in the same direction.

Alejandro and Jose (2013) developed two analytical models which describe the thermal behaviour of solar collectors: double parallel flow and double-pass counter-flow. Based on the local energy balances, they obtained algebraic expressions for the efficiency factor and overall heat loss coefficient as well as the air temperature distributions along the collectors. They also determined expressions for the mean temperatures of the two air streams and absorber plate. The model of the solar collector with a double parallel flow predicts that the mass of the airflow between the absorber plate and transparent cover is greater than that of the flow circulating through the other channel. The model for the solar collector with a double-pass

counter-flow indicates that increasing the airflow proportionally increases the percentage temperature rise of the channel.

Some researchers have suggested inserting the absorber plate between the lower glass cover (for double glazing) and bottom of the channel to divide the channel into two equal spaces. Thus, the air passes above and below the absorber plate in the same direction (Fudholi*et al.*, 2013), or the air first flows above the absorber plate fixed mid-channel and then circulates below the absorber plate (Aboul-Enein *et al.*, 2000).

Many modifications have been used to improve the coefficient of the heat transfer between the airflow and absorber plate. This can be achieved by increasing the absorber area or turbulence inside the flowing duct by inserting roughness, obstacles, and baffles (Njomo and Aguenet, 2006; Kasra and Majid, 2014; Ben Salma, 2007; Ming *et al*., 2014). Many researchers have used transverse ribs (Fudholi *et al*., 2013; Fudholi *et al*., 2011; Singh and Dhiman, 2014), fixed small wings (Ramani *et al*., 2010) or longitudinal fins (Omojaro and Aldabbagh, 2010; El-khawajah *et al*., 2011; Ben Salma, 2007; Ramadan *et al*., 2007; Fudholi *et al*., 2011;Youcef, 2005), or V-corrugated surfaces (Choudhury, 1995).

Fudholi*et al.* (2011) theoretically studied three types of counter-flow SAHs with longitudinal fins attached (I) on top, (II) on the bottom, or (III) on both the top and bottom of the flat-plate absorber of the collector. They showed that the thermal efficiency rapidly increases with both the number and height of the fins to reach maximum values of 73% for type I, 75% for type II, and 74% for type III at an airflow rate of 0.1 kg/s.

Yeh*et al.* (2002) experimentally and theoretically investigated solar collectors where an absorbing plate with fins was inserted inside the channel to divide the air passing through the collector into two equal parts. The maximum experimental efficiency was 70.8% at an airflow rate of 77.04 kg/h and solar intensity of 1100 W/m^2. Good agreement was achieved between the experimental data and theoretical solutions.

El-Sebaii*et al.* (2011) worked on theoretically and experimentally enhancing the thermal and thermo-hydraulic efficiencies of solar heaters. Their absorber plate was a sheet of copper with a finned collector dividing the upper and lower channels to have the same height of 0.05 m to form a double-pass SAH. The thermal efficiency was 55.7% at an airflow rate of 0.04 kg/s. They also investigated the effect of various airflow rates on the pressure drop.

Several groups have worked on packed bed absorbers like an aluminium foil matrix (Chiou*et al.*, 1965), porous matrix (Mohamad, 1997; Singh and Dhiman, 2014), and wire screen matrix (Omojaro and Aldabbagh, 2010; El-khawajah*et al.*, 2011) to improve the thermal performance of the solar collector. Many researchers have either experimentally or theoretically studied the effect of the packed bed on the thermal performance of a double-pass SAH.

Compared to conventional collectors, the results of packed-bed collectors have shown substantial improvement in the thermal efficiency. Mishra (2013) investigated the thermal performance of a double-pass counter-flow solar collector with porous material in the second air passage. They studied the behaviour of the solar collector with and without porous media and compared them according to

various governing parameters such as the air mass flow rate, inlet air temperature, spacing between the top cover and absorber plate, and intensity of the solar radiation. The SAH achieved a higher thermal efficiency with porous media than without. The thermal conductivity of the porous media was found to have a significant effect on the thermal performance of the SAH.

Some researchers such as Ramadan *et al.* (2007) and Singh and Dhiman (2014) inserted the packed bed above the absorber plate inside the channel. This forced the air to pass through the packed bed at the upper channel and then turn downward to pass through the second channel. Ramadan *et al.* (2007) considered a SAH with a 0.12 m gap between the lower cover and back bed. The solar collector with a packed bed of limestone or gravel in the upper channel showed a higher thermal efficiency than that without the packed bed. Other researchers put the packed bed below the absorber plate so that the air first passed through the empty upper channel and then turned downward to pass through a packed bed of gravel in the lower channel (El-Sebaii*et al.*, 2007;Elradi*et al.*, 2004).

El-Sebaii*et al.* (2007) showed that the thermal efficiency was higher with the packed upper channel than with the packed lower channel by 6.8%. In addition, they noted improvements in the thermo-hydraulic efficiency and exit air temperature of the system. The annual averages of the outlet air temperature and efficiency were 16.5 °C and 28.5% higher than those for the system without the packed bed. Yousef and Adem (2008) achieved a maximum thermal efficiency of 71.6% for a double-pass packed bed with an airflow rate of 0.04 kg/s, bed length of 1.5 m, upper channel height of 0.035 m, and lower channel height of 0.03 m.

Although using a porous medium increases the absorber area per unit volume ratio and thus the efficiency, it also increases the frictional losses. In other words, more pumping power is needed.

Bashria*et al.* (2007) studied the effect of increasing the airflow rate and channel depth on the pressure drop of the SAH. They noted that the pressure drop is a function of the airflow rate; the former increases with the latter. In addition, they found that increasing the channel depth decreases the pressure drop. Using porous media in the lower channel increased the bed efficiency. The double pass improved the efficiency over the single pass by 7%. The double flow mode with porous media was greater than the bed without porous media by 2%–3%.

The efficiency of the double-pass solar collector with fins and packed bed was found to be 7%–19% higher than that of the single-pass solar collector. The maximum efficiency of the double-pass SAH was 63.74% at 0.038 kg/s (Omojaro and Aldabbagh, 2010).

El-khawajah*et al.* (2011) improved the SAH by introducing porous media between the transverse fins along a snakelike airflow path.

Chapter 3

THERMAL ANALYSIS

This chapter explains the theoretical model of the conventional SAH in detail (Figure 3.1). The energy equation and assumptions are presented for a SAH without porous media between the absorber and the glass cover (Hsieh, 1986).

3.1 Conservation of Energy Equation

The following assumptions are usually made in applying the energy equation to the airflow in a SAH:

1. The airflow is under steady-state conditions and an ideal gas.
2. The heat capacities of the glass covers, absorber, back plate, and insulation are negligible.
3. The temperature of the passing air is constant in the y-direction and varies in the x-direction (Figure 3.1).
4. The outside convective heat transfer coefficient is constant along the length of the SAH.
5. The inside convective heat transfer coefficient is constant along the length of the SAH.
6. The thermal conductivity of the absorber plate is constant along the length of the SAH.
7. The air properties vary linearly with the temperature.
8. There is no temperature gradient across the thicknesses of the glass covers, absorber, and back plate.

3.1.1 An Energy Balance on the Absorber Plate of The Flat-Plate Solar Air Heater

The solar radiation is transmitted through the glass cover and then absorbed by the absorber plate. The absorber plate increase in temperature and transfer the heat to the airflow by convection. The passing air loses some heat to the glass covers by convection. The glass cover transfers heat to the surroundings by convection and radiation (Figure 3.1).

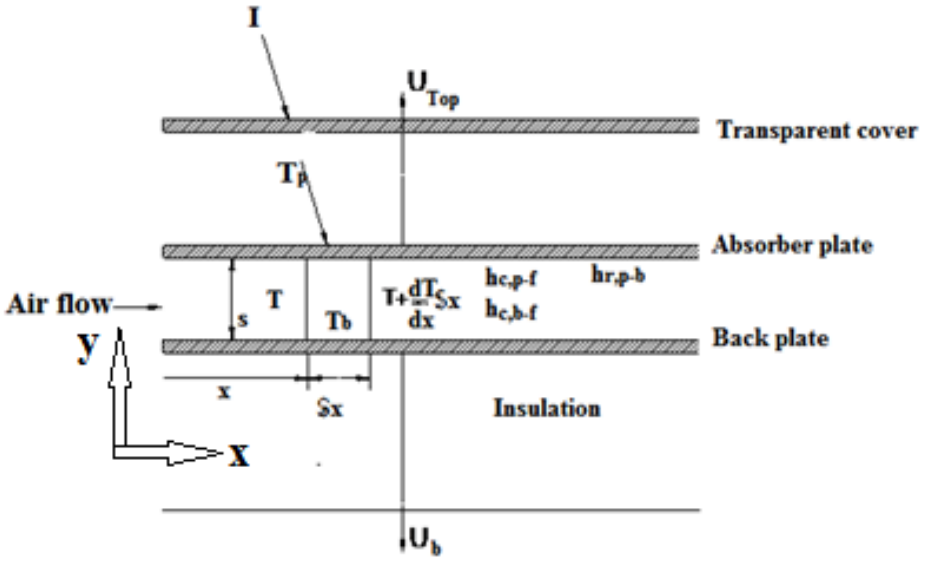

Figure 3.1: Thermal analysis of a SAH (Hsieh, 1986).

Energy balance for the absorber plate.

$$I(\tau\alpha)(\delta x) = U_{Top}(\delta x)(T_p - T_a) + h_{c,p-f}(\delta x)(T_p - T) + h_{r,p-b}(\delta x)(T_p - T_b) \quad (3.1)$$

where I is the solar intensity, $\tau\alpha$ is the transmissivity-absorptivity product of the glass cover, U_{top} is the top overall heat loss coefficient, T is the temperature of air, T_p is the temperature of absorber plate, T_a is the ambient temperature, $T_b$is the temperature of back plate, $h_{c,p-f}$ is the coefficient of the convective heat transfer

between the absorber plate and air, $h_{r,p\text{-}b}$ is the coefficient of convection heat transfer from absorber plate to the back plate.

$$h_{r,p-b} = \frac{\sigma(T_p^2 + T_b^2)(T_p + T_b)}{(1/\varepsilon_p) + (1/\varepsilon_b) - 1)} \quad (3.2)$$

where σ is the Stefan-Boltzmann constant (5.67×10^{-8} w. $m^{-2}.K^4$), ε_p and ε_b are emissivity of the absorber plate and top side of back plate, respectively.

3.1.2 An Energy Balance on the Air Stream

Energy balance for the air stream elementary volume ($s.1.\delta x$), where s is the air flow channel depth.

$$(\frac{m}{w})C_p(\frac{dT}{dx}\delta x) = h_{c,p-f}(\delta x)(T_p - T) + h_{c,b-f}(\delta x)(T_b - T) \quad (3.3)$$

where m is the airflow rate, w is the collector width, dT_f/dx is the change of air temperature along collector (x-direction), $h_{c,b\text{-}f}$ is the coefficient of the convection heat transfer between the back plate and air.

3.1.3 An Energy Balance on the Back Plate

Energy balance for the back plate of area ($1.\delta x$) gives

$$h_{r,p-b}(\delta x)(T_p - T_b) = h_{c,b-f}(\delta x)(T_b - T) + U_b(\delta x)(T_b - T_a) \quad (3.4)$$

where U_b is the coefficient of the back overall heat loss.

As $U_b << U_{top}$, we have $U_a \sim U_{top}$.

where $U_a$is the collector overall heat loss coefficient. Neglecting U_b and solving Eq. (3.4) for T_b yields

$$T_b = \frac{h_{r,p-b}T_p + h_{c,b-f}T}{h_{r,p-b} + h_{c,b-f}} \tag{3.5}$$

Substituting Eq. (3.5) in Eq. (3.1) yields

$$T_a(U_a+h)=I(\tau\alpha)+U_cT_a+ hT \tag{3.6}$$

where h is the convection heat transfer coefficient of air at $x=x$

$$h = h_{c,p-f} + \frac{1}{(1/h_{c,b-f} + 1/h_{r,p-b})} \tag{3.7}$$

Substituting Eq. (3.5) in Eq. (3.3) yields

$$hT_p = (\frac{m}{w})C_p \frac{dT}{dx} + hT \tag{3.8}$$

Combining Eq. (3.6) and Eq. (3.8) yields

$$(\frac{m}{w})C_p \frac{dT}{dx} = F'\left[I(\tau\alpha) - U_a(T - T_a)\right] \tag{3.9}$$

where F′ = collector efficiency factor

$$F' = \frac{1/U_a}{(1/U_a) + (1/h)} = \frac{h}{h + U_a} \tag{3.10}$$

Equation (3.10) is a linear differential equation of the first order. With the introduction of an integral factor of

$$\exp\left[\frac{U_aF'}{(m/w)C_p}x\right]$$

and the application of the initial condition of $T=T_{f,in}$ at x=0, the complete solution of Eq. (3.9) is given as (Hsieh, 1986).

$$T = \left(\frac{I(\tau\alpha)}{U_a} + T_a \right) - \frac{1}{U_a}\left[I(\tau\alpha) - U_a(T_{f,in} - T_a) \right] \exp\left[- \frac{U_a F'}{(m/w)C_p} x \right] \tag{3.11}$$

This is the temperature distribution equation for air in the duct. The temperature of air at outlet from the collector is obtained from Eq. (3.11) by letting $x=l$ and $A_c = wl$. Thus

$$T_{f,out} = T_{f,in} + \frac{1}{U_a}\left[I(\tau\alpha) - U_a(T_{f,in} - T_a) \right] \left[1 - \exp\left(- \frac{A_c U_a F'}{mC_p} \right) \right] \tag{3.12}$$

The useful energy gain (Q_g) by the airstream is then

$$\frac{Q_g}{w} = \left(\frac{m}{w}\right) C_p (T_{f,out} - T_{f,in}) \tag{3.13}$$

or

$$\left(\frac{Q_g}{A_c}\right) = \frac{mC_p}{A_c U_a}\left[I(\tau\alpha) - U_a(T_{f,in} - T_a) \right] \left[1 - \exp\left(- \frac{A_c U_a F'}{mC_p} \right) \right]$$

Let F_R= heat removal factor

$$F_R = \left(\frac{mC_p}{A_c U_a}\right) \left[1 - \exp\left(- \frac{A_c U_a F'}{mC_p} \right) \right] \tag{3.14}$$

It follows that

$$Q_g = A_c . F_R . [I(\tau\alpha) - U_a(T_{f,in} - T_a)] \tag{3.15}$$

The performance of a SAH can be measured in terms of the collector efficiency, which is defined as the ratio of the useful energy gain to the incident solar radiation.

$$\eta = \frac{Q_g}{A_c I} \tag{3.16}$$

As porous material is placed, the effective absorber area for convection to air will increase, so heat removal factor F_R will be greater than that given by equation (3.14) for a SAH with porous media.

3.2 Solar Air Heater Energy Losses

The solar radiation is transmitted through the glass cover and is then absorbed by the absorber plate. Most of this energy is delivered to the passing air to become useful energy. However, thermal energy can be lost to the environment transfer through the top, bottom and edge. An analysis is presented below.

The top loss coefficient U_{top} can be evaluated by considering convection and radiation losses from the porous media and baffles in the upward direction. Agarwal and Larson's (1981) empirical equation for the top loss coefficient is given by

$$U_{top} = \left[\frac{N}{(\frac{A}{T_p})\left(\frac{T_p - T_a}{N+B}\right)^{0.33}} + \frac{1}{h_w} \right]^{-1} + \left[\frac{\sigma(T_p - T_a)(T^2{}_p - T^2{}_a)}{\frac{1}{[\varepsilon_p + 0.05N(1-\varepsilon_p)]^{-1}} + \left(\frac{2N+B-1}{\varepsilon_g}\right) - N} \right] \tag{3.18}$$

where N is the number of glass covers, A=520[1-0.0044(c-90)]; c is the collector tilt angle, B=(1-0.04h_w+0.0005$h^2{}_w$)(1+0 .091N), ε_g is the emissivity of glass, h_w is the wind heat transfer coefficient. Bottom and edge have been neglected in the preceding analysis.

Chapter 4

DESCRIPTION OF EXPERIMENTAL SETUP

SAHs are the most important component of a solar energy utilisation system, as discussed in previous chapters. The air path, glass cover, and absorber plate are the main parts of a typical SAH. Active solar heating methods use an air fan to enhance the airflow and heat transfer. In the present study, some modifications were made to a conventional air heater. The path of the air flowing inside the channel was increased, and the effects of the second pass height and number of baffles on the thermal performance of the solar collector were studied. This chapter presents the construction and experimental setup of air heaters with different numbers of baffles, various bed heights, and with wire mesh layers as the absorber plate. The chapter also presents an uncertainty analysis for the mass flow rate and thermal efficiency.

4.1 Solar Air Heater with Various Arrangements

An outdoor experimental setup was developed to test SAHs (single- and double-pass with 16 wire mesh layers and baffles as well as different bed heights and numbers of baffles). Table 4.1 lists the different SAH setups. The main components in each setup were the numbers of baffles, duct of various heights, and glass or double-glass cover. Figure 4.1 shows the photo of the system, Figure 4.2 shows the assembly scheme of the single-pass SAH system, 3 baffles and wire mesh layers. Figure 4.3 shows the assembly scheme of the double-pass SAH system, 5 baffles and wire mesh layers and the assembly scheme of the double-pass SAH, 7 baffles and wire mesh layers is presented in Figure 4.4

Table 4.1: Different set-ups of the SAH.

#	**Collector**	**Number of baffles**	**Bed height (cm)**
1	Single- pass	3	3 cm
2	Single- pass	5	3 cm
3	Single- pass	7	3 cm
4	Single- pass	3	5 cm
5	Single- pass	5	5 cm
6	Single- pass	7	5 cm
7	Single- pass	3	7.5 cm
8	Single- pass	5	7.5 cm
9	Single- pass	7	7.5 cm
10	Double- pass	3	3 cm
11	Double- pass	5	3 cm
12	Double- pass	7	3 cm
13	Double- pass	3	5 cm
14	Double- pass	5	5 cm
15	Double- pass	7	5 cm
16	Double- pass	3	7.5 cm
17	Double- pass	5	7.5 cm
18	Double- pass	7	7.5 cm

Figure 4.1: Pictorial view of the experimental set up of SAH.

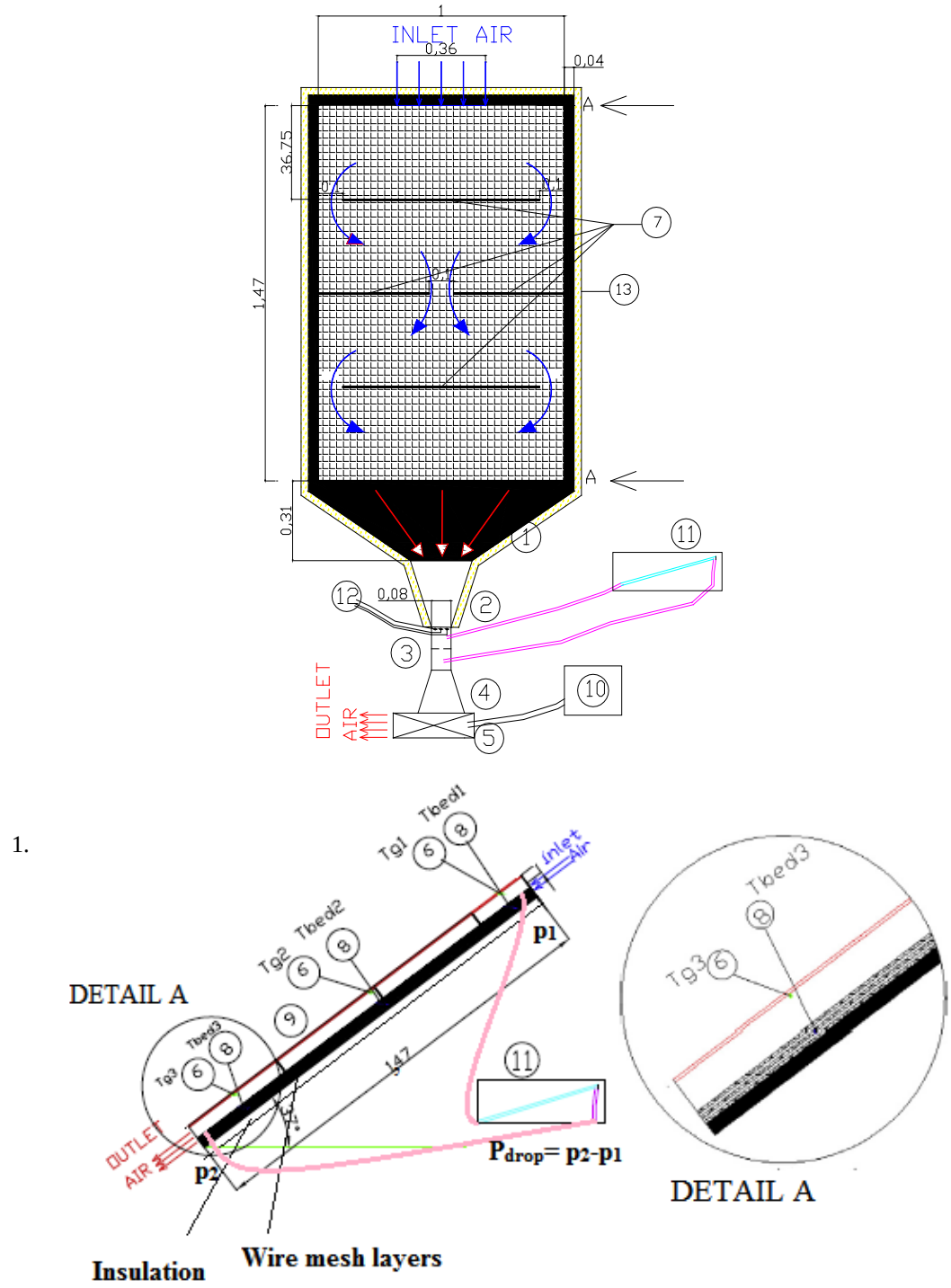

Converging section., 2. Converging duct, 3. Orifice meter, 4. Diverging duct, 5. Air blower.6. Glass thermocouples (Temperature of the airflow close to glass), 7. Baffles, 8. Bed thermocouples (Temperature of the airflow inside the bed). 9. Glass, 10. Speed controller,11. Incline manometer,12. Outlet air thermocouple.

Figure 4.2: Assembly scheme of the single-pass SAH system 3 baffles and wire mesh layers, section A-A, side view of single-pass SAH.

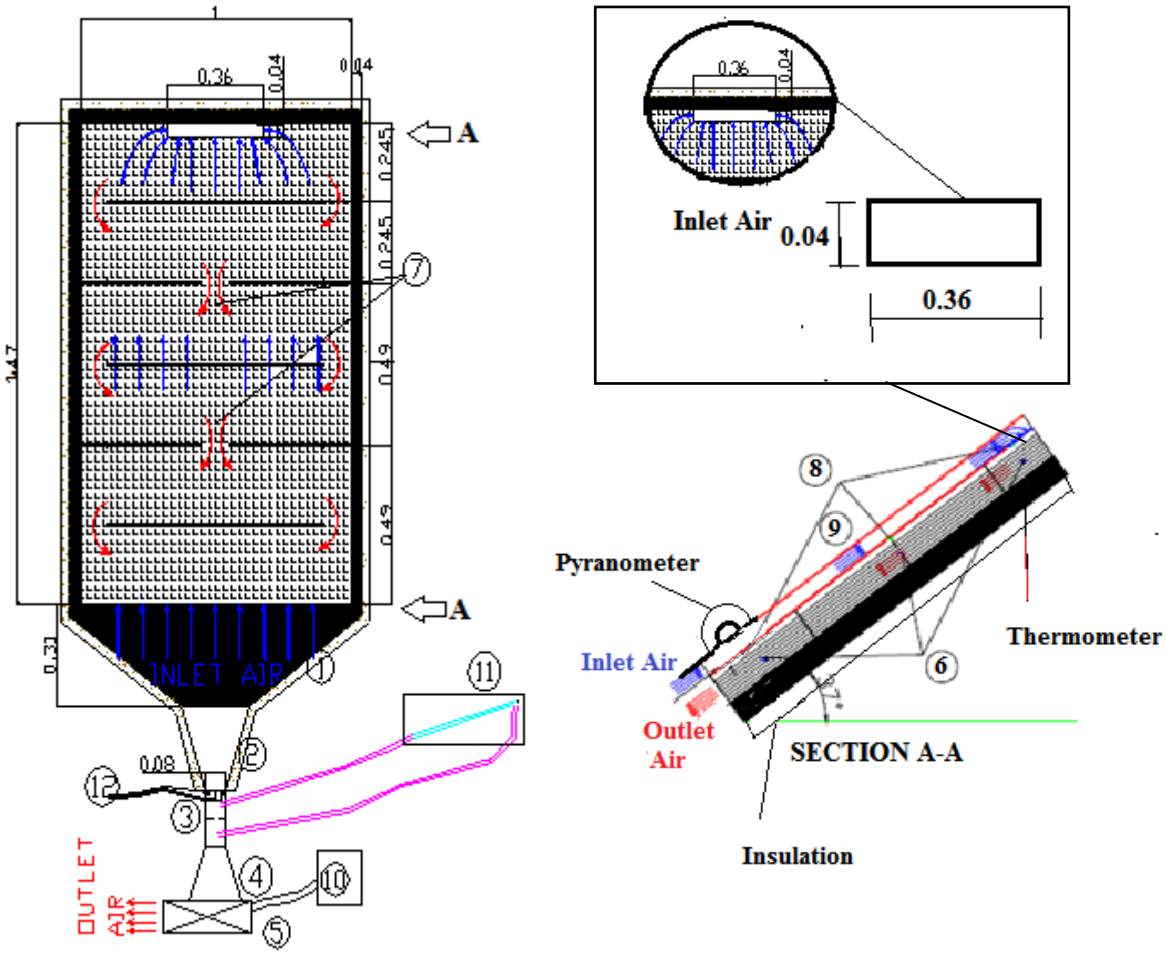

1. Converging section., 2. Converging duct, 3. Orifice meter, 4. Diverging duct, 5. Air blower.6. Glass thermocouples (Temperature of the airflow close to glass), 7. Baffles, 8. Bed thermocouples (Temperature of the airflow inside the bed). 9. Glass, 10. Speed controller,11. Incline manometer,12. Outlet air thermocouple.

Figure 4.3: Schematic assembly of the double-pass SAH, 5 baffles and wire mesh layers, section A-A, side view of double-pass SAH.

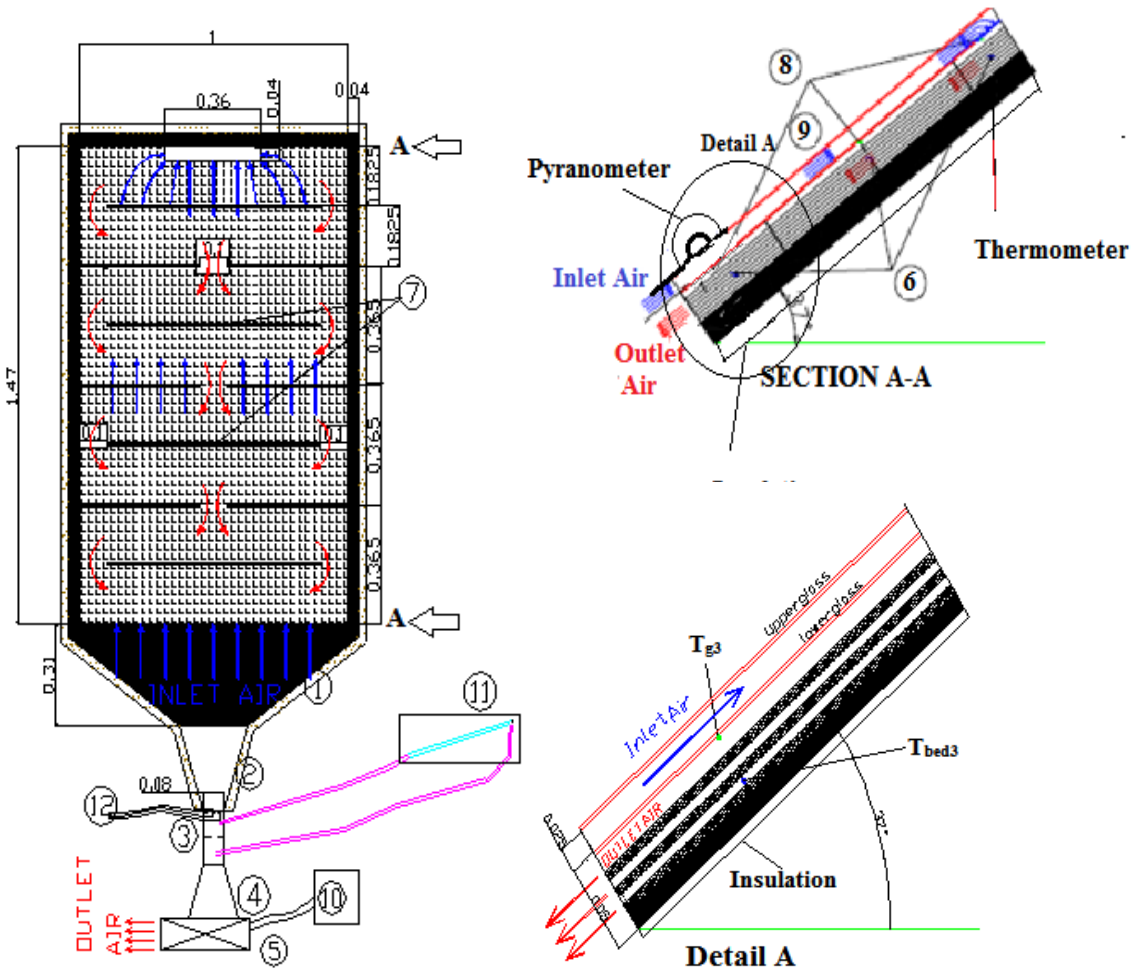

1. Converging section, 2. Converging duct, 3. Orifice meter, 4. Diverging duct, 5. Air blower.6. Glass thermocouples (Temperature of the airflow close to glass), 7. Baffles, 8. Bed thermocouples (Temperature of the airflow inside the bed). 9. Glass, 10. Speed controller,11. Incline manometer,12. Outlet air thermocouple.

Figure 4.4: Schematic assembly of the double-pass SAH, 7 baffles and wire mesh layers, section A-A, side view of double-pass SAH.

4.2. Experimental Setup

The flat-plate SAH was constructed in Famagusta, North Cyprus for the thermal efficiency experiments. A wooden collector was used with dimensions of 1.47 m × 1 m (Figure 4.2) and channel with a depth of 0.03, 0.05, or 0.075 m. There was a rectangular hole on top with dimensions of 0.36 m × 0.03 m to act as the airflow entrance. Table 4.2 presents the design and operating parameters.

Table 4.2. The basic design and operating parameters used for the experimental study.

Parameters	Value
Location of collector	Famagusta, North Cyprus
Collector slope	37^{o} degree (35.125 ^{o}N and 33.95 ^{o}E)
Collector orientation	South
Experiment Period	August 2011, August 2012 and August 2013
Length of collector	1.47 m
Width of collector	1 m
Air channel depths	0.03 m, 0.05 m, 0.075 m
Absorber	16 wire mesh layers (porosity Φ= 0.98)
Number of glazing	1 or 2
Glass thickness	4 mm
Glass covers space	25 mm
Blower power	0.62 kW centrifugal fan
Mesh layer	Absorptivity of 0.96
	Emissivity of 0.87

The wooden bed base and frame were coloured black to absorb the solar radiation and improve the efficiency. All sides of the bed were thermally insulated with Styrofoam (thickness of 20 mm) except for the top of the channel. Ordinary panes of glass with a thickness of 4 mm were used as the cover for the single- and double-pass beds. The space between the upper glass and lower glass for the double-pass collector was 0.025 m. The single-pass air collector was fabricated simply by removing the first glass on top of the collector. Sixteen wire mesh layers with square voids of 1.81 mm × 1.81 mm were used in three groups located 5 mm apart. The first and second sets each contained six wire mesh layers fixed to the bottom of the channel and set parallel to the glass cover. The third group consisted of four wire mesh layers located 5 mm above the first two groups. All of the layers, which corresponded to an overall porosity of 0.98, were painted black prior to installation. Aluminium baffles were positioned transversely along the channel to divide the bed into many equal parts. All of these baffles were painted black before insertion in the bed. These baffles were 27, 47, or 72 mm high and 3 mm thick. Some were 0.8 m long, while the others were 0.45 m long. A black slot rubber band that was 5 mm wide and 3 mm thick was used to prevent the baffles from touching the glass and prevent air from passing above them. In this manner, the air flowed along the pattern and gained heat as it passed through the channel (Figures 4.2 and 4.3). For the double-pass collector, the flow first entered from above the exit of the lower channel and passed through the upper channel. The flow then reversed direction in the lower channel prior to turning to flow from the top side to the bottom side through a 0.36 m × 0.04 m opening in the upper middle of the second glass pane (Figure 4.3). The calibrated orifice meter used to measure the airflow rate followed Holman’s design (Holman, 1989). Flow straighteners were placed before and after the orifice meter to create a uniform flow through it. These straighteners were

plastic straw tubes with a diameter of 4.6 mm and length of 20 mm. A 0.62 kW blower was joined to the discharge side, this is explained in detail in Section 4.4.2. An alcohol manometer tube set at an angle of 15° and possessed a liquid density of 803 kg/m^3, was used to measure the pressure difference across the orifice. Five airflow readings were obtained between airflows of airflow rate 0.011 and 0.032 kg/s. A speed controller, which was connected to the fan, was adjusted in order to control the speed of the fan. Two holes were made one at the inlet of the collector and one at the outlet to measure the pressure drop across the collector. The pressure drop across the collector is recorded by using the inclined alcohol manometer tube for the various flow rates.

4.3 Experimental Procedure

The ambient temperature T_{in} was recorded by using two mercury thermometers that hung underneath the bed. A calibration test confirmed an accuracy of ±0.5 °C. Nine T-type thermocouples were distributed in three groups of three thermocouples each to measure the temperatures at three locations. A calibration test confirmed an accuracy of ±0.15 °C. The first group was used to measure the average outlet air temperatures T_{out} (T_{out1}, T_{out2}, and T_{out3}) and was fixed 5 cm in front of the orifice meter. The second group was used to measure the average bed temperature T_{bed} (T_{bed1}, T_{bed2}, and T_{bed3}) and was mounted inside the wire mesh. The last group was used to measure the average glass temperature T_g (T_{g1}, T_{g2}, and T_{g3}) and was fixed on the lower side of the glass by silicon glue and adhesive tape inside the channel at three different place. T_g was the mean temperature of the air very close to the second glass. All of the measured temperatures were obtained by using digital thermometers (OMEGASAYS) with an accuracy of ±0.5 °C, as shown in Figure 4.5.

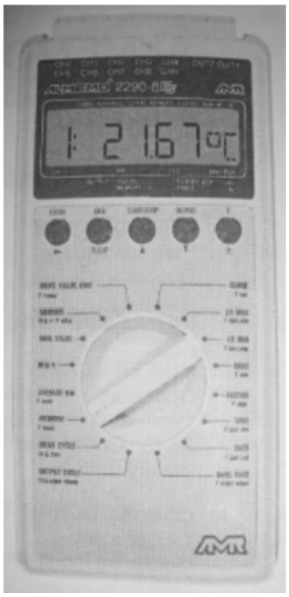

Figure 4.5: Digital thermometer (OMEGASAYS).

The solar radiation was determined by using a pyranometer located adjacent to the bed (Eppley Radiometer Pyranometer, PSP model HHM1A digital, ±0.5% accuracy over a range of 0–2800 W/m^2). This is explained in detail in Section 4.4.3. The solar heater collector was oriented facing south and tilted at an angle of 37° with respect to the horizontal. The inlet temperature T_{in} (ambient temperature), average outlet temperature T_{out}= (T_{out1}+ T_{out2}+ T_{out3})/3, average bed temperature T_{bed}= (T_{bed1}+ T_{bed2}+ T_{bed3})/3 (temperature of air passing inside the bed at three positions), average glass temperature T_g= (T_{g1}+ T_{g2}+ T_{g3})/3 (temperature of air passing very close to the glass), wind speed, relative humidity ratio, and solar radiation I were recorded every 60 min. All data were recorded from 8:00 am to 5:00 pm. The device was operated under steady-state conditions; the air was circulated for 30 min prior to the period in which the data were taken.

4.4 Measurements and Calibration of the Instruments

4.4.1 Airflow

The orifice meter was calibrated and installed between the outlet discharge duct (end of bed) and fan (Figure 4.6) to measure the volume airflow rate. The orifice

meter was designed according to Holman (1989). As shown in Figure 4.6, the orifice was a steel pipe having an outer diameter (D) of 0.16 m, inner diameter (d) of 0.08 m, and length of 0.5 m. The airflow inside the orifice meter was made uniform by fixing plastic straw tubes with a length of 20 mm and diameter of 4.6 mm at the inlet and outlet of the orifice meter. The orifice pipe was located between the converging section of the collector and inlet centrifugal fan. The blower rated at 0.62 kW and was of OBR 200 M-2K type.The volume airflow rate can be calculated as follows:

$$Q = CM.A.\left[\frac{2g_c}{\rho}\right]^{\frac{1}{2}}.[\Delta P]^{\frac{1}{2}} \qquad (4.1)$$

where Q is the volume flow rate (m^3/s), A is the area of the inner diameter d (m^2) section, CM is the flow coefficient (0.64), ρ is the density of air (kg/m^3), g_c is the specific gravitational force (1 kg m N^{-1} s^{-2}), and ΔP is the pressure difference (N/m^2).

Substituting the numerical values into equation 4.1 produces

$$Q = 0.002148\ [\Delta P]^{1/2} \qquad (4.2)$$

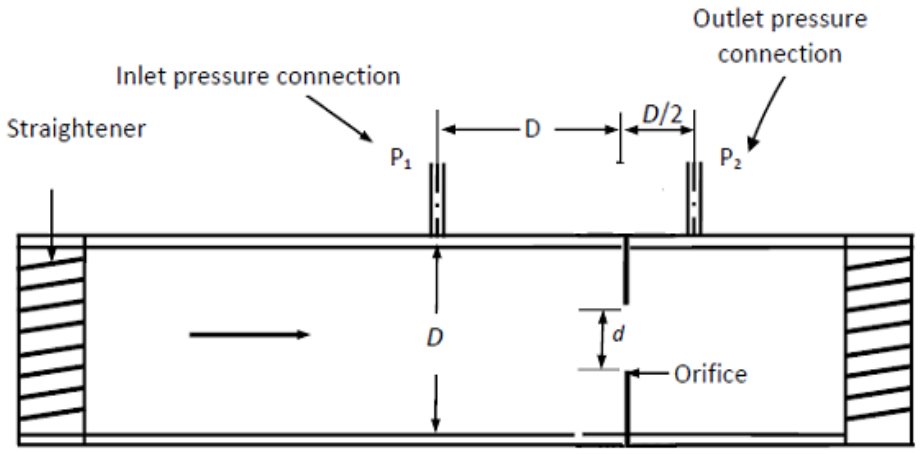

Figure 4.6: Cross sectional view of the designed orifice meter.

Figure 4.7: An Eppleypyranometer.

4.4.2 Blower

A blower was employed at the end of the collector to suck ambient air from the top side through the wire mesh layers. The blower (OBR 200 M-2K type, power of 0.62 kW) was used to enhance the required airflow velocity. Five airflow rates from 0.011 to 0.038 kg/s were used during the experemants.

4.4.3 Solar Radiation

The amount of solar radiation was determined by using a pyranometer located adjacent to the bed (Eppley Radiometer Pyranometer, PSP model HHM1A digital) with a ±0.5% accuracy over the range of 0–2800 W/m^2 (Figure 4.7). Based on the geographical location of Cyprus (33.95°E, 35.125°N), the solar heater bed was oriented south and tilted 37°withrespect to the horizontal. The pyranometerwas fixed beside the glass cover of the collector.

4.4.4 Wire Mesh Layers

Although the absorber plate is one of the major components of the SAH, increasing the absorber area definitely increases the thermal efficiency of the collector. In this

study, the absorber plate was replaced with wire mesh layers and baffles, which are much cheaper than a metal absorber plate and are readily available in the market. The use of wire mesh layers tends to substantially increase the surface area per unit volume ratio and improve the thermal efficiency of a SAH.

Sixteen steel wire mesh layers with voids of 0.181 cm× 0.181 cm and wire diameters of 0.025 cm were fixed inside the collector's duct parallel to the glazing. The wire mesh layers were arranged as follows. Six wire mesh layers were attached to each other as one matrix and placed at the bottom of the collector. Six more layers were attached to each other and placed in the middle. The last four meshes were connected to each other and located on top of the other layers. The distances between the three sets of wire meshes were fixed to 0.5 cm. Moreover, a spacing of 0.5 cm was between the second glazing and the upper layers.

The porosity of the mesh sheet Φ was calculated as the total void volume divided by the total volume occupied by the solid matrix. The value of the porosity Φ was obtained by using the wetting liquid method (Nield and Bejan, 1999). A piece of the wire screen with known dimensions was immersed in a container filled with water. After the container was shaken well, the displaced water would be equal to the volume of the solid. Subtracting the displaced water volume from the total volume of the specimen gave the volume of the voids of the wire mesh. The porosity was obtained by dividing the void volume by the volume of the bed:

$$\Phi = \frac{Volume\ of\ voids}{Total\ volume} \tag{4.3}$$

Volume of voids: (volume of wire mesh layers and volume of water container - volume of water container) - total volume of wire mesh layers (equal to the volume bed height of 3 cm).

Total volume: Volume of bed with a height of 3 cm.

4.5 Uncertainty Analysis

The errors associated with the practical measurements were obtained prior to the experiment. The uncertainty analysis for the fluid flow and thermal efficiency is presented below. The airflow rate of air passing across the bed is defined by

$$m = \rho Q \tag{4.4}$$

The fractional uncertainty (ω_m/m) for the airflow rate is given by Gill *et al.* (2012); Kalogirou (2004) and Duffie and Beckman (1991):

$$\frac{\omega_m}{m} = \left[\frac{1}{4}\left(\frac{\omega_{T_{air}}}{T_{air}} \right)^2 + \frac{1}{4}\left(\frac{\omega_{\Delta P}}{\Delta P} \right)^2 \right]^{1/2} \tag{4.5}$$

where, T_{air} is the film air temperature between the outlet and inlet,ω_{Tair} is uncertainty for the film air temperature, ΔP is the pressure difference, $\omega_{\Delta p}$ is the uncertainty for the pressure differences.

The thermal efficiency η of the solar bed is given by

$$\eta = \frac{\dot{m} C_p (T_{out} - T_{in})}{I A_c} \tag{4.6}$$

where I is the solar intensity and A_c is the area of the collector.

Because A_c is constant, if C_p is assumed to be constant for the range of working temperatures, the fractional uncertainty of the solar thermal efficiency of the bed (ω_η/η) is related to m, I, and ΔT.

The fractional uncertainty (Holman 1989; Esen 2008) is given by

$$\frac{\omega_\eta}{\eta} = \left[\left(\frac{\omega_{\dot{m}}}{\dot{m}} \right)^2 + \left(\frac{\omega_{\Delta T}}{\Delta T} \right)^2 + \left(\frac{\omega_I}{I} \right)^2 \right]^{1/2} \quad (4.7)$$

Where ω_m is the uncertainty for the airflow rate, $\omega_{\Delta T}$is the uncertainty for the temperature difference and ω_I is the uncertainty for the solar radiation.

The performance was investigated for different numbers of fins and airflow rates, and the results were averaged for each day to obtain the fractional uncertainty. Table 4.3 indicates the mean average values of the variables T_{out}, T_{in}, ΔT, T_{air}, m, η, and I for all days along with the fractional uncertainties of the airflow rate and efficiency.

Table 4.3: The mean average value for single and double- pass SAH.

Case	Height of bed (cm)	Mean Average							ω_m %	$\omega\eta$ %
		ΔT ^oC	T_{in} ^oC	T_{out} ^oC	T_{air} ^oC	m (kg/s)	I (w/m^2)	η (%)		
SPSAH	3	21.69	33.72	55.41	44.57	0.022	699.30	42.57	0.35	0.92
	5	19.2	33.07	52.27	42.67	0.021	729.00	41.62	0.34	0.92
	7.5	18.10	33.70	51.80	42.75	0.027	727.65	39.20	0.34	0.91
DPSAH	3	23.80	34.92	58.70	46.81	0.024	687.57	48.62	0.13	0.72
	5	22.50	34.80	57.30	42.94	0.025	711.97	47.34	0.15	0.73
	7.5	21.70	34.30	56.00	45.15	0.027	717.15	45.00	0.15	0.73

Chapter 5

RESULTS AND DISCUSSION

5.1 Heat Flux and Inlet Temperature

In general, the solar intensity values followed a similar pattern for all of the days of the experiments. The solar intensity increased from morning until midday, at which point it reached the maximum value, and then slowly decreased until sunset. The ranges of the solar intensity for each experiment were close to each other. Figure 5.1 shows the hourly variation in the measured solar intensity for the single- and double-pass SAHs with airflow rates of 0.011–0.032 kg/s. The peak value of the solar intensity I between 12:00 and 1:00 pm was 1081 W/m^2 for the single-pass SAH and 1005 W/m^2 for the double-pass SAH. However, the solar radiation and inlet temperature reached their maximum values at noon (Figure 5.2). The maximum inlet temperature T_{in} between 12:00 and 1:00 pm was 37and 36.9 °C for the single- and double-pass SAHs, respectively. The inlet temperature depended on the environmental state. The fluctuations during some days were caused by the wind speed. The wind speed was an important factor that affected the inlet temperature and humidity ratio.

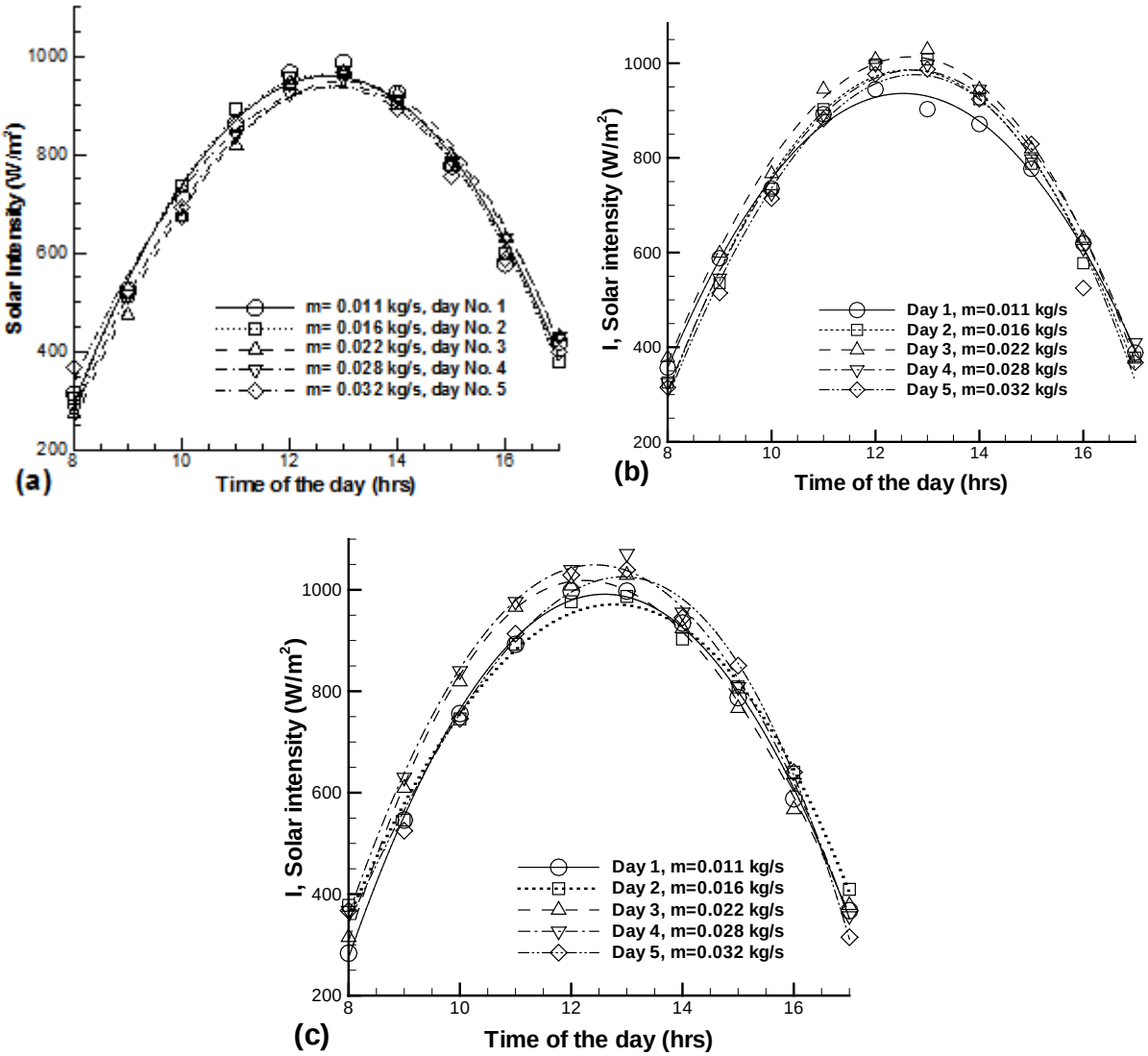

Figure 5.1: Solar intensity versus time of the day for double- pass SAH, during testing of the SAHs having (a) 3 baffles (b) 5 baffles and (c) 7 baffles, with7.5 cm bed height.

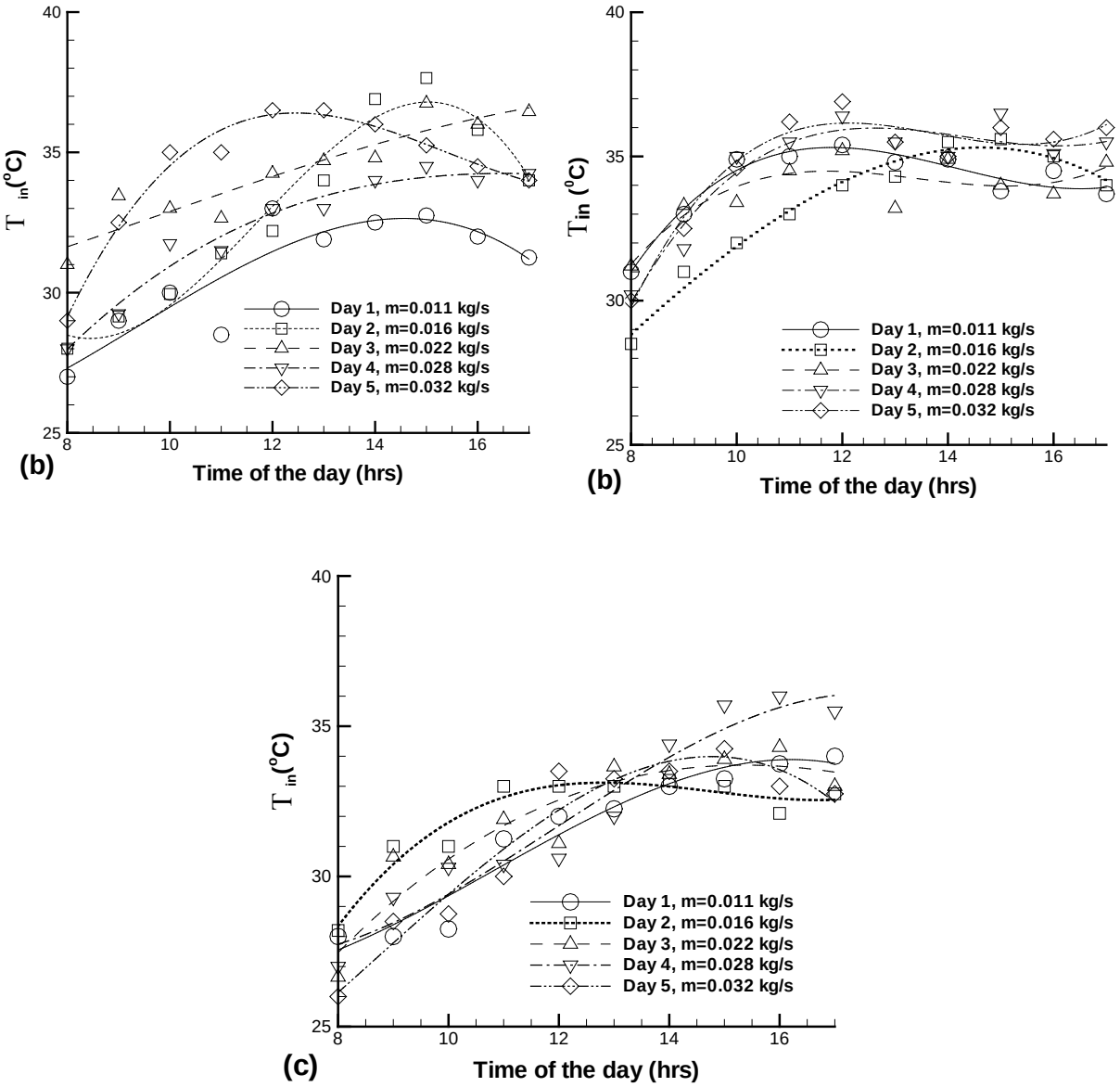

Figure 5.2: Inlet temperature versus time of the day for: (a) 3 baffles (b) 5 baffles and (c) 7 baffles, for double- pass SAH, with 7.5 cm bed height.

5.2 Temperature Differences between the Outlet and Inlet Temperatures (ΔT)

Figures 5.3–5.5 show the temperature differences (average outlet temperature - inlet temperature) for single- and double-pass SAHs with a bed height of 3 cm and airflow rate of 0.011–0.032 kg/s with the time of day. For all airflow rates, the temperature difference ($\Delta T = T_{out} - T_{in}$) increased from the morning to reach its maximum at noon and then slowly decreased from 1:00 pm to the end of the day at 5:00 pm in a similar manner as the solar radiation. For all curves, ΔT increased to reach its maximum value at noon and then decreased at the end of day (similar manner as the solar radiation). In addition, ΔT was greater for the double-pass SAH than for the single-pass SAH at the same airflow rate. In the case of the double-pass SAH, the inlet air was preheated in the upper channel before entering the bed, which caused ΔT to increase. Figures 5.6 and 5.7 show the temperature difference ($\Delta T = T_{in} - T_{out}$) with the time of day for different airflow rates of the SAHs with a bed height of 5 cm. The maximum values of ΔT with three, five, and seven baffles were 39, 39.8, and 44.7 °C, respectively, for the single-pass SAH and 45, 48.3, and 51 °C, respectively, for the double-pass SAH.

Figures 5.8–5.10 show the temperature difference ΔT for the SAHs with a bed height of 7.5 cm. The maximum ΔT was 49.8 °C for the double-pass SAH with seven baffles at 1:00 PM. This is less than ΔT for the bed heights of 3 and 5 cm which is given above. The graphs clearly show that ΔT decreased as the bed height increased. Decreasing the bed height reduced the cross-sectional area of the bed, which increased the airflow velocity through the bed and convection heat transfer ratebetween the porous media and passing air. At the same airflow rate, ΔT

increased with the number of baffles, as shown in Figure 5.11. The maximum value of ΔT was 54 °C at a solar intensity of 953 W/m^2, airflow rate of 0.011 kg/s, bed height of 3 cm, and seven baffles. Increasing the number of baffles increased the airflow path through the bed, which increased the air velocity and convection heat transfer rate between the porous media and passing air). Figure 5.12 shows the effect of the solar intensity and temperature difference on the single-pass SAH with a bed height of 5 cm. There was a very strong correlation between the temperature difference and solar intensity; the temperature difference increased similarly to the solar intensity. Figure 5.13 shows the relation between T_{in} and T_{out} for the single- and double-pass SAHs with a bed height of 5 cm. The outlet temperature increased with the inlet temperature. Table 5.1 and Figure 5.14 present the maximum temperature differences of the SAHs with different bed heights and numbers of baffles at an airflow rate of 0.011 kg/s. When the new design results were compared with the previously published data presented earlier in the introduction, the former showed an enhancement in the heat transfer performance. Fudholi*et al.* (2011) obtained the highest ΔT of 42 °C with 49 baffles and a bed area of 2.4 m × 1 m at m = 0.02 kg/s and I = 700 W/m^2. Aldabbagh*et al.* (2010) obtained a maximum ΔT of 38.8 °C for a double-pass SAH at 13:00 for an airflow rate of 0.012 kg/s and absorber area of 1.5 m × 1 m. Sopian*et al.* (2009) numerically investigated a double-pass SAH with porous media and achieved ΔT = 20 °C at a solar intensity of 480 W/m^2, airflow rate of 0.037 kg/s, and bed area of 1.2 m × 2.2m.

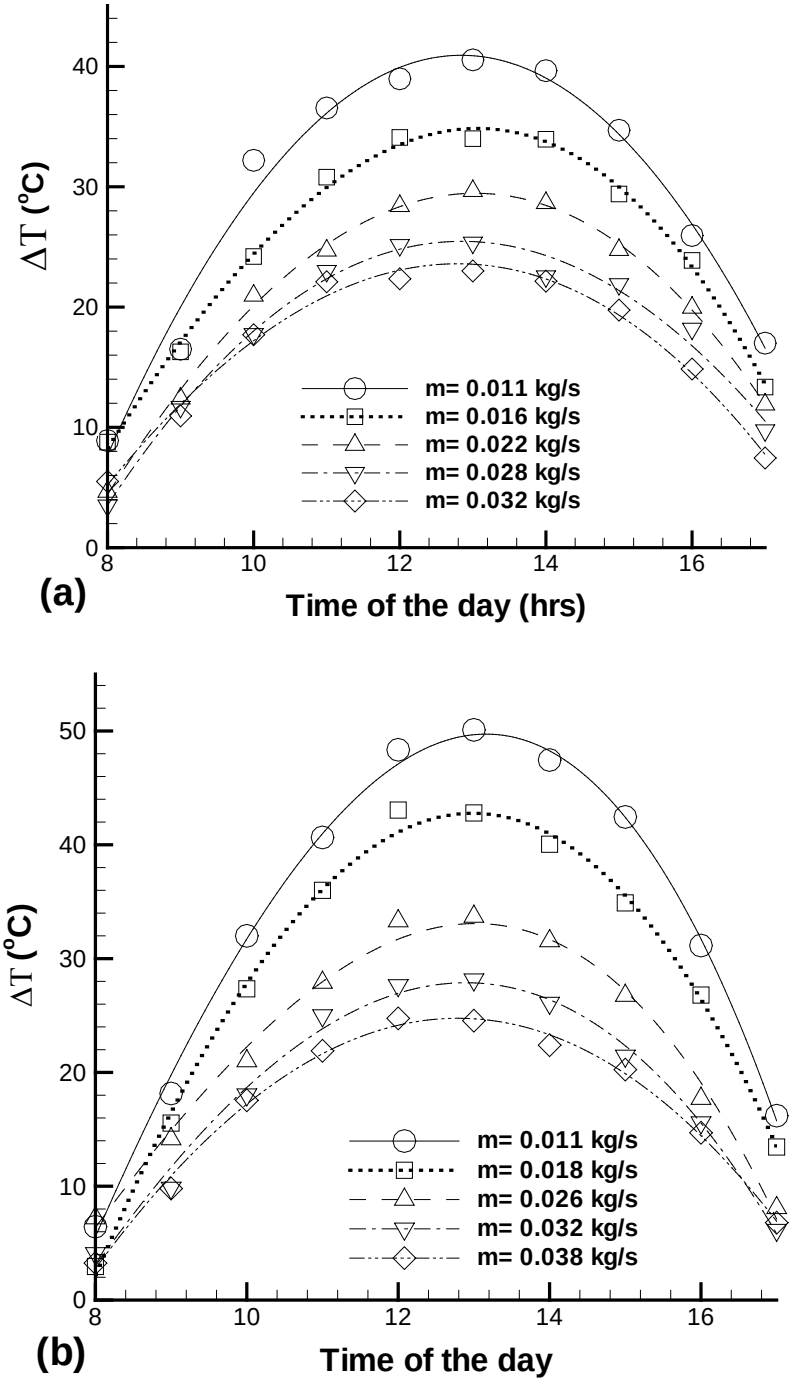

Figure 5.3: Temperature difference versus time of the day at different mass flow rates: (a) Single- pass SAH, (b) Double- pass SAH, 3 baffles, 3cm bed height.

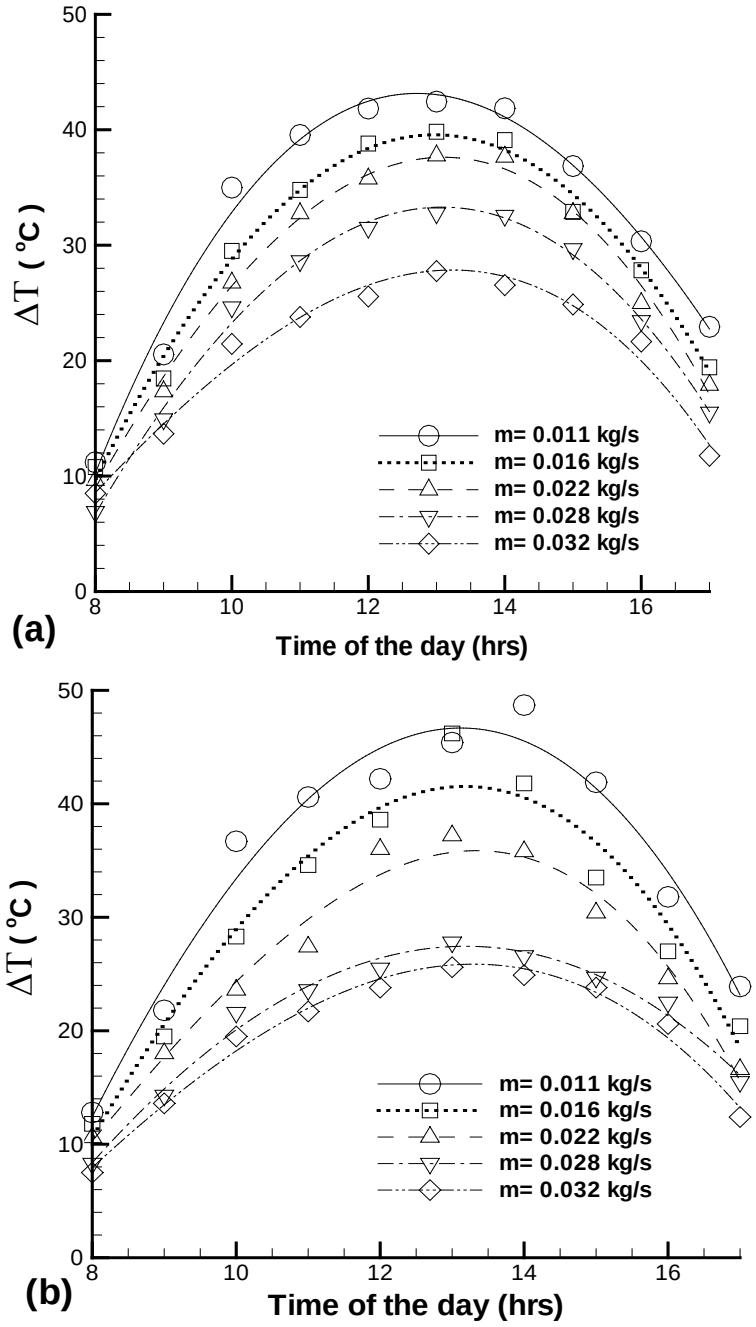

Figure 5.4: Temperature difference versus standard local time of the day at different mass flow rates: (a) Single- pass SAH, (b) Double- pass SAH, 5 baffles, 3cm bed height.

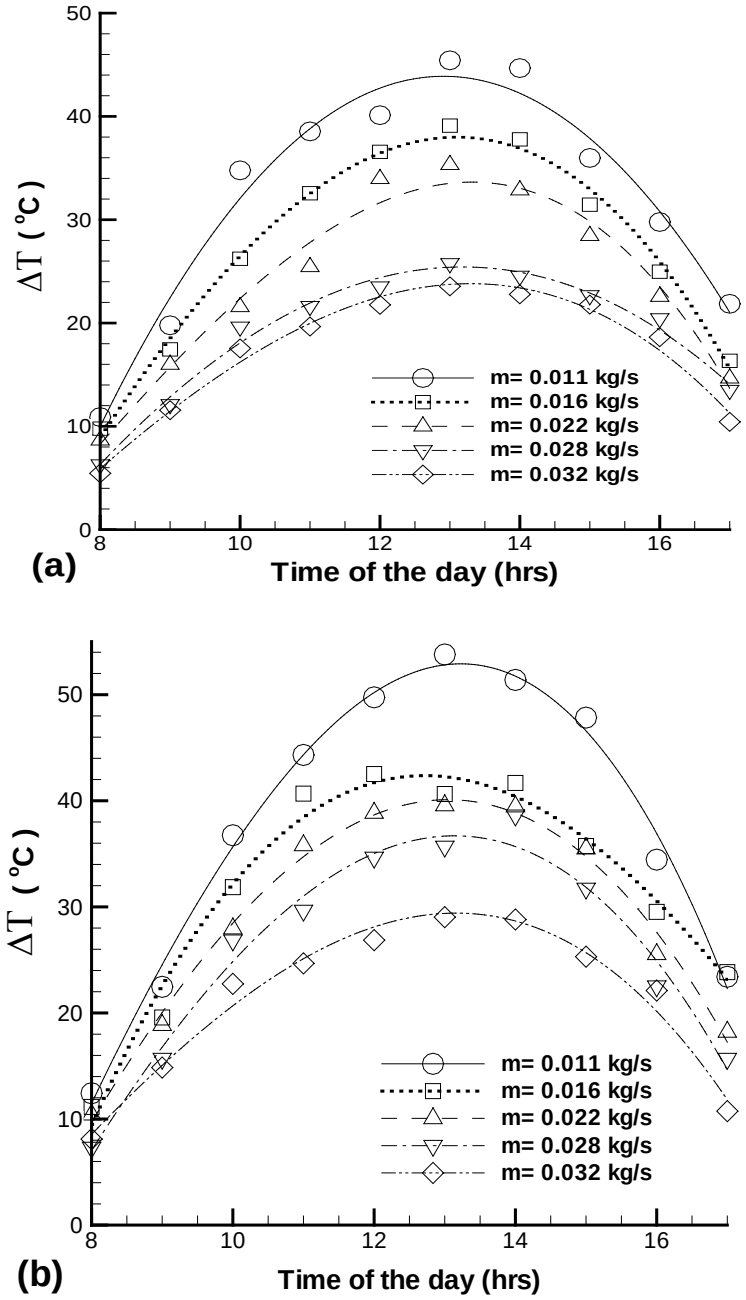

Figure 5.5: Temperature difference versus standard local time of the day at different mass flow rates: (a) Single- pass SAH, (b) Double- pass SAH, 7 baffles, 3cm bed height.

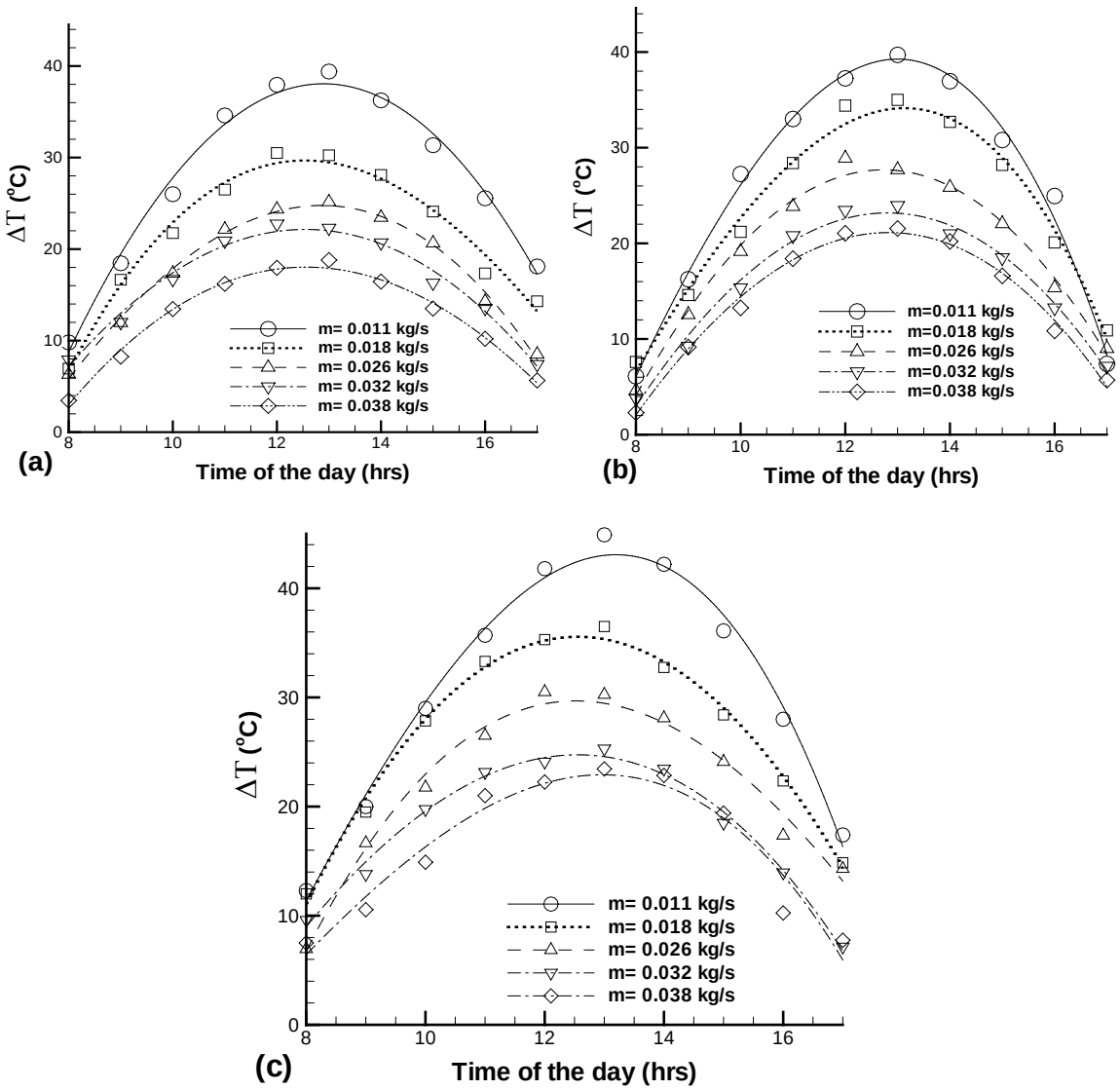

Figure 5.6: Temperature difference versus standard local time of the day at different mass flow rates : (a) 3 baffles (b) 5 baffles and (c) 7 baffles, for single- pass SAH, 5cm bed height.

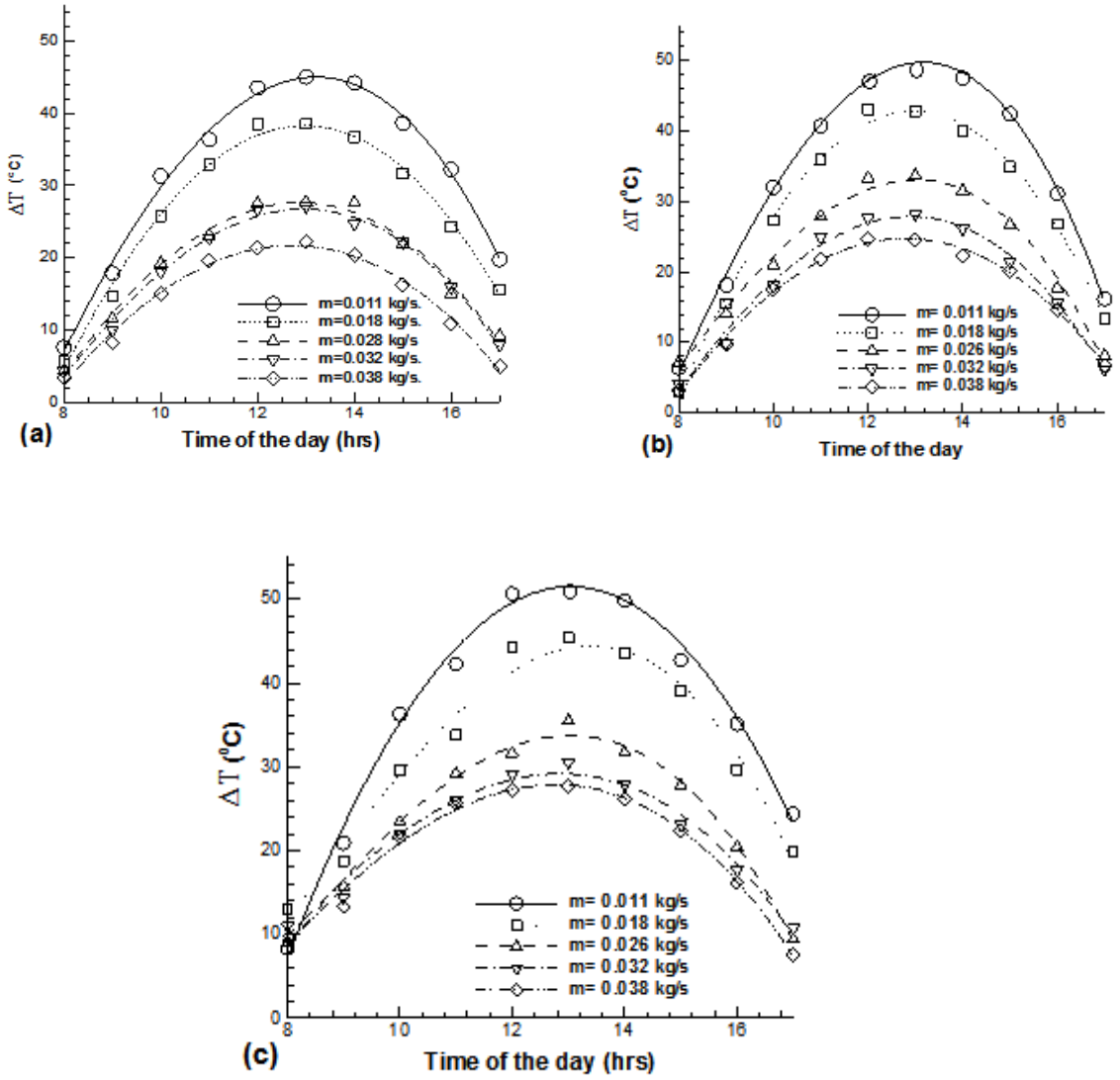

Figure 5.7: Temperature difference versus standard local time of the day at different mass flow rates: (a) 3 baffles (b) 5 baffles and (c) 7 baffles, for double- pass SAH, 5cm bed height.

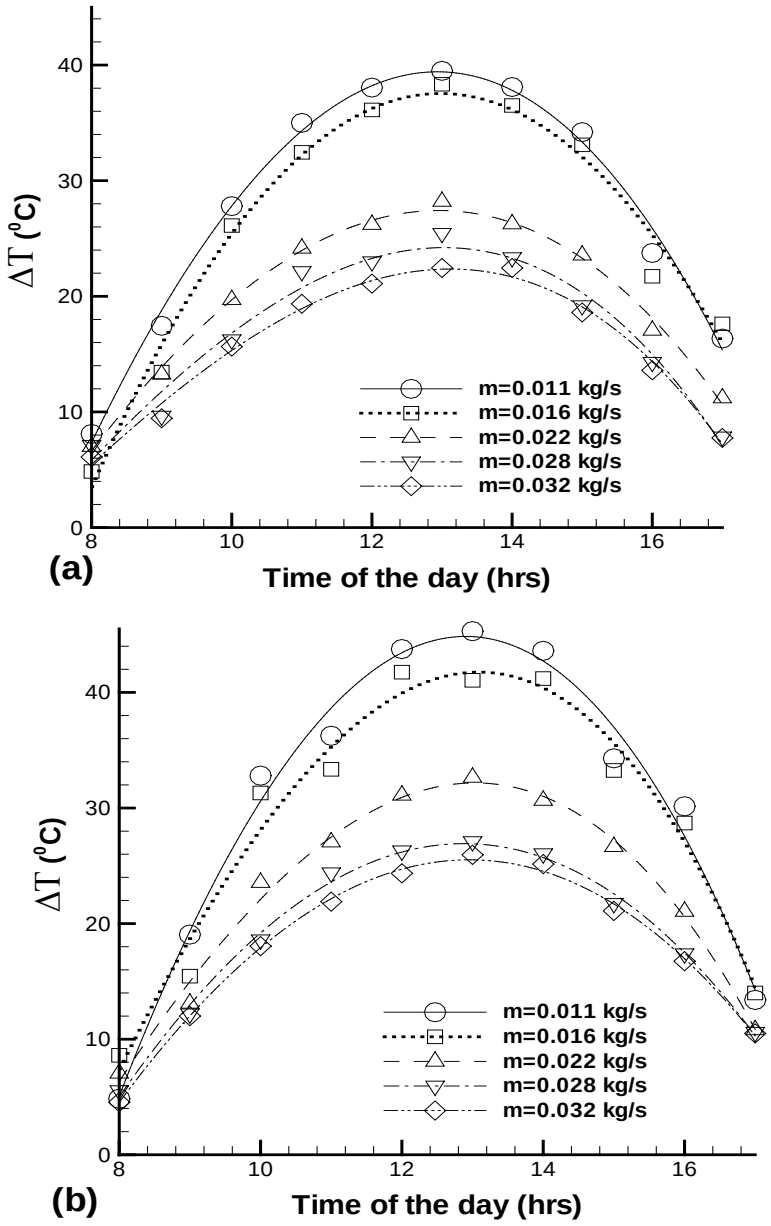

Figure 5.8: Temperature difference versus standard local time of the day at different mass flow rates: (a) Single- pass SAH, (b) Double- pass SAH, 3 baffles, 7.5cm bed height.

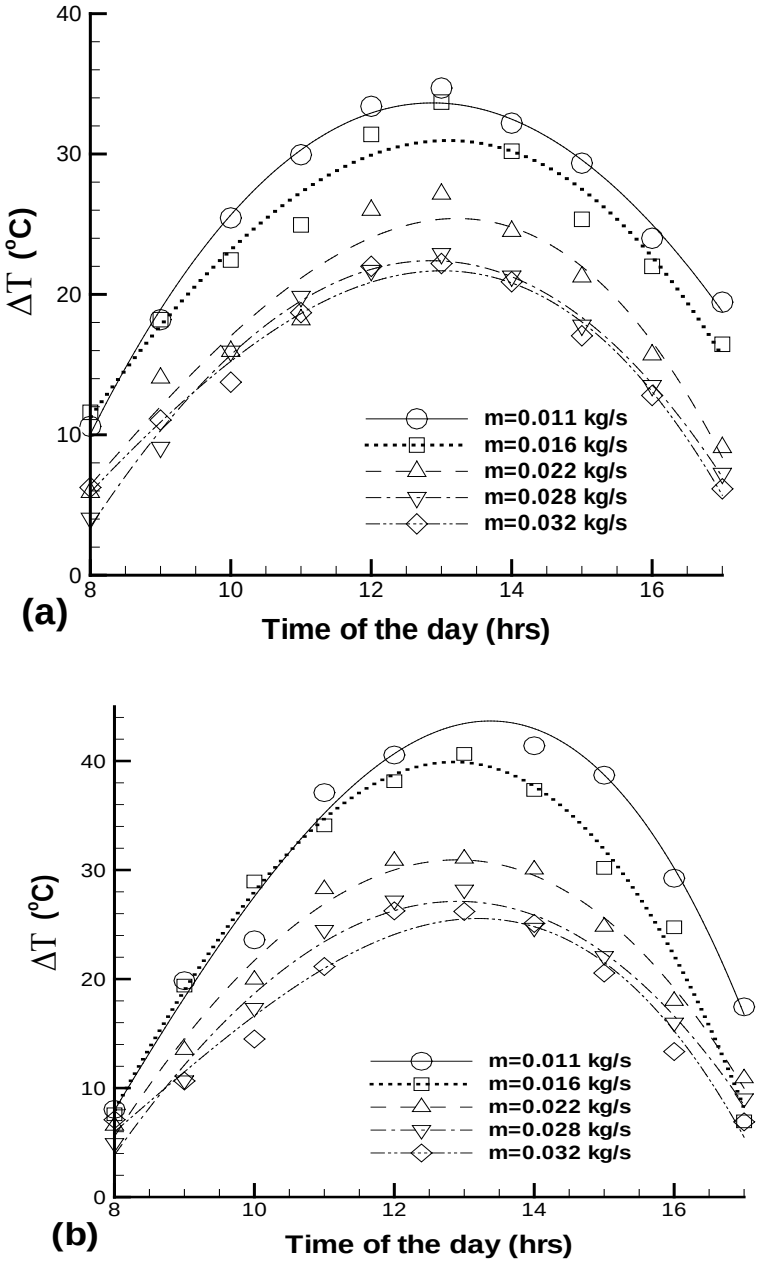

Figure 5.9: Temperature difference versus standard local time of the day at different mass flow rates: (a) Single- pass SAH, (b) Double- pass SAH, 5 baffles, 7.5cm bed height.

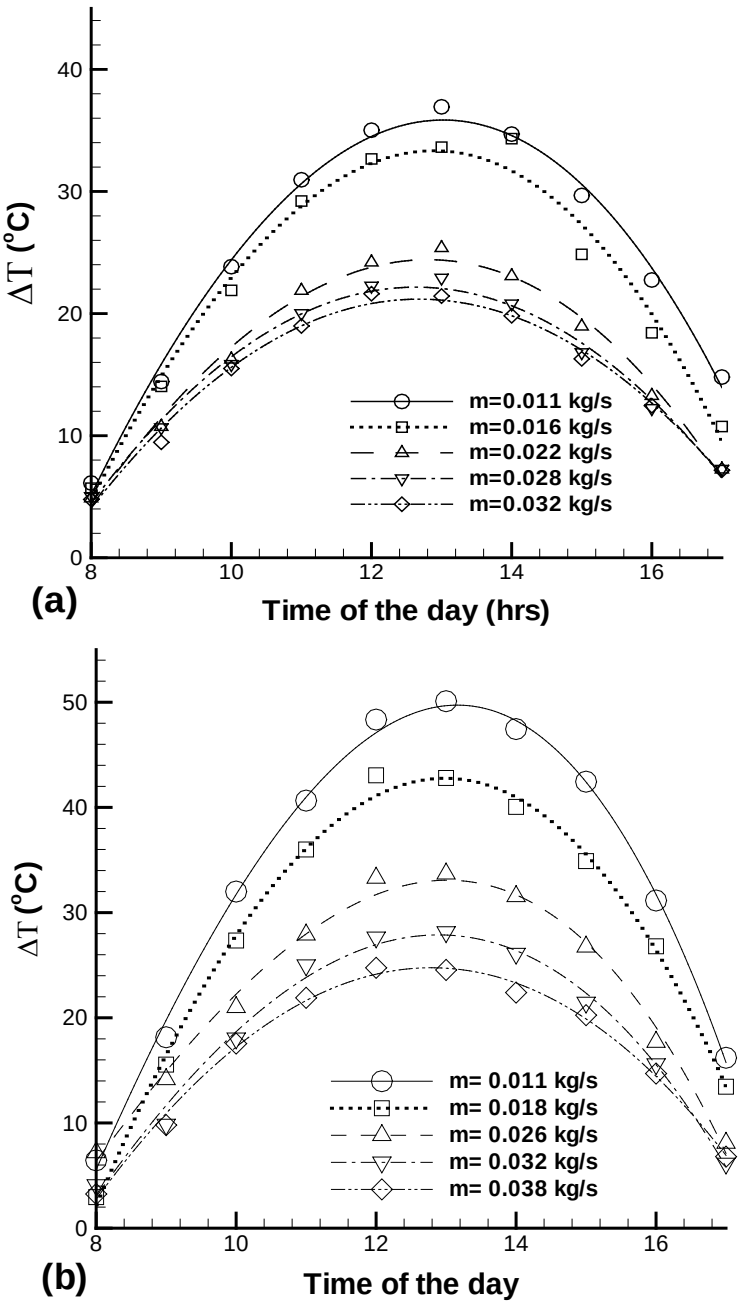

Figure 5.10: Temperature difference versus standard local time of the day at different mass flow rates: (a) Single- pass SAH, (b) Double- pass SAH, 7 baffles, 7.5cm bed height.

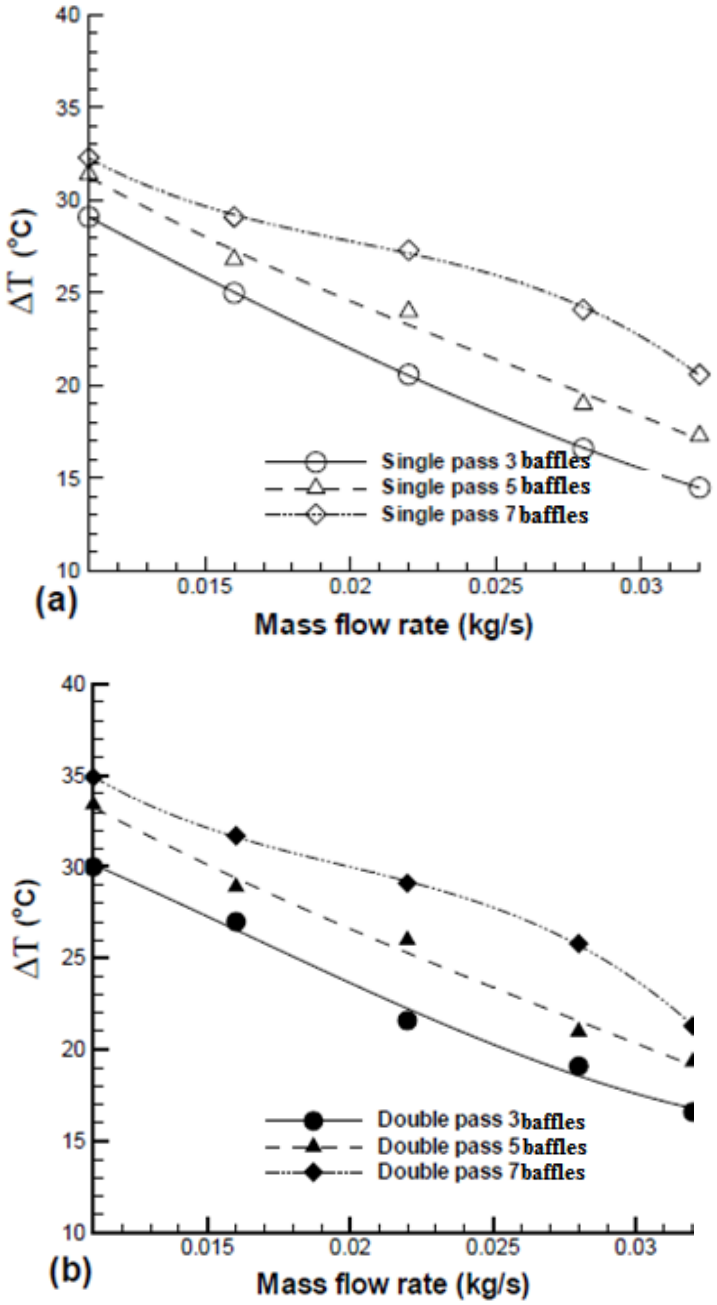

Figure 5.11: Effect of number of baffles (3, 5 and 7) on the temperature difference at different mass flow rates: a) Single- pass SAH, b) Double- pass SAH, 5cm height of bed.

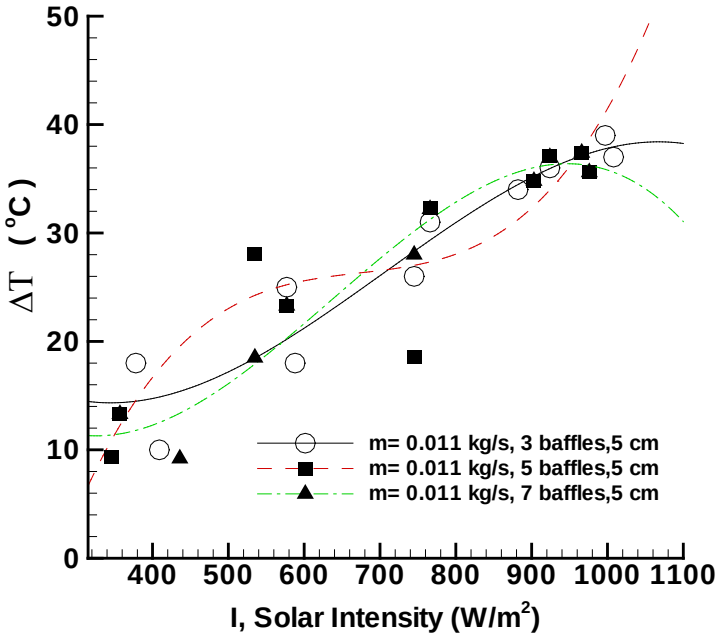

Figure 5.12: Temperature difference versus solar intensity at 0.011kg/s airflow rate for single- pass SAH with 5 cm bed height.

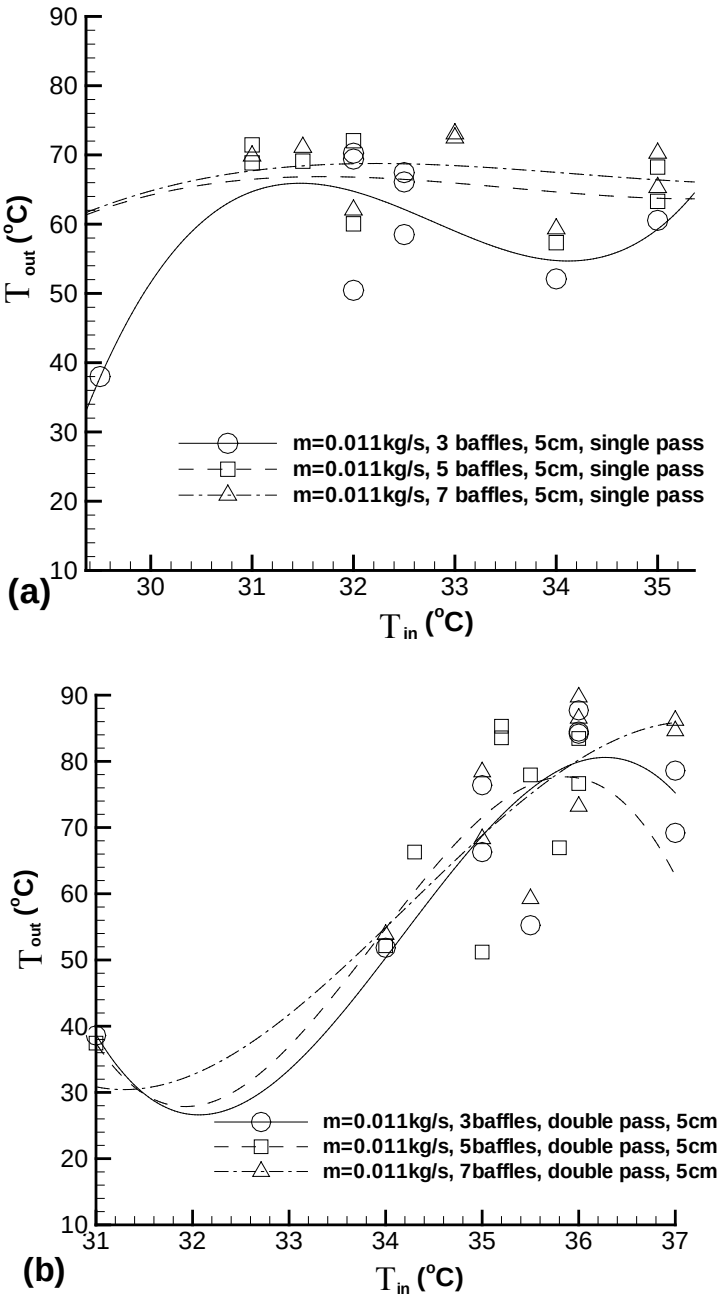

Figure 5.13: Outlet temperature versus Inlet temperature for: a) Single- pass SAH, b) Double- pass SAH with 5cm bed height.

Table 5.1: Maximum temperature differences of the solar air heater with different height of collectors and number of baffles at minimum airflow rate 0.011 kg/s.

#	Number of baffles	Bed height (cm)	Max. ΔT, single pass, ^{0}C	Max. ΔT, double pass, ^{0}C
1	3	3 cm	40.4	45.7
2	5	3 cm	42.3	48.7
3	7	3 cm	45.6	54
4	3	5 cm	39	45
5	5	5 cm	39.8	48.3
6	7	5 cm	44.7	51
7	3	7.5 cm	39.7	44.3
8	5	7.5 cm	34.4	45
9	7	7.5 cm	36.3	49.8

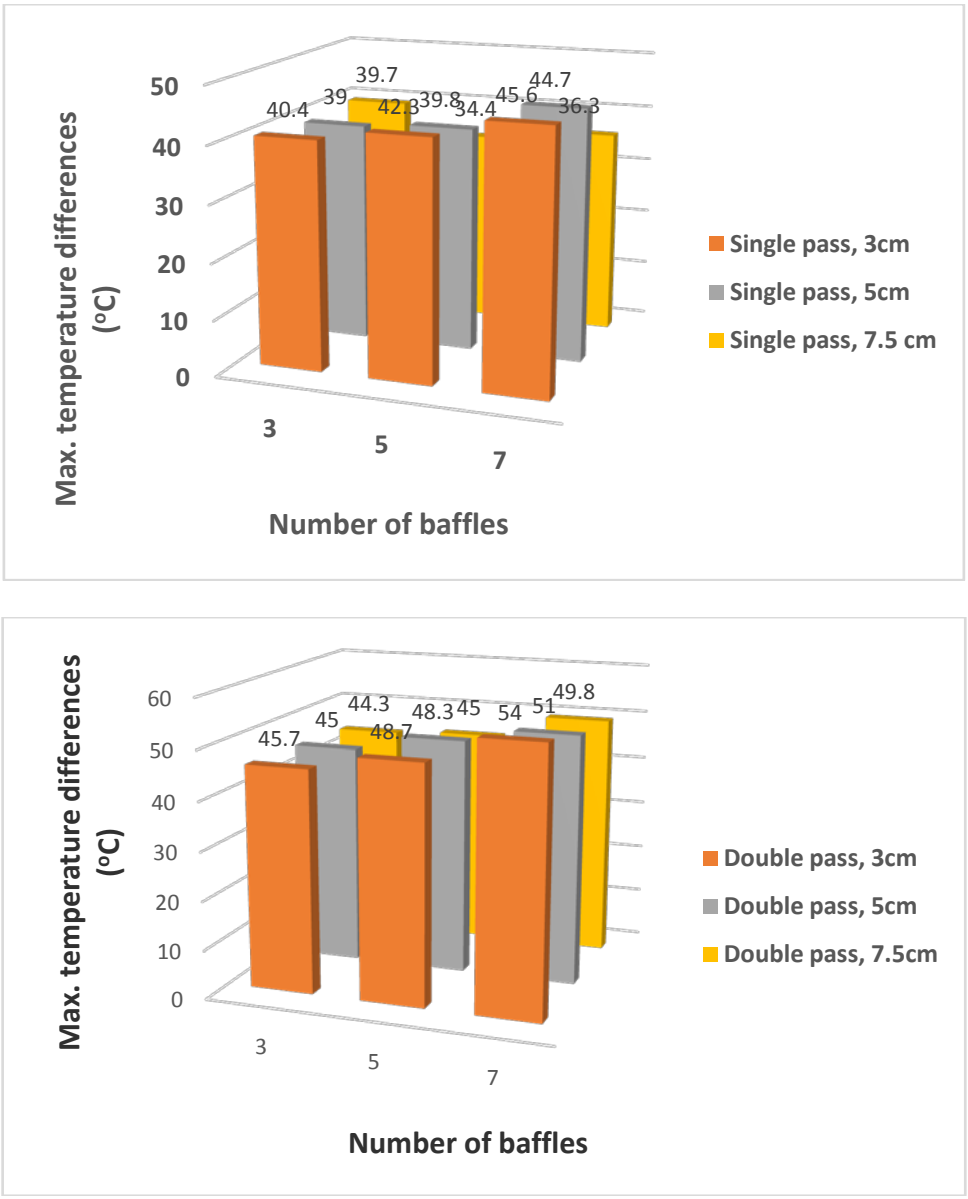

Figure 5.14: Maximum temperature differences of the solar air heater with different height of collectors and number of baffles, as 3D columns.

5.3 Temperature Differences of Bed ΔT_{bed} and Glass ΔT_g

Figures 5.15 and 5.16 show the variation in the bed temperature difference $\Delta T_{bed} = T_{bed} - T_{in}$ and glass temperature difference $\Delta T_g = T_g - T_{in}$ with the time of day for the single- and double-pass SAHs with three longitudinal baffles. The maximum value of ΔT_{bed} was 62.3 °C for the double-pass SAH with a 3 cm bed height and seven longitudinal baffles. The maximum ΔT_g was 46.3 °C for the double-pass SAH with a 3 cm bed height and seven longitudinal baffles. The bed temperature difference ΔT_{bed} and glass temperature difference ΔT_g were greater for the double-pass SAH than for the single-pass SAH, as shown in Figures 5.17 and 5.18. For the double-pass SAH, the counter-flow meant that the air was preheated in the upper channel before it turned down to enter the lower channel through the 36 cm × 4 cm opening in the second glass and flow in the reverse direction. Note that the temperatures of the bed and glass were averaged from the measurements of the three thermocouples at three different positions, as described in Chapter 4.

As shown in Figure 5.19 a and Figure 5.19 b, the curve of outlet temperature difference ΔT and the curve of bed temperature difference ΔT_{bed} were found to converge (the curve of ΔT close to to the curve of ΔT_{bed}) for the single- and double-pass SAHs. The small difference between the bed temperature difference ΔT_{bed} and temperature difference ΔT is strong evidence for the strong heat transfer from the wire mesh layers acting as an absorber plate to the airflow. The outlet temperature difference ΔT was closer to the bed temperature difference ΔT_{bed} in the single-pass SAH than in the double-pass SAH. This is because, with the double-pass SAH, there was a high radiative heat transfer between the wire mesh layers and second glass. Thus, the outlet temperature difference ΔT was closer to the glass temperature difference ΔT_g than the bed temperature difference ΔT_{bed}.

Increasing the number of baffles increased the airflow path through the bed, which increased the heat absorbed by the airflow from the porous media, as shown in Figures 5.20 and 5.21. In addition, ΔT_g increased as the airflow rate was decreased from 0.032 to 0.011 kg/s, the time that the air took to move from the inlet section of the collector to the end of the collector was increased. Hence, the air carried more heat from the porous media, which increased ΔT_g temperature.

Table 5.2 shows the maximum bed temperatures differences and glass temperatures differences of the SAH with different height of collectors and number of baffles at airflow rate 0.011 kg/s.

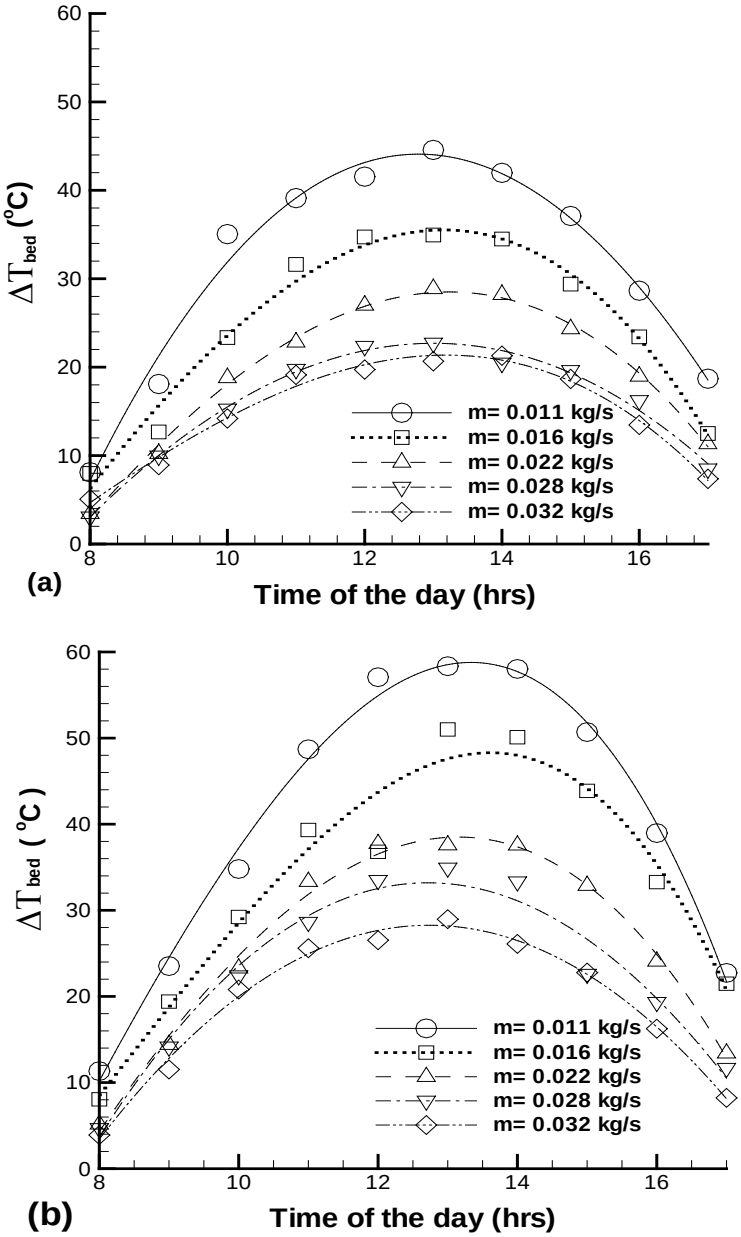

Figure 5.15: Bed temperature difference versus standard local time of the day at different mass flow rates for: (a) single- pass SAH, (b) double- pass SAH, 3 baffles and 3cm bed height.

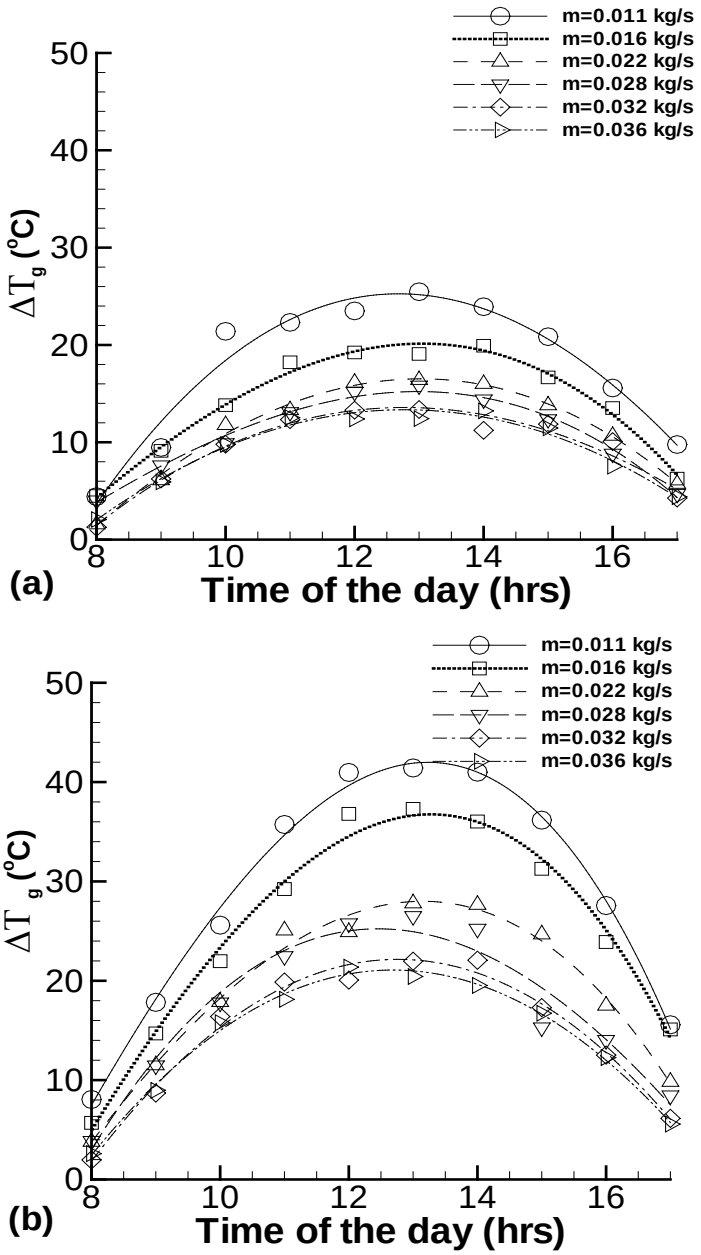

Figure 5.16: Glass temperature difference versus standard local time of the day at different mass flow rates for: (a) single- pass SAH, (b) double- pass SAH, 3 baffles and 3cm bed height.

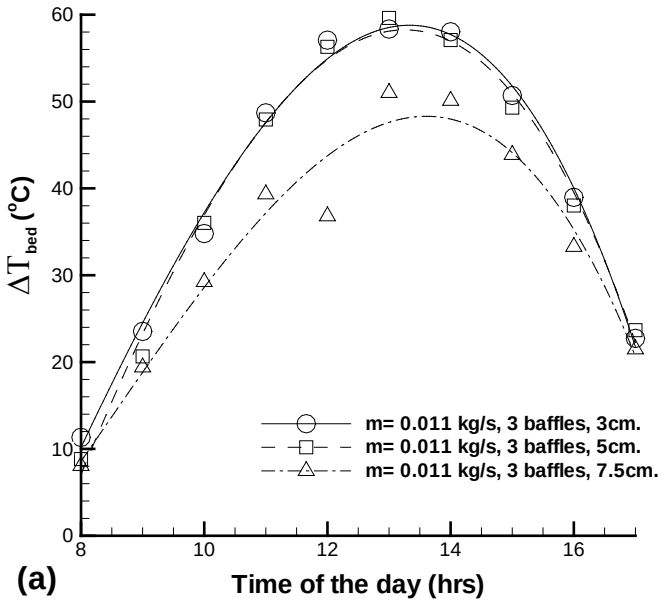

Figure 5.17: Bed temperature difference versus standard local time of the day at airflow rates 0.011 kg/s for double- pass SAH, 3 baffles.

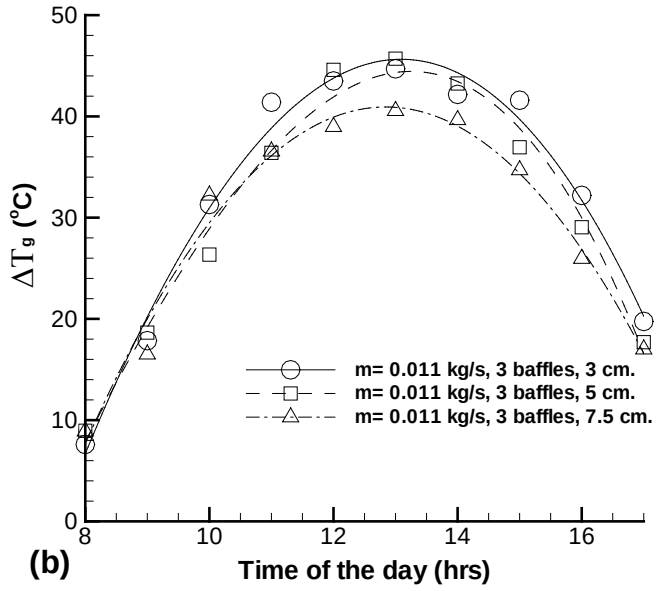

Figure 5.18: Glass temperature difference versus standard local time of the day at airflow rates 0.011 kg/s for double- pass SAH, 3 baffles.

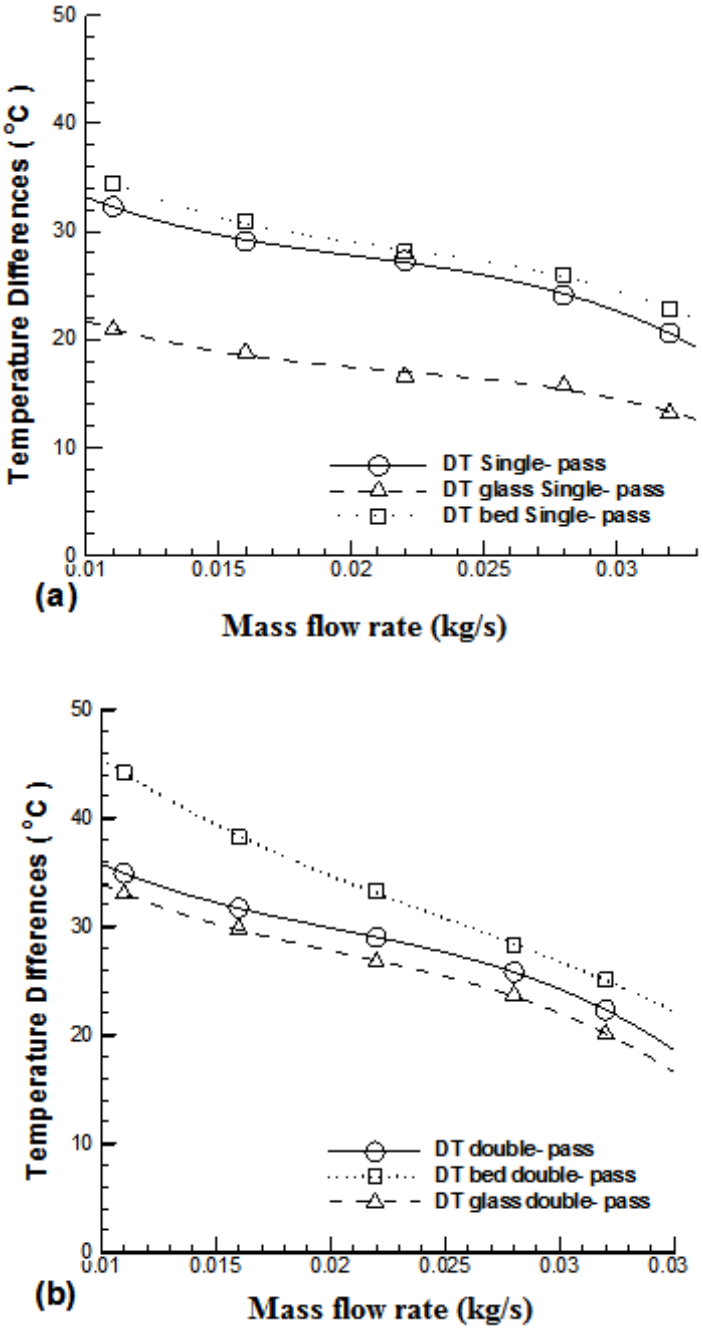

Figure 5.19: Bed temperature difference and Glass temperature difference versus standard local time of the day, at airflow rates 0.011 kg/s, for a) Single- pass SAH, b) Double- pass SAH, 7 baffles with 5 cm bed height.

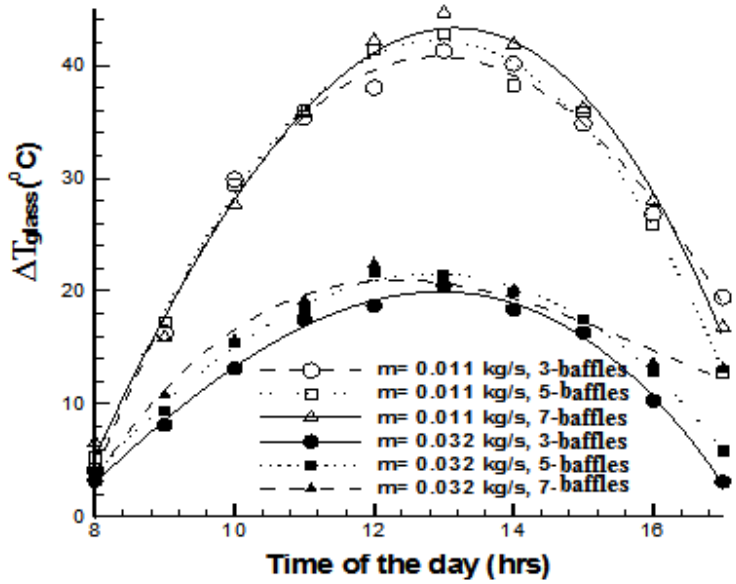

Figure 5.20: Glass temperature difference versus standard local time of the day, for double- pass SAH: 3,5,7 baffles, 5 cm height of bed.

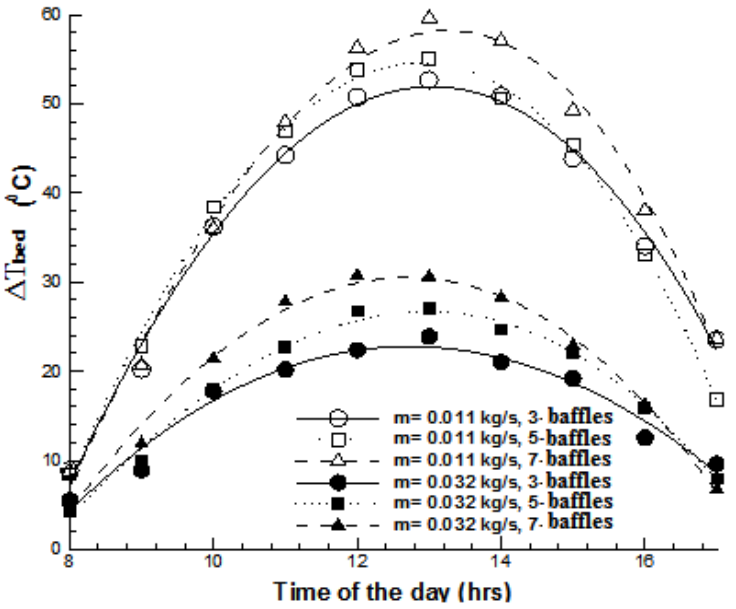

Figure 5.21: Bed temperature difference versus standard local time of the day, for double- pass SAH: 3,5,7 baffles, 5 cm height of bed.

Table 5.2: Maximum bed temperatures differences and glass temperatures differences of the SAH with different height of collectors and number of baffles at airflow rate 0.011 kg/s.

#	Number of baffles	Bed height (cm)	Max. ΔT_{bed}, ^0C, double- pass SAH	Max. ΔT_g, ^0C, double-pass SAH
1	3	3 cm	58.4	41.2
2	5	3 cm	61.1	45.1
3	7	3 cm	62.3	46.3
4	3	5 cm	52.3	41.7
5	5	5 cm	55.1	43
6	7	5 cm	59.3	44.5
7	3	7.5 cm	52.8	38.4
8	5	7.5 cm	56.7	40.4
9	7	7.5 cm	58.2	41.3

5.4 Thermal Efficiency (η)

Figures 5.22–5.24 present the thermal efficiency versus hour of the day at different airflow rates. The efficiency continuously increased with the airflow rate (*i.e.* the heat transfer rate was directly proportional to the airflow rate), As the velocity increased the convective heat transfer coefficient increases thus enhancing heat transfer from the collector to the working fluid . The maximum efficiencies obtained for single- and double-pass SAHs with an airflow rate of 0.032 kg/s, bed height of 3 cm, and seven baffles were 66.3% and 68.1%, respectively. At the maximum airflow rate as shown in Figure 5.22, the thermal efficiency reached the maximum value between 12:00 PM and 1:00 PM then starting to decrease until sunset. This observation was also reported by Omojaro*et al.* (2010). Depending on the solar intensity and the outlet air temperatures of the bed, the efficiency results generally continue to increase from morning until evening as shown in Figures 5.23 and 5.24. This observation was similar to that of El-khawajah*et al.* (2011). It was observed that the efficiency increased at higher airflow rates, this is due to the energy stored in the porous media and shorter flow time of the working fluid within the collector. This energy was received from the sun and the energy absorbed from the mesh layers. Another explanation for this observation was the continual addition of heat to the inlet temperature from morning to afternoons on days with a low wind speed.

The double-pass SAHs were more efficient in all cases than the single-pass SAHs, the flow was preheated in the first channel before it turned down to enter the lower channel; this increased the outlet temperature and useful energy gain. In addition, as shown in Figure 5.25, using seven baffles was more efficient than using five or

three baffles at the same airflow rate. Increasing the number of baffles increased the velocity between these baffles and created a turbulent airflow inside the narrow space that increased the heat transfer coefficient and heat transfer rate. In addition, the path length with seven baffles was clearly longer than that with five or three baffles; thus, the air carried more heat from the bed.

Figure 5.26 presents the thermal efficiency versus time of day at different number of baffles for SAHs with a bed height of 5 cm. The efficiency continuously increased with the airflow rate. The maximum efficiencies for the double-pass SAHs were 62% with three baffles, 64% with five baffles, and 66.3% with seven baffles at a maximum airflow rate of 0.032 kg/s. For the single-pass SAHs, the maximum thermal efficiencies were 56.3% with three baffles, 57.4% with five baffles, and 59.3% with seven baffles. As shown in Figure 5.27 and Figure 5.28, the average thermal efficiency increased with the number of baffles because increasing the path length increases the air velocity for the same mass flow rate. The maximum average efficiencies for the double-pass SAHs were 53.47% with three baffles, 55.7% with five baffles, and 58.36% with seven baffles at an airflow of 0.032 kg/s. The average efficiencies increased to 55%, 58.4%, and 61.8% with three, five, and seven baffles, respectively, when the airflow was increased to 0.038 kg/s. The average thermal efficiency was higher for the double-pass SAH than for the single-pass SAH at airflows of 0.011–0.038 kg/s. This was the result of the air being preheated in the upper channel before turning down to flow inside the lower channel.

Figure 5.29 presents the thermal efficiency versus time of the day at different airflows for SAHs with three baffles and a bed height of 7.5 cm. The efficiency

continuously increased with the airflow rate. Increasing the airflow rate decreases the heat loss from the cover because the heat removal capacity depends directly on the mass flow rate. The maximum values obtained by the single- and double-pass SAHs with a maximum airflow rate of 0.032 kg/s were 55% and 62.5%, respectively. Figure 5.30 present the maximum thermal efficiencies for single- and double-pass SAHs with different bed heights and numbers of baffles. Figure 5.31 present the average efficiencies for single- and double-pass SAHs with different bed heights and numbers of baffles at the maximum airflow rate of 0.032 kg/s. Increasing the number of baffles increased the average thermal efficiency (Figure 5.32) because of the increased air velocity inside the channel. The air velocity between the baffles increased with the reduced cross-sectional area between the baffles.

Figure 5.33 shows the efficiency of the single-pass SAH compared to double-pass SAH versus standard local time of the day when decreasing lower channel heights, 7.5-cm, 5-cm and 3-cm were applied. The thermal efficiency was found to increase by decreasing the space between the second cover and bottom bed for the double-pass SAH. The maximum efficiency of 65.8% for height 3-cm at airflow rate 0.032 kg/s was shown to be the best for double pass solar collector compared to 64% and 62.5% for 5-cm and 7.5-cm respectively. For minimum air flow rate of 0.011 kg/s, the result shows similar behaviour as for the maximum air flow rate of 0.032 kg/s.

In general, increasing the gap between second cover and the bottom of the duct reduces the average air velocity and decreases the heat transfer coefficient.

Figures 5.34 and 5.35 show that the solar intensity and inlet temperature were important factors that affected the thermal efficiency. Figure 5.34 shows the thermal efficiency versus the solar intensity for a single-pass SAH. The thermal efficiency clearly increased with the solar intensity. The increase in the solar intensity increased the outlet temperature and thermal efficiency. Figure 5.35 shows the thermal efficiency versus inlet temperature for single- and double-pass SAHs. The thermal efficiency increased with the inlet temperature. The average thermal efficiencies in the present work were compared with the reported data. For the double-pass SAH, the proposed collector showed an improvement with seven baffles and a bed height of 3 cm (Figure 5.36). Omojaro and Aldabbagh (2010) set up a bed with seven wire mesh layers (1.5 m × 1 m) and longitudinal baffles with a height of 7 cm. Their maximum average efficiency was 51% at a flow rate of 0.035 kg/s. Sopian*et al.* (2009) presented a collector with a saturated absorbent and obtained efficiencies of 32%–67% for flow rates of 0.031–0.071 kg/s. They fixed the heights of the upper and lower channels to 2.5 and 7 cm, respectively. El-Khawajah*et al*. (2011) used a snakelike flow path with twelve wire mesh layers (1.5 m × 1 m), transverse baffles, and a channel height of 7 cm. They reported efficiencies of 46%–79% for fluid flows of 0.012–0.042 kg/s. Musa *et al.* (2004) experimentally tested a double-pass SAH where porous media were inserted in the 2.4-m-long lower channel and the upper and lower channels had depths of 0.035 and 0.075 m, respectively. Their experimental efficiencies were 18%–67% for fluid flow rates of 0.035–0.075 kg/s. Table 5.3 shows the thermal efficiencies for single- and double-pass SAHs with different height of bed and number of baffles at airflow rate 0.032 kg/s and Table 5.4 shows the average thermal efficiencies for single- and double-pass SAHs with different height of bed and number of baffles at airflow rate 0.032 kg/s.

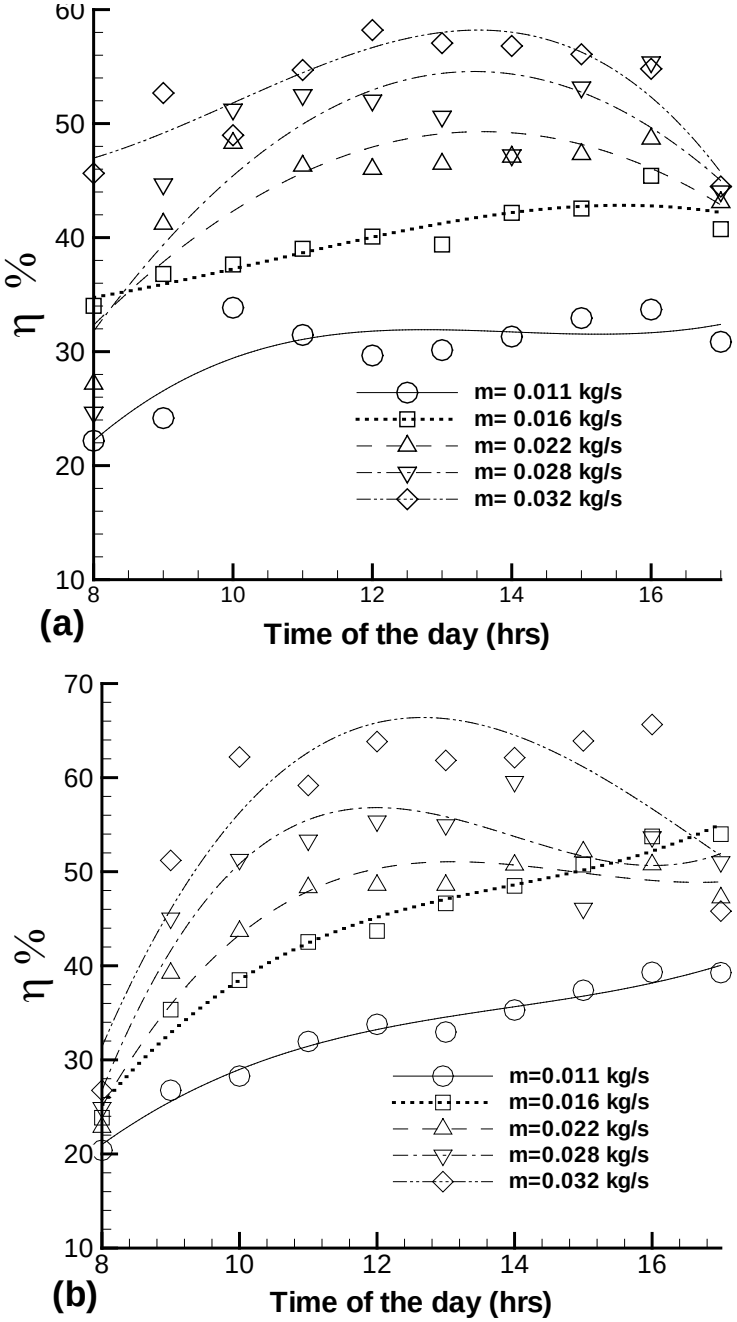

Figure 5.22: Variation of collector efficiency at different mass flow rates for (a) Single- pass SAH, (b) Double- pass SAH, for 3 baffles, 3cm bed height.

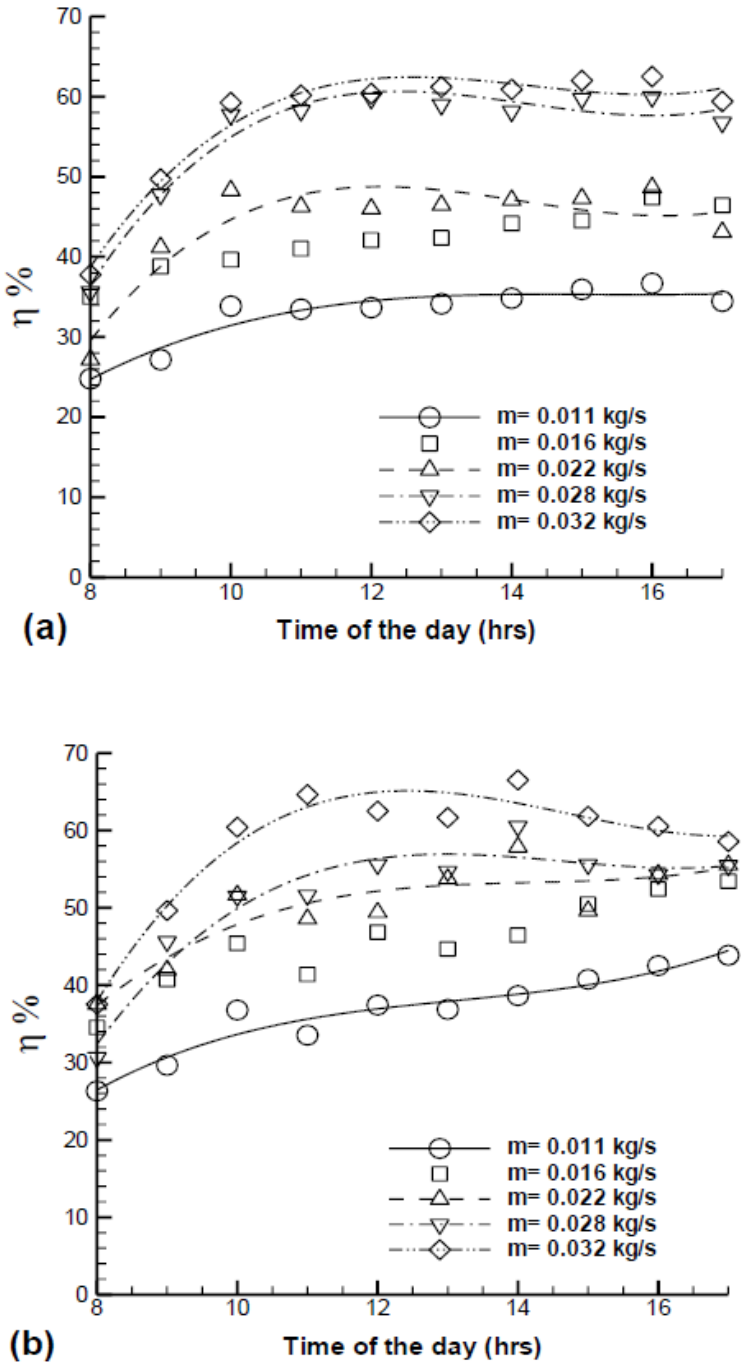

Figure 5.23: Variation of collector efficiency at different mass flow rates for (a) Single- pass SAH, (b) Double- pass SAH, for 5 baffles, for 3cm bed height.

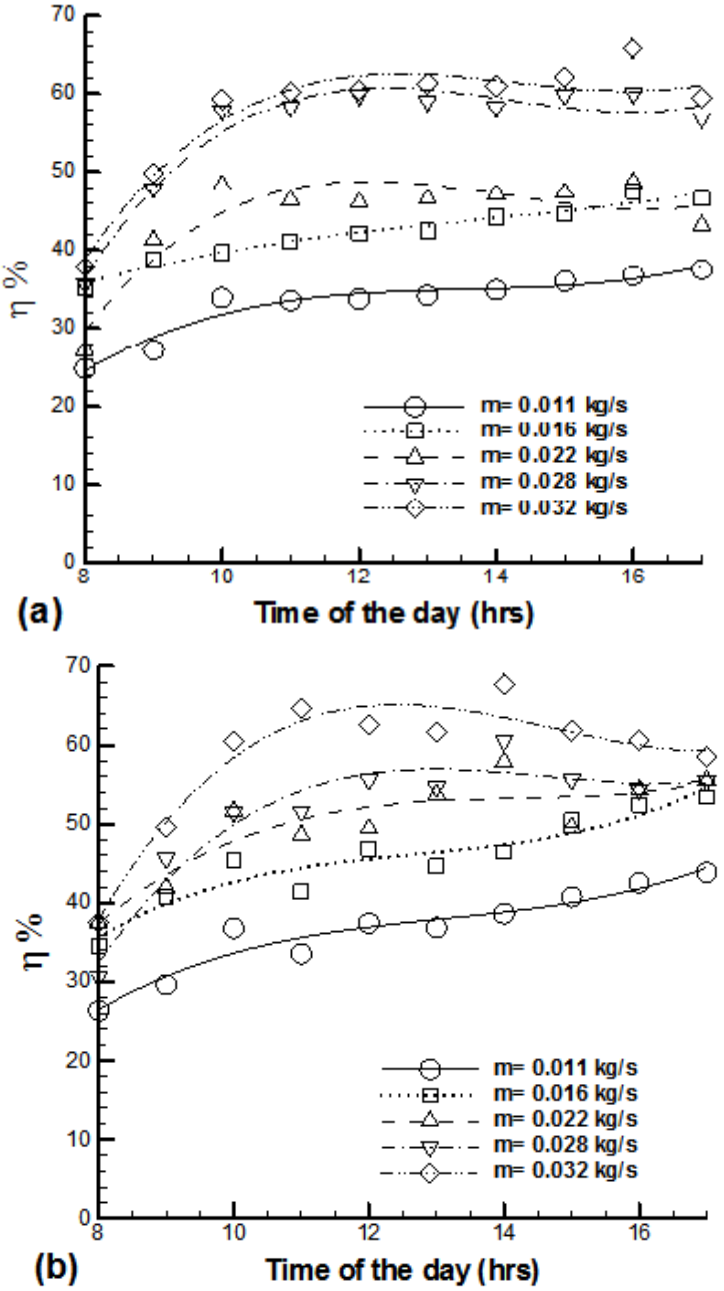

Figure 5.24: Variation of collector efficiency at different mass flow rates for (a) Single-pass SAH, (b) Double-pass SAH, for 7 baffles, 3cm bed height.

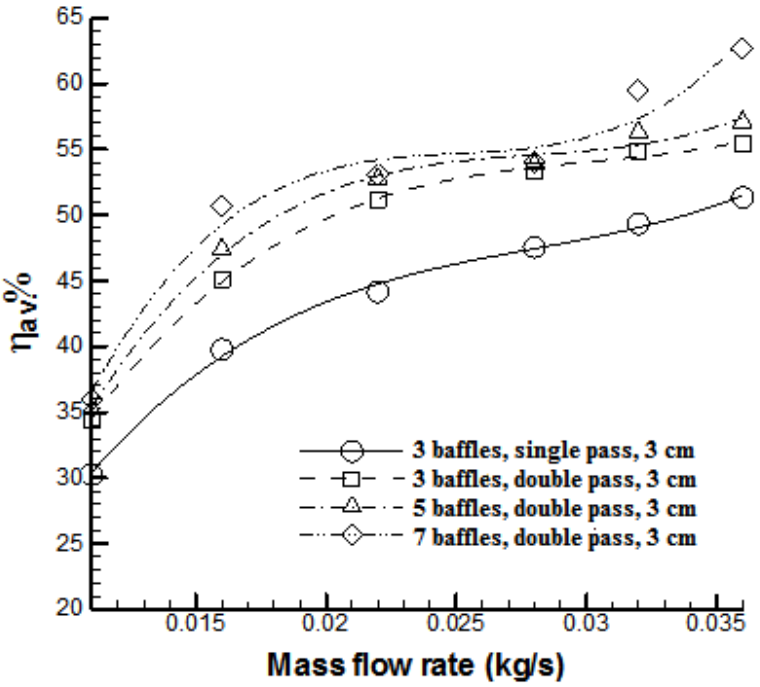

Figure 5.25: Average efficiency across the single- and double-pass SAHs versus mass flow rate, for 3cm bed height.

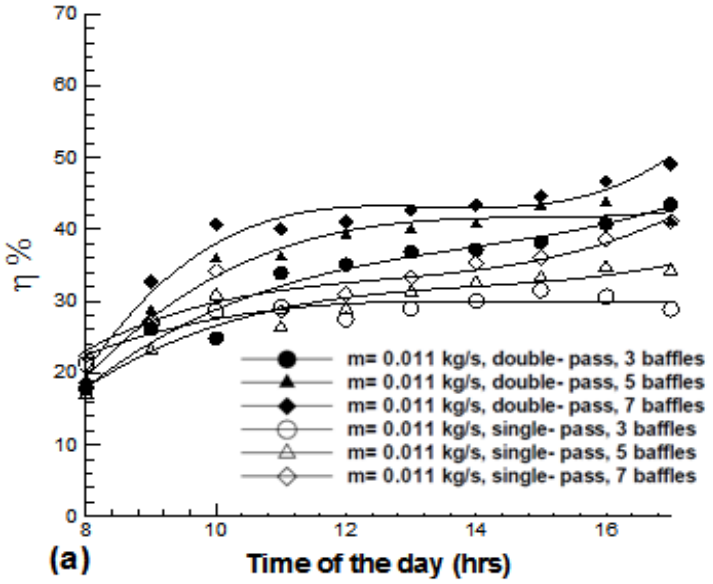

(a)

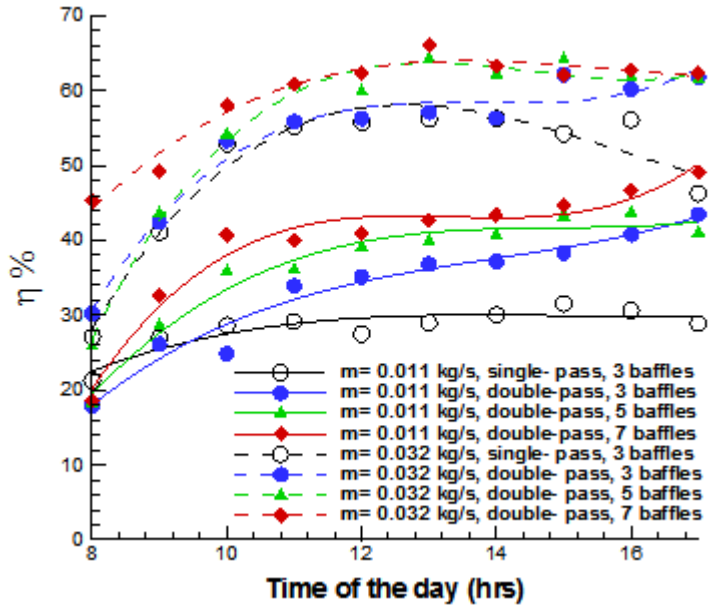

(b)

Figure 5.26: Efficiency comparison between single- pass and double- pass SAHs, for 5cm bed height.

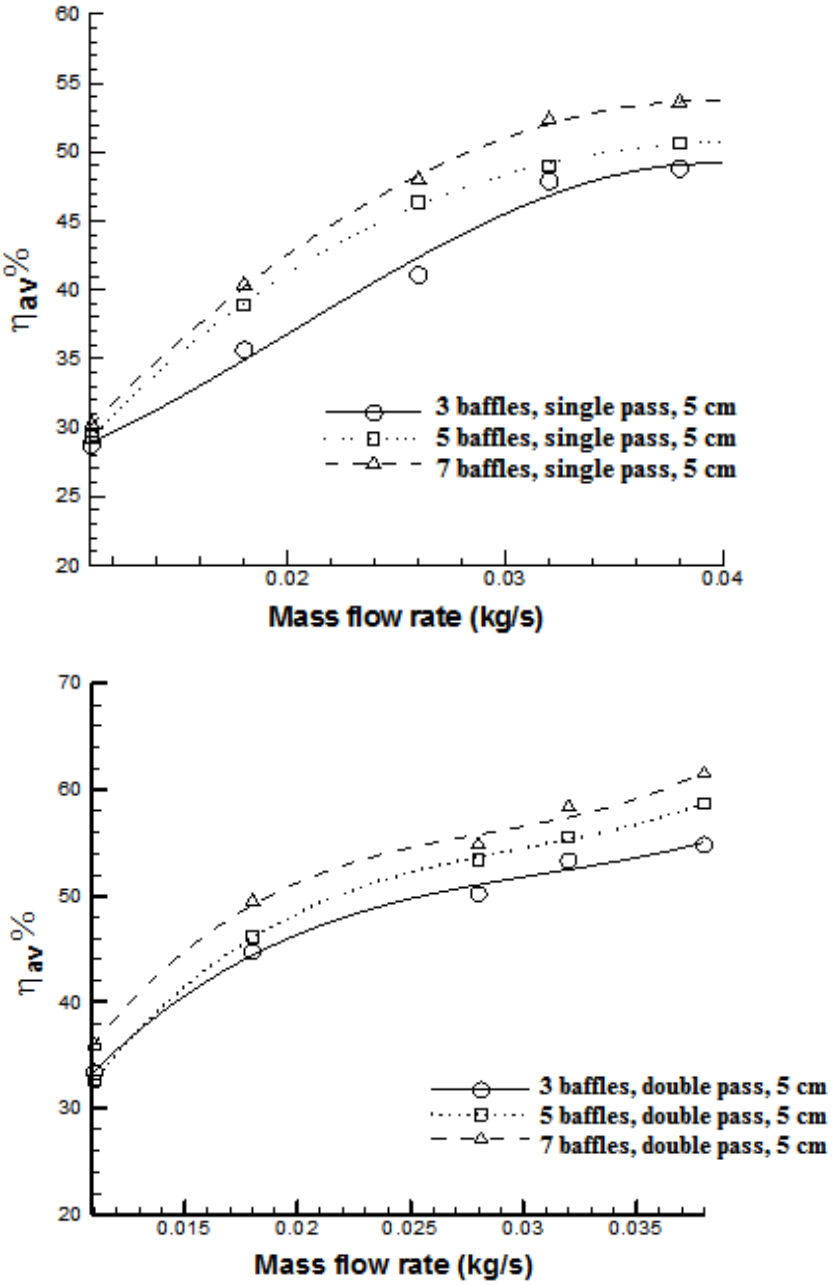

Figure 5.27: Average efficiency across the single- and double- pass SAHs versus mass flow rate, for 5cm bed height.

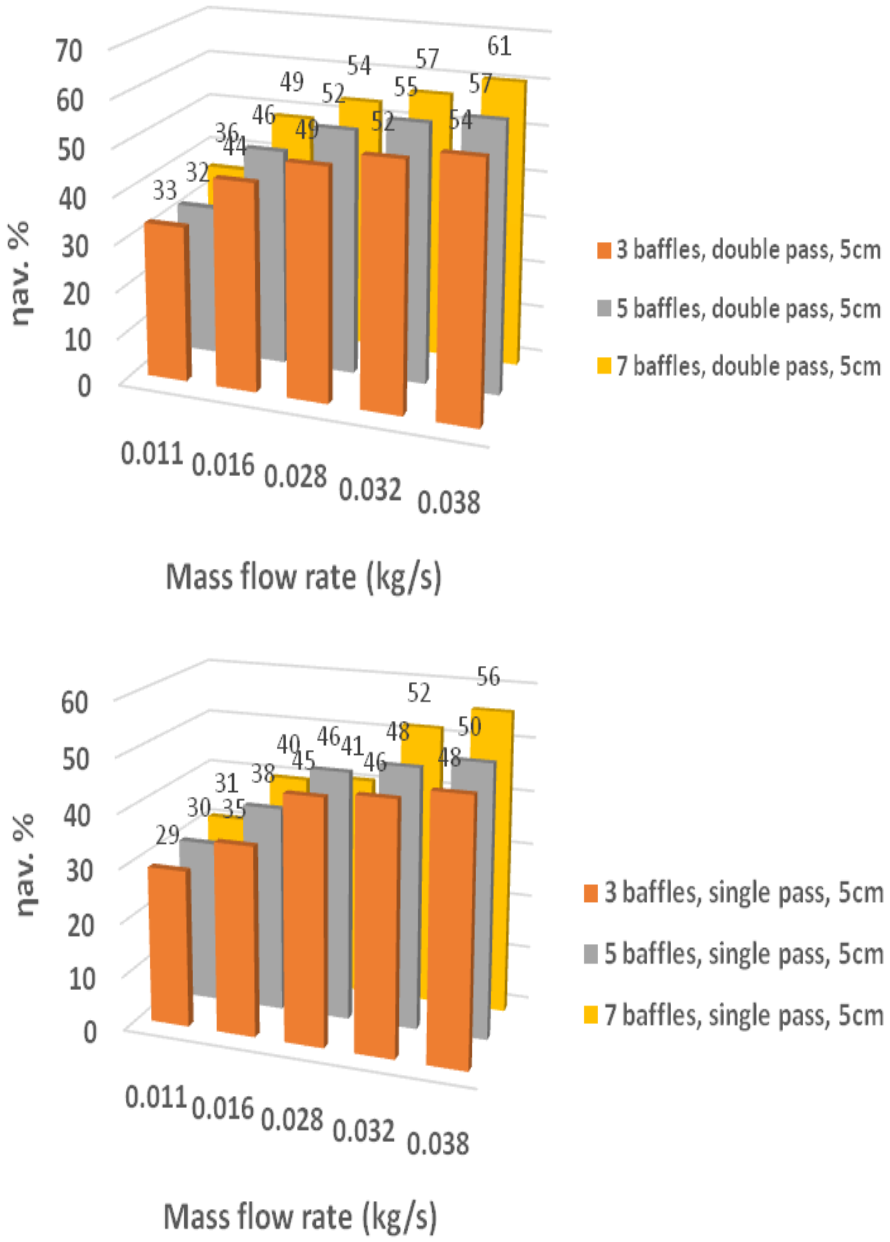

Figure 5.28: Average efficiency across the single- and double- pass SAHs versus mass flow rate, for 5cm bed height as 3D columns.

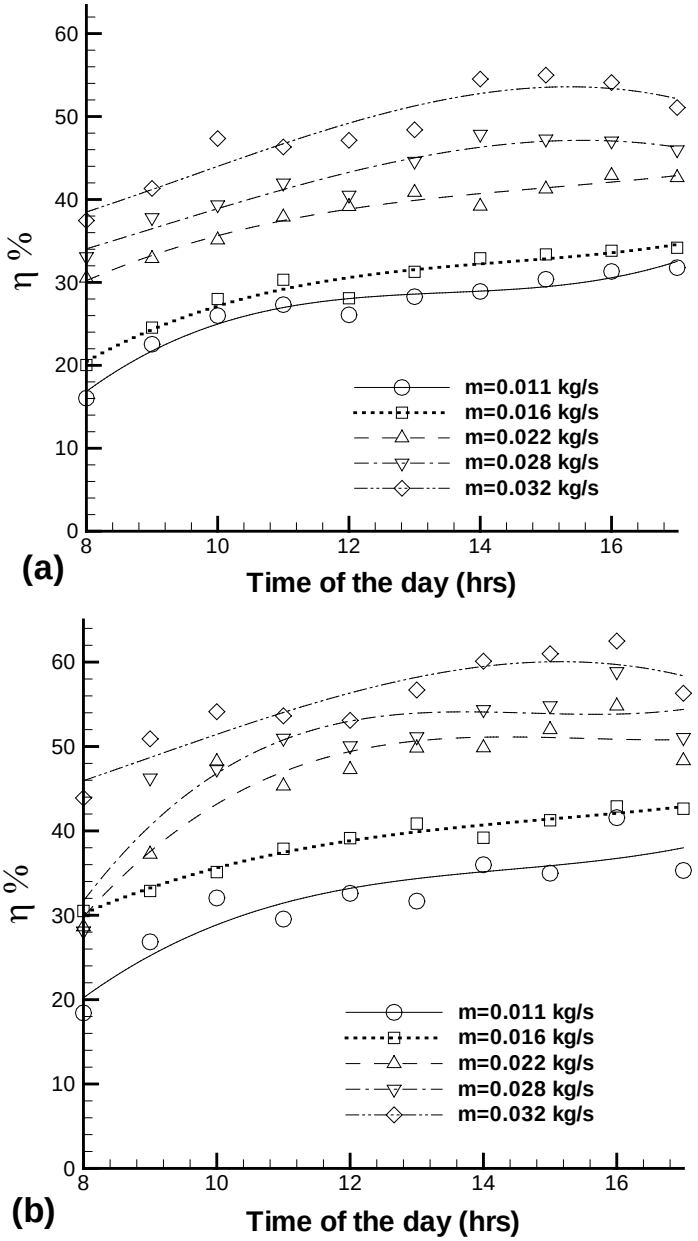

Figure 5.29: Variation of collector efficiency at different mass flow rates for: (a) Single- pass SAH, (b) Double- pass SAH, for 3 baffles, for 7.5cm bed height.

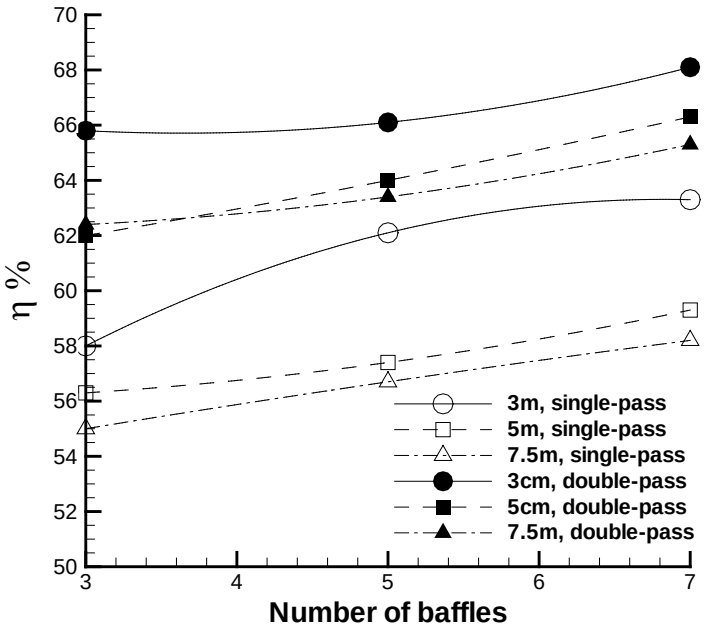

Figure 5.30: The maximum thermal efficiencies for single- and double- pass SAHs with different height of bed and number of baffles at mass flow rate 0.032 kg/s.

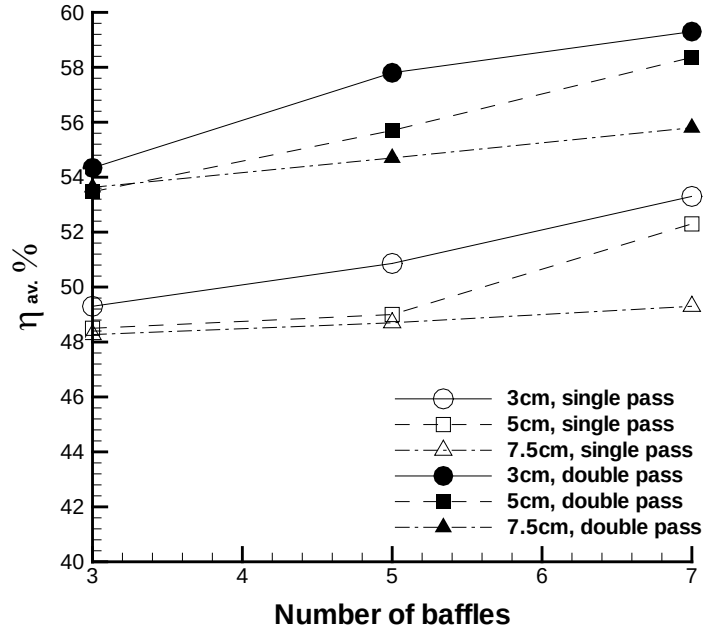

Figure 5.31: The maximum average thermal efficiencies from single- and double-pass SAHs with different height of bed and number of baffles at airflow rate 0.032 kg/s.

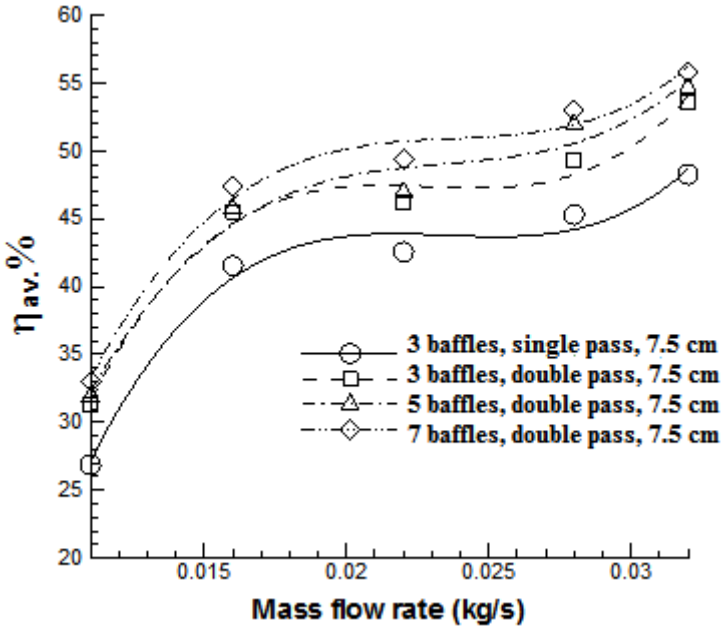

Figure 5.32: Average efficiency versus air flow rate for 7.5 cm with 3,5 and 7 baffles, for 7.5cm bed height.

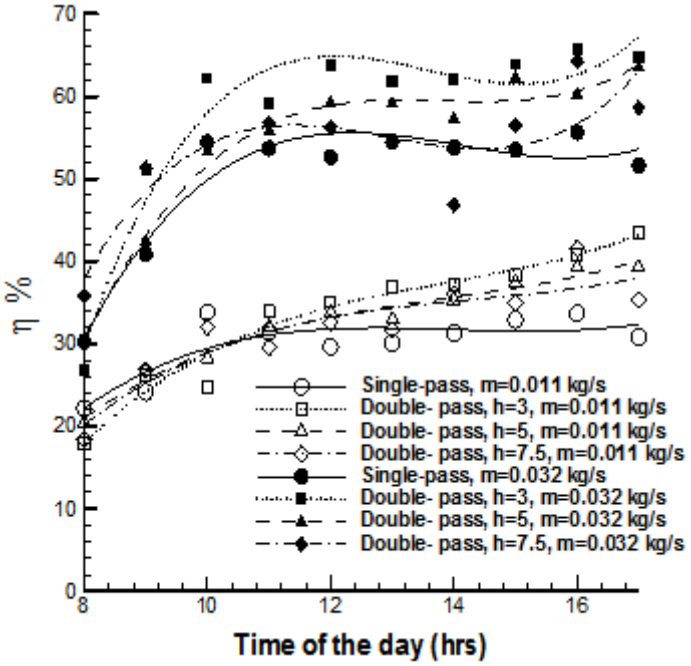

Figure 5.33: Efficiency comparison between single- pass and double- pass SAHs for 3baffles.

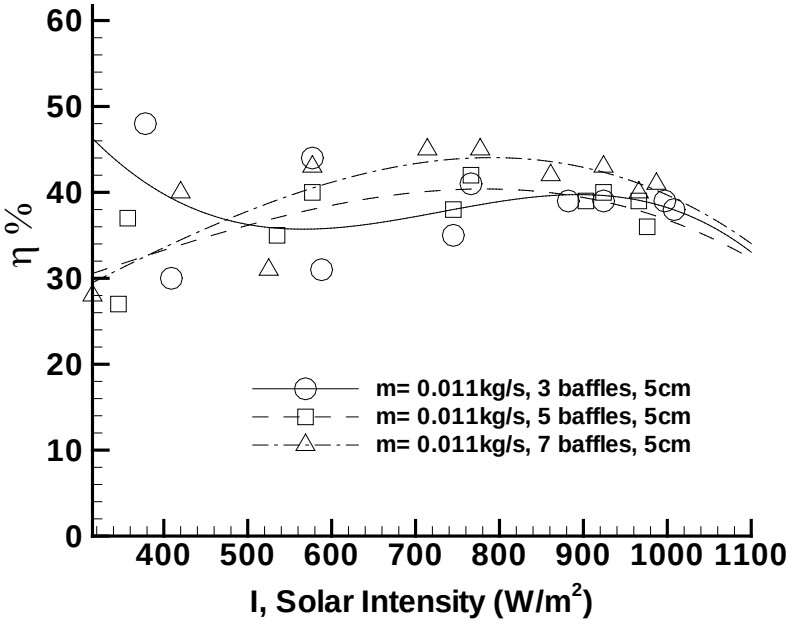

Figure 5.34: Thermal efficiency versus solar intensity for 5 cm with 3,5 and 7 baffles, for single- pass SAH.

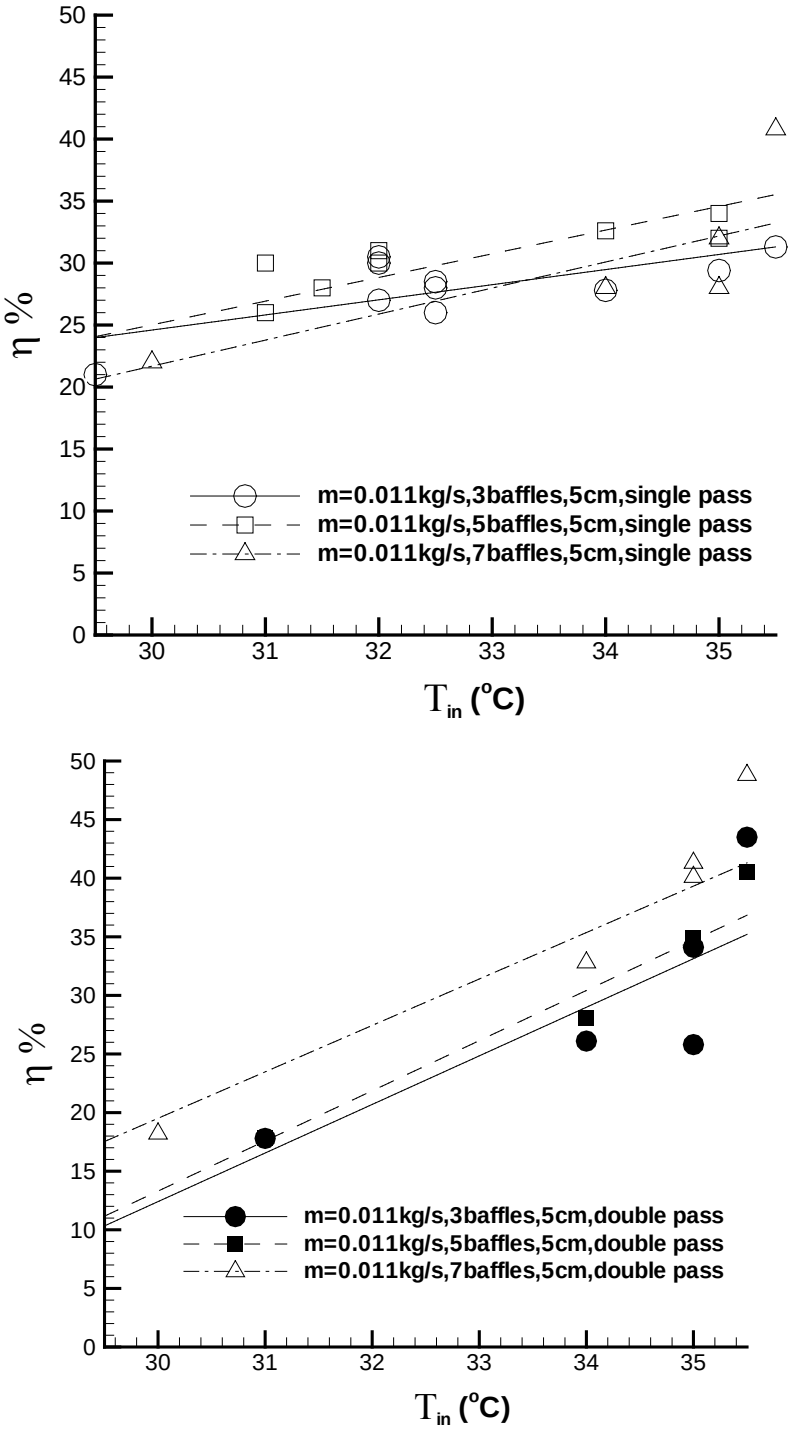

Figure 5.35: Thermal efficiency versus inlet temperature for 5 cm with 3,5 and 7 baffles, for single- pass and double- pass SAHs.

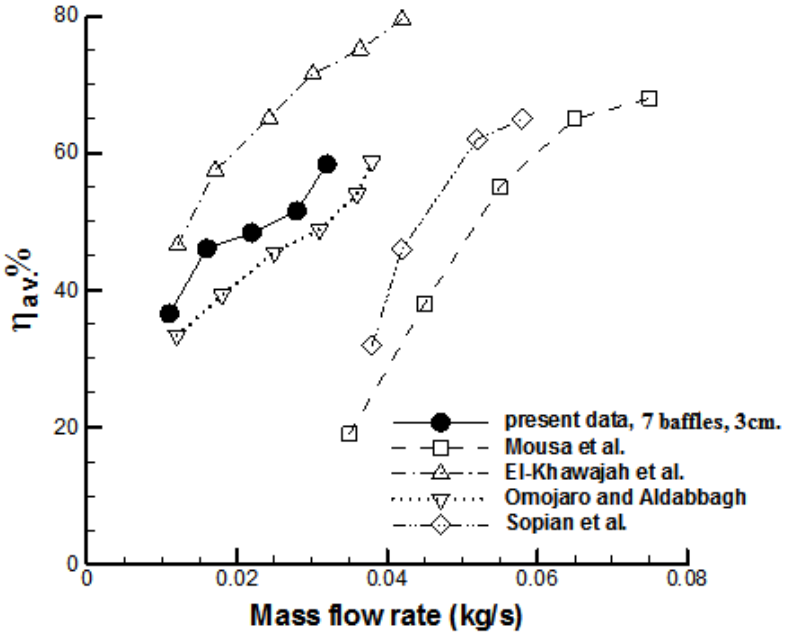

Figure 5.36: Efficiency comparison between the double- pass SAH (7 baffles- 3cm) with same double- pass SAHs in literature.

Table 5.3: The thermal efficiencies for single- and double-pass SAHs with different height of bed and number of baffles at airflow rate 0.032 kg/s.

#	Number of baffles	Bed height (cm)	Max. η%, single pass	Max. η%, double pass
1	3	3 cm	58	65.8
2	5	3 cm	62.1	66.1
3	7	3 cm	66.3	68.1
4	3	5 cm	56.3	62
5	5	5 cm	57.4	64
6	7	5 cm	59.3	66.3
7	3	7.5 cm	55	62.5
8	5	7.5 cm	56.7	63.4
9	7	7.5 cm	58.2	65.3

Table 5.4: The average thermal efficiencies from single- and double-pass SAHs with different height of bed and number of baffles at airflow rate 0.032 kg/s.

#	Bed height (cm)	Max. η_{av}%, single- pass	Max. η_{av}%, double- pass
1	3 cm	49.34	54.34
2	3 cm	50.86	57.86
3	3 cm	53.3	59.3
4	5 cm	48.5	53.47
5	5 cm	49	55.7
6	5 cm	52.3	58.36
7	7.5 cm	48.27	53.63
8	7.5 cm	48.67	54.7
9	7.5 cm	49.3	55.8

Figures 5.37-5.39 represent the thermal efficiency of the collectors versus (T_o - T_i)/I, for 3, 5 and 7.5 cm bed height, 3baffles.

The thermal efficiency decreased as the temperature parameters (T_o - T_i)/I) increased. Increasing (T_o - T_i)/I, increased the heat losses from the cover to the surroundings and reduced the thermal efficiency of the collector. The explanation is: at noon the maximum solar radiation is transmitted through the glass cover and then absorbed by the wire mesh layers. The mesh layers increase in temperature and increase the heat loss to environment by radiation.

The curves were characterised by straight lines (see Equation 5.5, straight-line equations), the intercept $F_R(\tau\alpha)$, and slope $F_R U_L$ (El-Sebaii and Shalaby, 2013).

The temperature parameter (T_o - T_i)/I and thermal efficiency in Figures 5.37- 5.39 represent the values of I, T_o, T_i, and η at noon (13:00 pm), for single- and double-pass SAHs at airflow rates of 0.011–0.032 kg/s). Figures 5.38 and 5.39 show the effect of increasing the bed height of the single- and double-pass collectors to 5 and 7.5 cm. The efficiencies decrease as (T_o - T_i)/I increase, the main reason is the increase in temperature difference (T_o-T_i) which is due to increased wire mesh temperature thus lowering the thermal efficiency. At higher mass flow rates and lower channel depths the air velocity increases and this improves the heat transfer rate from the absorber to air and thermal efficiency of SAH. The scatter in the data around the straight line was due to fluctuations in the wind speed and heat losses from the top cover.

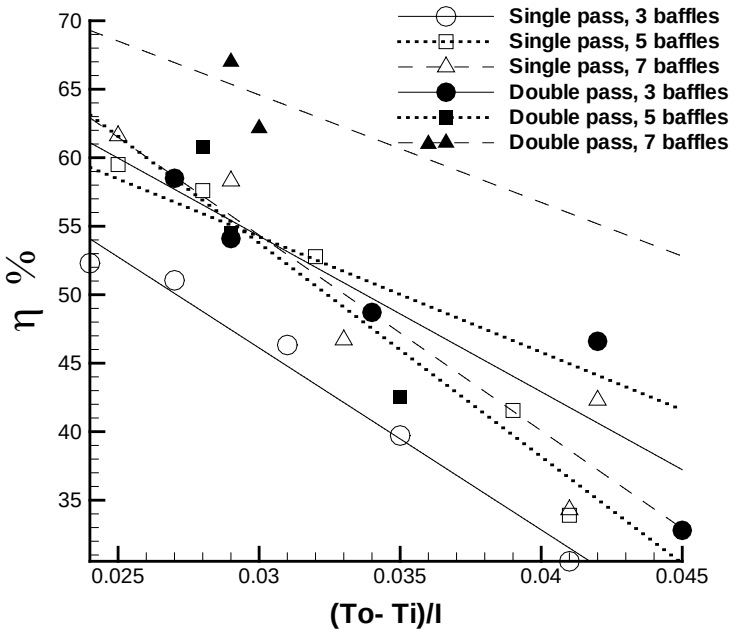

Figure 5.37: The thermal efficiency of the collectors versus $(T_o - T_i)/I$, for 3cm bed height, 3baffles.

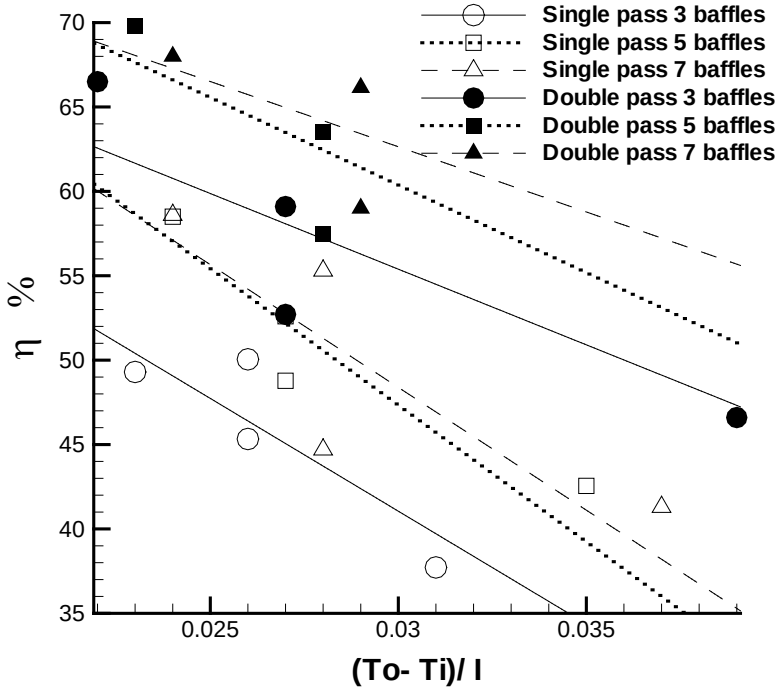

Figure 5.38: The thermal efficiency of the collectors versus $(T_o - T_i)/I$, for 5cm bed height, 3baffles.

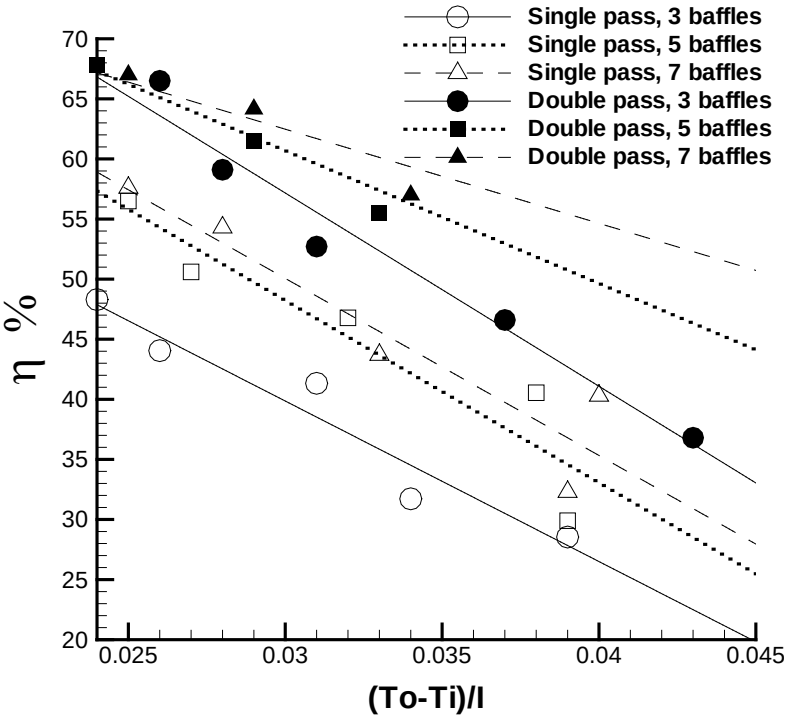

Figure 5.39: The thermal efficiency of the collectors versus $(T_o - T_i)/I$, for 7.5cm bed height, 3baffles.

5.5 Pressure Drop

When the air flows through the channel in the air heater, due to friction the air pressure drops along the length of the flow channel. This pressure drop across the flow duct is given by the following expression (Ratna*et al*., 1992):

$$P_{drop} = f\left(\frac{m^2}{\rho}\right)\left(\frac{L}{w}\right)^3 \quad (5.6)$$

$$f = f_o + y\left(\frac{w}{L}\right) \quad (5.7)$$

where P_{drop} is the pressure drop, *f* is the friction factor, m is the airflow rate, L is the collector length and w is the collector width.

The values of f_o and y are

f_o= 24/Re, y= 0.9 for laminar flow (Re<2550).

f_o= 0.0094, y= 2.92 $Re^{-0.15}$ for transitional flow ($2550<Re<10^4$).

f_o= 0.059 $Re^{-0.2}$, y= 0.73 for turbulent flow ($10^4<Re<10^5$).

In the SAH, the energy gain was maximised and heat transfer was enhanced by using transverse baffles and mesh layers. This was accompanied with an increased pressure drop through the channel. However, the increased pressure drop within the bed with the proposed design was not very high when compared with that of a commercial SAH without porous media. The pressure drop was greater for seven longitudinal baffles than for five or three baffles at the same airflow rate, as shown in Figure 5.40 (7 baffles create high turbulent airflow inside the solar collector, for 7 baffles turbulent airflow greater than for 5 and 3 baffles, the turbulent airflow increased the friction factor and pressure drop inside the solar collector). The

maximum pressure drop for a double-pass SAH with a bed height of 5 cm, airflow rate of 0.032 kg/s, and three baffles was 100 Pa. With five baffles, the maximum pressure drop was 194 Pa. With seven baffles, the maximum pressure drop was 225 Pa. The pressure drop increased with the airflow rate increase as shown in eq. 5.6. The transverse baffles caused turbulent flow inside the duct and increased the convective heat transfer coefficient and thermal energy. The turbulent airflow increased the pressure drop inside the solar collector (friction factor increased for turbulent flow). The maximum pressure drops for single- and double-pass SAHs with a bed height of 3 cm and three baffles were 281 and 312 Pa, respectively (Figure 5.41). The maximum pressure drops for single- and double-pass SAHs with a bed height of 7.5 cm and three baffles were 62 and 66 Pa, respectively (Figure 5.42). Increasing the bed height decreased the pressure drop. The velocity was lower at a bed height of 7.5 cm than at 3 cm, and the airflow was less turbulent. Table 5.5 presents the maximum pressure drops for single- and double-pass SAHs with different bed heights and numbers of baffles at a maximum flow rate of 0.032 kg/s.

Table 5.5: shows the maximum pressure drop from with different height of bed and number of baffles at airflow rate 0.032 kg/s.

#	Number of baffles	Bed height (cm)	Max. pressure drop (Pa), single pass	Max. pressure drop (Pa), double pass
1	3	3 cm	281	312
2	5	3 cm	341	360
3	7	3 cm	375	393
4	3	5 cm	89	100
5	5	5 cm	154	194
6	7	5 cm	194	225
7	3	7.5 cm	64	66
8	5	7.5 cm	123	114
9	7	7.5 cm	147	165

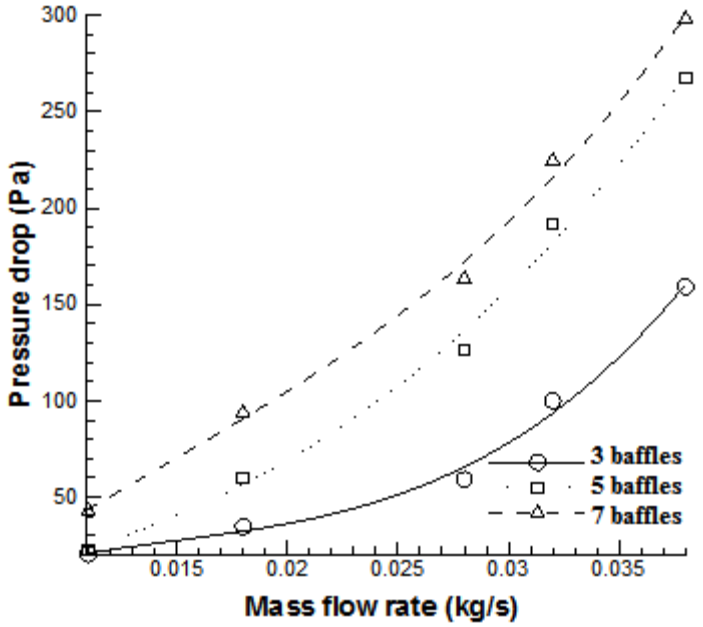

Figure 5.40: Pressure drop across the bed versus mass flow rates for: (a) 3 baffles (b) 5 baffles and (c) 7 baffles, for double pass SAH, 5cm bed height.

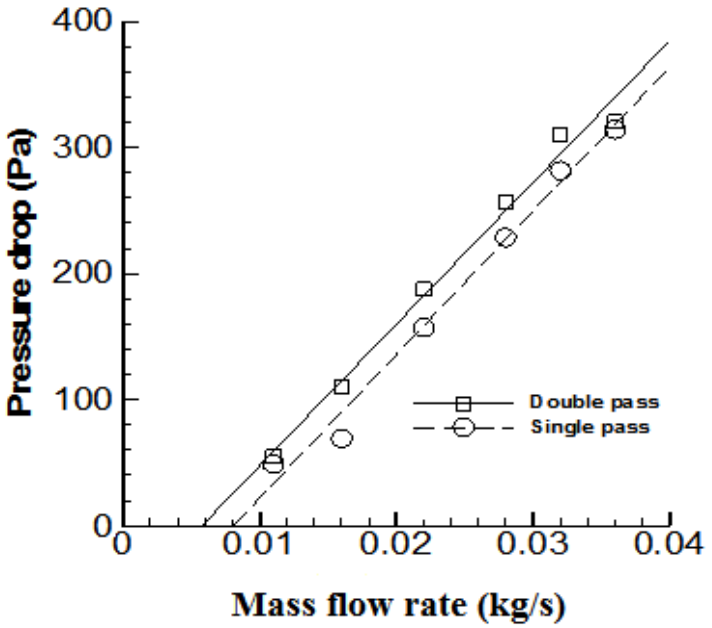

Figure 5.41: Pressure drop across the bed of 3 baffles versus mass flow rates for single and double pass. For 3cm bed height.

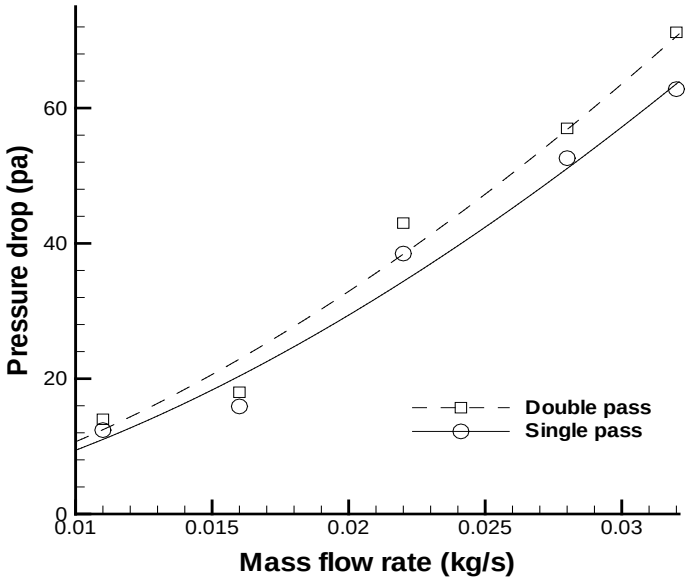

Figure 5.42: Pressure drop across the bed versus mass flow rates for single- pass and double- pass SAHs, for 3 baffles, for 7.5cm bed height.

5.6 Performance Implications of the New Porous Media and Baffles Arrangement

The available literature on SAHs show that many considerable research works are performed on such systems in order to increase the performance of the air heaters; however further modifications can prove worthwhile in the optimization of the overall performance also reducing the construction costs of collectors. In many experimental studies porous media are used as absorber plates but, studies where large quantities of the packed materials used in a small bed height of the collector are very few. This study evaluated the improvement in the performance of the SAH collector by using aluminium transverse baffles and wire mesh layers in a new arrangement, which increases the heat transfer rate from the porous media to the airflow. The improvement in the collector efficiency is obtained when the collector is constructed with baffles and low channel depth to create turbulent flow between these baffles. In solar air heater design where the heat transfer to the working fluid is by convection, it is important to determine the convection heat transfer coefficient (h). Where, h is used for the calculation of heat transfer rate between the surface and the working fluid. For the design purposes empirical relations are relied on for the evaluation of the convection heat transfer coefficient. Empirical correlations are usually presented in dimensionless quantities such as Reynolds number (Re), Nusselt number (Nu) Prandtl number and etc. The flow becomes turbulent if the Reynolds number is higher than the critical Reynolds number. Reynolds number is the ratio of the inertia forces to viscous forces in the fluid and it is directly proportional to the fluid velocity. The Nusselt number is expressed as:

$$Nu=hD_e/k \tag{5.8}$$

where, D_e is the characteristic dimension of the surface, and k is the thermal conductivity of the fluid. The Nusselt number for solar air heaters where the flow is turbulent can be evaluated by the following approximate equation (Kays, 1966):

$$Nu=0.0158Re^{0.8} \quad (5.9)$$

As the velocity increases the Reynolds number also increases. It is clear from Eq. 5.9 that Nu increases as Re increased. Therefore, in a solar air collector increasing the velocity increases the Re, Nu and thus h also increases (see Eq. 5.8). Increased convection heat transfer coefficient enhances the heat transfer between the surface and the working fluid.

Increasing the number of baffles increases the path length of the airflow (i.e., the average velocity of the air increases) and this improves the useful heat gain in the collector. Using wire mesh layers instead of sheet metal as the absorber increased the contact area (i.e., heat transfer area between the air and absorber) of the working fluid inside the channel thus enhancing heat transfer to the working fluid from the absorber. See equation in section 3.1; in particular Eqs. (3.13)- (3.15).

Five airflow rates were considered for single- and double-pass SAHs with different numbers of baffles and bed heights. These experimental results are important in this research field. The new study was a successful improvement in the thermal efficiencies and outlet air temperatures of the SAH system by increasing the path of the airflow inside the channels of single- and double-pass SAHs with porous media in the lower channel without an absorber plate. Transverse baffles were fixed inside the duct to direct the air inside the channel to produce a special path shape (Figures 4.2–4.4). Those baffles divided the channel into equal sections. In this case, the air

at the entrance was divided into two equal parts: one part moved to the left and the other part to right. Then, the two parts entered the second section of the channel through the two openings made at the two sides. The two parts of the airflow were mixed together at the midsection of the second part of the channel and passed to the third section through the opening made at the midsection of the second baffles. In this manner, the path of the airflow was repeated. Increasing the number of baffles increases the length of the airflow path from the inlet to the outlet of the collector, so the airflow gains more heat from the wire mesh layers.

The wire meshes used in this collector were similar to those used by El-khawajah*et al.* (2011), Gill *et al.* (2012) and AL-Kamil *et al.* (1996) with differences in the total number of layers, number of layers in each matrix, and distance between matrices considered in order to further reduce the pressure drop. The effect of the height of the second pass on the thermal performance of the SAH was also considered. Tests were conducted under actual outdoor conditions. The double pass was used in this study to reduce the losses from the cover; the inlet air was preheated by absorbing radiation heat from the absorber wire mesh layers (Mohamad, 1997).

In the present study, the maximum efficiencies for the single- and double- pass SAHs were achieved with seven baffles, a bed height of 3 cm, and airflow rate of 0.032 kg/s. The maximum temperature difference (*i.e.* average outlet temperature - average inlet temperature) was achieved with seven baffles, a bed height of 3 cm, and minimum airflow rate of 0.011 kg/s. First, single- and double-pass SAHs were constructed with a bed height of 3 cm and three, five, or seven transverse baffles, which divided the channel into four, six, or eight equal sections. The transverse baffles were arranged in a special shape to allow the air to move between these

baffles. Experiments were conducted at Famagusta, Cyprus (35.125°N latitude and 33.95°E longitude) during the summer months from 8 July to 20 August 2011. The average of the hourly mean wind speed was measured to be 5.65 m/s (wind speed data from the Department of Meteorology, Ministry of Public Works and Transport, Turkish Republic of Northern Cyprus; http://kktcmeteor.org/). The absorber plate was replaced with sixteen wire mesh layers. The airflow rate was varied from 0.011 kg/s to 0.032 kg/s. For the double-pass SAH, the heights of the upper and lower channels were fixed to 2.5 and 3 cm, respectively. Second, single- and double-pass SAHs were constructed with a bed height of 5 cm and three, five, or seven transverse baffles, which divided the channel into four, six, or eight equal sections. This experiment was conducted from 8 July to 20 August 2012 under clear skies. The airflow rate was varied from 0.011 kg/s to 0.038 kg/s. For the double-pass SAH, the heights of the upper and lower channel were fixed to 2.5 and 5 cm, respectively. Third, single- and double-pass SAHs were constructed with a bed height of 7.5 cm and three, five, or seven longitudinal baffles that were painted black and placed transversely to create four, six, or eight equally spaced sections. Sixteen steel wire mesh layers were inserted between these baffles as an alternative to an absorber plate. This experiment was conducted from 14 August to 22 September 2013 under clear skies. The airflow rate was varied from 0.011 kg/s to 0.032 kg/s. For the double-pass SAH, the heights of the upper and lower channels were fixed to 2.5 and 7.5 cm, respectively.

Chapter 6

CONCLUSION AND FUTURE WORK

6.1 Conclusions of Present Work

The thermal performances of single- and double-pass SAHs with different numbers of transverse baffles and steel wire mesh layers acting as an absorber plate were investigated experimentally under the prevailing weather conditions at Famagusta, Cyprus. The effects of air mass flow rates of 0.011- 0.032 kg/s on the outlet temperature and thermal efficiency were studied. The bed heights of the lower channel were varied between 3 and 7.5 cm. The upper channel of the double-pass SAH was fixed to a depth of 2.5 cm for all cases.

In general, the cost of the SAH was reduced by the use inexpensive wire mesh layers instead of the absorber plate.

The results showed that the efficiency increased with the air mass flow rate at the same bed height and a fixed number of baffles. At the same air flow rate and a fixed height channel and number of baffles, the double-pass SAH was found to be 7% more efficient than the single-pass SAH. In addition, the efficiencies of the single- and double-pass SAHs increased with the number of baffles for the same air mass flow rate and bed height. The maximum efficiencies for the single- and double- pass SAHs with seven baffles and bed height of 3 cm were 64.3% and 69.3%, respectively, for an air mass flow rate of 0.032 kg/s. The thermal efficiency decreased when the height of the first pass of the single- and double-pass SAHs was

increased. The instantaneous and average efficiency were higher with a 3 cm channel height than with channel heights of 5 and 7.5 cm for the same air mass flow rate and a fixed number of baffles.

For both the single- and double- pass SAHs, the temperature difference between the outlet flow and ambient decreased as the air mass flow rate increased for the same channel height and number of baffles. The temperature rise increased with the number of baffles for the same channel height and air mass flow rate. The temperature rise was higher with seven baffles than with three or five baffles. Decreasing the channel height of the first pass increased the temperature rise at the same air mass flow rate and number of baffles. The maximum temperature rise obtained in this work for the single- and double-pass SAHs were 45.6 and 54.6 °C, respectively at the minimum air flow rate of 0.011 kg/s with seven baffles and a channel height of 3 cm. The temperature differences with a channel height of 5 cm were 44.7 and 50.1 °C, respectively. With a 7.5 cm channel height, they were 36.3 and 49.8 °C, respectively. In general, the temperature rise increased with an increase in the number of baffles or decrease in the lower channel height at the same air mass flow rate. It was found that increasing the number of baffles and lowering the channel height resulted in an increase in the pressure drop, along with increasing the thermal efficiency and temperature difference. The pressure drop was higher with seven baffles than with five or three baffles. The double-pass collector showed a higher pressure drop than the single-pass collector for the same number of baffles and air mass flow rate. Increasing the air flow was accompanied with an increase in the pressure drop. Decreasing the bed height from 7.5 cm to 5 or 3 cm produced a high pressure drop. The maximum pressure drops for the single- and double-pass

SAHs were 375 and 393 Pa, respectively, with seven baffles, a bed height of 3 cm, and air flow of 0.032 kg/s.

The present experimental work showed that the proposed SAH design provides improvements compared to a conventional SAH. These improvements are due to the use of packed wire layers and transverse baffles as an alternative to the absorber sheet and the low bed height (3 cm). The thermal efficiencies for the single- and double- pass SAHs in the present work showed an improvement compared to the SAHs of Omojaro and Aldabbagh, 2010, Sopian*et al.*, 2009 and Musa *et al.*, 2004). The results demonstrated that the proposed design produced significant improvements in the thermal efficiency and outlet air temperature.

6.2 Future Work

For future studies, the design should be performed on a software program before any experimental work to identify the weak points and optimise the design to reduce the expenses and time. Moreover, the theoretical work can also be compared with the experimental work. The heat lost from the glazing face of the collector can be decreased by increasing the space between the first mesh layer of the package and the glazing cover. More study is needed for the new arrangement of mesh layers to determine the effect on the outlet temperature, thermal efficiency, and pressure drop. Experiments can also be conducted with different numbers of mesh layers to obtain the best design with the fewest mesh layers in order to reduce the pressure drop and improve the performance.

REFERENCES

Aboul-Enein S., El-Sebaii A.A., Ramadan M.R.I., El-Gohary H.G. (2000). Parametricstudy of a solar air heater with and without thermal storage for solar drying applications. *Renewable Energy*. 21, 505- 522.

Adnane L., Noureddine M., Adel B., Kamel A., Abdelhafid M. (2012). Performance investigation of single- and double-pass solar air heaters through the use of various fin geometries. *International Journal of Sustainable Energy*. 31, 423-434.

Aghaie A.Z., Rahimi A. B., AlirezaAkbarzadeh A. (2015). A general optimized geometry of angled ribs for enhancing the thermo-hydraulic behavior of a solar air heater channel - A taguchi approach. *Renewable Energy*. 83, 47- 54.

Ahern C., Norton B. (2015). Energy savings across EU domestic building stock by optimizing hydraulic distribution in domestic space heating. Energy and Buildings. 91, 199- 209.

Akpinar E. K., Kocyigit F. (2010). Energy and exergy analysis of a new flat plate solar air heater having different obstacles on absorber plates. *Applied Energy.* 87, 3438- 3450.

Alam T., Saini R. P., Saini J. S. (2014). Heat and flow characteristics of air heater ducts provided with turbulators. *Renewable and Sustainable Energy Reviews*. 31, 289- 304.

Aldabbagh L.B.Y., Egelioglu F., Ilkan M. (2010). Single and double pass solar air heaters with wire mesh as packing bed. *Energy*. 9, 3783- 3787.

Alejandro L.H.,José E.Q. (2013). Analytical models of thermal performance of solar air heaters of double parallel flow and double-pass counter flow. *Renewable Energy*. 55, 380- 391.

AL-Kamil M.T., Al-Ghareeb A.A. (1996). Effect of thermal radiation inside solar air heaters. *Energy Conversation Management*. 38, 1451- 1458.

Alta D., Bilgili E., Ertekin C., Yaldız O. (2010). Experimental investigation of three different solar air heaters: Energy and exergy analyses. *Applied Energy*. 87, 2953- 2973.

Bahrehmand D., Ameri M. (2015). Energy and exergy analysis of different solar air collector systems with natural convection. *Renewable Energy*. 74, 357- 368.

Bashria A, Yousef A., Adam N.M., Sopian K., Zaharim A., Alghoul M. (2007). Analysis of single and double passes V-grooves solar collector with and without porous media. *International Journal of Energy And Environment*. 1 Issue 2.

Ben Salma R. (2007). The air solar collectors: Comparative study, introduction of baffles. *Solar Energy*. 8, 139- 149.

Bhargava A.K., Jha R., Garg H.P. (1990). Analysis of a solar air heater with thermosym- phon flow in one channel and forced flow in other channel. *Conservation and Management*. 30, 231-236.

Chamolia S., Chauhana R., Thakura N.S.,Sainib J.S. (2012). A review of the performance of double pass solar air heater. *Renewable and Sustainable Energy Reviews*. 16, 481- 492.

Chiou J.P., El-Wakil M.M., Duffie J.A. (1965). A slit and expanded aluminium-foil matrix solar collector. *Solar Energy*. 9, 73- 80.

Chongjie W., Zhenzhong G., Xueyi Z., Delin W. (2006). Numerical simulation study on transpired solar air collector. *Renewable Energy Resources and a Greener Future*. 3, 40- 47.

Choudhury C., Chauhan P.M., Garg H.P. (1995). Design curves for conventional solar air heaters. *Renewable Energy*. 7, 739- 749.

Denga J., Yang X., Ming Y. ,Zhifeng W. (2015). Experimental study of a single-pass flat plate solar air collector with severe dust deposition on the transparent glass cover. *Energy*. 70, 32- 40.

Duffie J.A. and Beckman W.A. (1991). Solar engineering of thermal processes. *(John Wiley& Sons, New York)*, pp.1-379.

Ekechukwu O.V., Norton B. (1999). Review of solar-energy drying systems III: low temperature air-heating solar collectors for crop drying applications. *Energy Conversion and Management*. 40, 657- 667.

El-khawajah M.F., Aldabbagh L.B.Y., Egelioglu F. (2011). The effect of using transverse fins on a double pass flow solar air heater using wire mesh as an absorber.*Solar Energy*. 85, 1479- 1487.

Elradi A.M., Sopian K., Shahrir A. (2004). Heat transfer analysis and pressure drop correlations for the double-pass solar collector with porous media. *Journal of Energy & Environment*. 3, 15- 24.

El-Sebaii A.A., Abou-Enein S., Ramadan M.R.I., El-Bialy E. (2007). Year round performance of double pass solar air heater with packed bed. *Conservation and Management*. 48, 990-1003.

El-Sebaii A.A., Aboul-Enein S., Ramadan M.R., Shalaby S.M., Moharram B.M. (2011). Thermal performance investigation of double pass-finned plate solar air heater. *Applied Energy*. 88, 1727- 1739.

El-Sebaii A.A., Shalaby S.M. (2013). Experimental investigation of an indirect-mode forced convection solar dryer for drying thymus and mint. *Energy Conversion and Management* 74, 109- 116.

Esen H. (2008). Experimental energy and exergy analysis of a double-flow SAH having different obstacles on absorber plates. *Build Environ*. 43, 1046-1054.

Fan Jing-Li, Yu H., Yi-Ming W. (2015). Residential energy-related carbon emissions in urban and rural China during 1996–2012: From the perspective of five end-use activities. *Energy and Buildings*. 96, 201- 209.

Fudholi A., Sopian K., Mohd H.R., Mohd Y.O., Muhammad Y. (2011). Thermal efficiency of double pass solar collector with longitudinal fins absorbers. American. *Journal of Applied Sciences*. 8, 254- 260.

Fudholi A., Sopian K., Othman M.Y., Ruslan M.H., Bakhtyar B. (2013). Energy analysis and improvement potential of finned double-pass solar collector. *Energy Conversion and Management*. 75, 234- 240.

Gill R.S., Sukhmeet S., Parm Pal S.(2012). Low cost solar air heater. *Energy Conversion and Management*. 57, 131- 142.

Gupta M.K, Kaushi S.C. (2008). Exergetic performance evaluation and parametric studies of solar air heater .*Energy.* 33, 1691- 1702.

Hanemann M., Labandeira X., Labeaga José M., López-Otero X. (2013). Energy demand for heating: short run and long run. *Economic for energy*. 9, 8-13.

Hegazy A. A. (1996). Optimization of flow-channel depth for conventional flat plate solar air heaters. *Renewable Energy*. 7, 15- 21.

Heiskanen E., Lovio R., Jalas M. (2011). Path creation for sustainable consumption: promoting alternative heating systems in Finland. *Journal of Cleaner Production*. 19, 1892-1900.

Holman JP. (1989). Experimental methods for engineers. *New York: McGraw-Hill*.

Hsieh J.S. (1986). Solar energy engineering. *Englewood Cliffs, New Jersey: Prentice-Hall.*

Jesko V. (2008). Classification of solar collectors. *Engineering For Rural Development. Jelgava*. 29, 30-35.

Kalogirou S.A. (2004). Solar thermal collectors and applications. *Progress in Energy and Combustion Science*. 30, 231- 295.

Kalogirou S.A. (1997). Solar distillation systems: a review. Proceedings of first international conference on energy and the environment. *Limassol, Cyprus*. 2, 832- 838.

Kasra M., Majid S. (2014). Appraising the performance of a baffled solar air heater with external recycle. *Energy Conversion and Management*. 88, 239- 250.

Kumar C., Singh H.(2014). Experimental performance analysis of solar air heater with three different modifications in absorber plate. *International Journal of Advanced Technology in Engineering and Science*. 2, 2348- 7550.

Kays W.M. Convective heat and mass transfer. *New York: McGraw-Hill*, 1966.

Ming Y., Xudong Y., Xing Li., Zhifeng W. (2014). Pengsu W. Design and optimization of a solar air heater with offset strip fin absorber plate. *Applied Energy*. 113, 1349- 1362.

Mishra K. A. (2013). *A CFD* Investigation and pressure correlation of solar air heater. *International Journal of Mechanical Engineering and Technology*. 4, 401- 417.

Mittal M.K., Varshney L. (2006). Optimalthermohydraulic performance of a wire mesh packed solar air heater. *Solar Energy*. 80, 1112- 1120.

Mohamad A.A. (1997). High efficiency solar air heater. Solar Energy. 60, 71- 76.

Mohammadia K., Sabzpooshani M. (2013). Comprehensive performance evaluation and parametric studies of single pass solar air heater with fins and baffles attached over the absorber plate. *Energy*. 57, 741- 750.

Mohammadi K., Sabzpooshani M. (2014). Appraising the performance of a baffled solar air heater with external recycle. *Energy Conversion and Management*. 88, 239- 250.

Musa E.A., Sopian K., Shahrir A. (2004). Heat transfer analysis and pressure drop correlations for the double-pass solar collector with porous media. *Energy Environ*. 3, 15- 24.

Naveed A.T., Kang E.C., Lee E. J. (2006). Effect of unglazed transpired collector on the performance of a polycrystalline silicon photovoltaic module. *Journal of Solar Energy Engineering*. 128, 349- 353.

Nield D.A., Bejan A. (1999). Convection in porous media. *Springer-Verlag New York.*

Njomo D., Aguenet M. (2006). Sensitivity analysis of thermal performances of flat plate solar air heaters. *Heat and Mass Transfer*. 42, 1065- 1081.

Omojaro A.P., Aldabbagh L.B.Y. (2010). Experimental performance of single and double pass solar air heater with fins and steel wire mesh as absorber. *Apply Energy*. 87, 3759- 3765.

Pakdaman M. F., Lashkari A., Tabrizi H.B., Hosseini R. (2011). Performance evaluation of a natural-convection solar air-heater with a rectangular finned Absorber Plate. *Energy Conservation and Management*. 52, 1215- 1225.

Ramadan M.R.I., El-Sebaii A.A., Aboul-Enein S., El-Bialy E. (2007). Thermal performance of a packed bed double pass solar air heater. *Energy*. 32, 1524- 1535.

Ramani B.M., Akhilesh G.B., Ravi K. (2010). Performance of a double pass solar air collector. *Solar Energy*. 84, 1929- 1937.

Ratna V., Ram Ch., Garg H.P. (1992). Technical note- optimization of solar air heaters of different designs. *Renewable Energy*. 2, 521- 531.

Saxena A., Varun A., El-Sebaii A.A. (2015). Athermodynamic review of solar air heaters. *Renewable and Sustainable Energy Reviews*. 43, 863- 890.

Singh S., Dhiman P. (2014). Using an analytical approach to investigate thermal performance of double-flow packed-bed solar air haters with external recycle. *Journal of Energy Engineering*. 211, 4001- 4031.

Sopian K., Alghoul M.A., Ebrahim M., Sulaiman M.Y., Musa E.A. (2009). Evaluation of thermal efficiency of double-pass solar collector with porous–nonporous media. *Renewable Energy*. 34, 640- 645.

Struckmann F. (2008). Analysis of a flat-plate solar collector. *Project report 2008 MVK160 Heat and Mass Transport*, May 08, Lund, Sweden.

Suleyman K. (2006). Performance analysis of new-design solar air collectors for drying applications. *Renewable Energy*. 32, 1645- 1660.

T.R.N.C. (Turkish Republic of Northern Cyprus), *ministry of public works and transport, department of meteorology*. http://kktcmeteor.org/.

Ürge-Vorsatz D., Cabeza L.F., Serrano S., Barreneche C., Petrichenko K. (2015). Heating and cooling energy trends and drivers in buildings. *Renewable and Sustainable Energy Reviews*. 41, 85- 98.

Yeh H.M., Ho C.D. (2009). Effect of external recycle on the performances of flat-plate solar air heaters with internal fins attached. *Renewable Energy*. 34, 1340- 1347.

Yeh H.M., Ho C.D., Hou J.Z. (2002). Collector efficiency of double-flow solar air heaters with fins attached. *Energy*. 27, 715- 727.

Yongsiri K., Eiamsa-ard P., Wongcharee K., Eiamsa-ard S. (2014). Augmented heat transfer inaturbulent channel flow with inclined detached-ribs. *Case Studies Therm. Eng*. 3, 1- 10.

Youcef-Ali S. (2005). Study and optimization of the thermal performances of the offset rectangular plate fin absorber plates, with various glazing. *Renewable Energy*. 31, 271- 280.

Youcef-Ali S., Desmons J.Y. (2006). Numerical and experimental study of a solar equipped with offset rectangular plate fin absorber plate. *Renewable Energy*. 31, 2063- 2075.

Yousef B.A.A., Adem N.M. (2008). Performance analysis for flat plate collector with and without porous media. *Journal of Energy in Southern Africa*. 19, 32- 42.